Lecture Notes in Statistics 206

Dihedral Fourier Analysis

Data-Analytic Aspects and Applications

Springer

Lecture Notes in Statistics 206

Edited by
P. Bickel, P. Diggle, S. Fienberg, U. Gather, I. Olkin, S. Zeger

For further volumes:
http://www.springer.com/series/694

Marlos A.G. Viana • Vasudevan Lakshminarayanan

Dihedral Fourier Analysis

Data-Analytic Aspects and Applications

Springer

Marlos A.G. Viana
University of Illinois at Chicago
Eye Center
Chicago Illinois
USA

Vasudevan Lakshminarayanan
University of Waterloo
School of Optometry
University Ontario
Canada

ISBN 978-1-4614-5561-5 ISBN 978-1-4614-5562-2 (eBook)
DOI 10.1007/978-1-4614-5562-2
Springer New York Heidelberg Dordrecht London

Library of Congress Control Number: 2012949361

Printed on acid-free paper

Springer is part of Springer Science+Business Media (www.springer.com)

To Ingram Olkin

Preface

The theory and applications of dihedral Fourier analysis presented in these notes are aimed at the study of experimental data indexed by, or associated with, the points in a dihedral symmetry orbit such as the images of a retina's visual field. The images

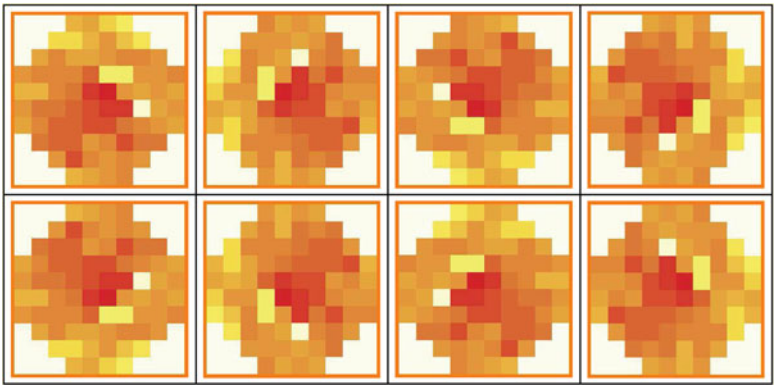

are iterated 90° rotations and/or horizontal reflections of each other, and together, the resulting set of images gives a symmetry orbit generated by *any* one of the images. The orbit has the symmetries of the rotations $\{1, r, r^2, r^3\} = C_4$ and reversals $\{h, rh, r^2h, r^3h\} = C_4h$ that together define the dihedral group $D_4 = C_4 \cup C_4h$. Similarly, the vector field illustrated in the diagram below gives a D_4 orbit when the rotations in C_4 and reversals in C_4h are represented with the (homomorphic) substitutions

$$r \mapsto R = \begin{bmatrix} \cos\phi & -\sin\phi \\ \sin\phi & \cos\phi \end{bmatrix}, \quad h \mapsto H = \begin{bmatrix} 1 & 0 \\ 0 & -1 \end{bmatrix},$$

where $\phi = 2\pi/4$, and applied to the position (q) and the direction (p) of a given field vector (q, p), thus defining the dihedral orbit shown below

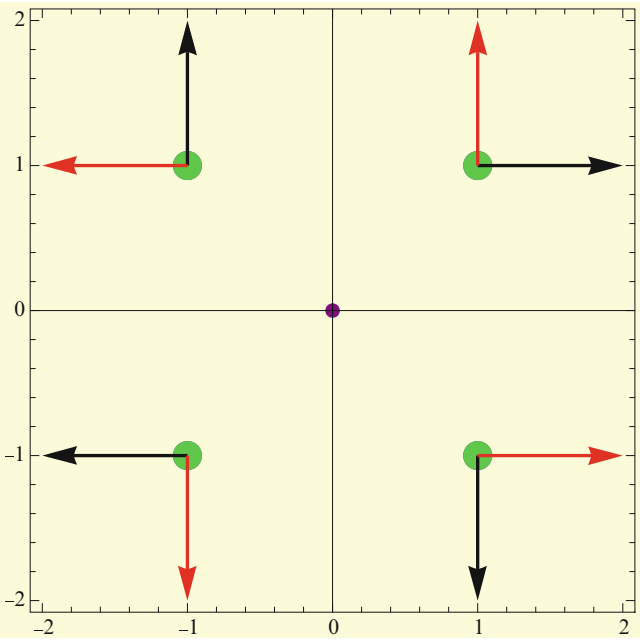

$$\mathcal{O} = \{(\tau q, \tau p);\ \tau \in D_4\}.$$

Here a reversal was defined as a counterclockwise rotation preceded by an x-axis reflection. Note that any two distinct-color vectors are line-reflection image of each other, whereas any two vectors of the same color are double-reflection (or rotation) image of each other. In that orbit, for example, we may want to evaluate the gradients

$$x_\tau = [\nabla f(\tau q)] \cdot \tau p, \quad \tau \in D_4,$$

of a response function f evaluated at τq in the direction of the vector τp along each field vector in the orbit $\mathcal{O}$, or the behavior of the center of mass

$$X_\sigma = \frac{\sum_\tau m_\tau \sigma F_\tau}{\sum_\tau m_\tau}, \quad \sigma \in D_4,$$

in the homogeneous field

$$F_\tau = (\tau q, p);\ \tau \in D_4,$$

with fixed direction p and allocated masses m_τ.

The dihedral orbits generated by D_n, as planar transformations, are simply the $2n$ symmetries of an n-sided regular polygon for $n > 2$, whereas the planar transformations in $D_2 = \{1, r, h, rh\}$ describe the symmetries of a 180° rotation

(r) and of two line reflections $(h,\ rh = v)$ along the vertical and horizontal axes, respectively. We often write, then, $D_2 = \{1, r, h, v\}$.

The orbits illustrated above are generated by applying the symmetries $\tau \in D_4$ to any one of the eight components in the orbit, so that they are independent of the orbit's generator or initial condition.

It is precisely this arbitrariness that is characteristic of the resulting *invariants* in any dihedral analysis. They are always invariant (in a way to be made precise throughout the text) to the different choices in initial conditions. Obviously, the image

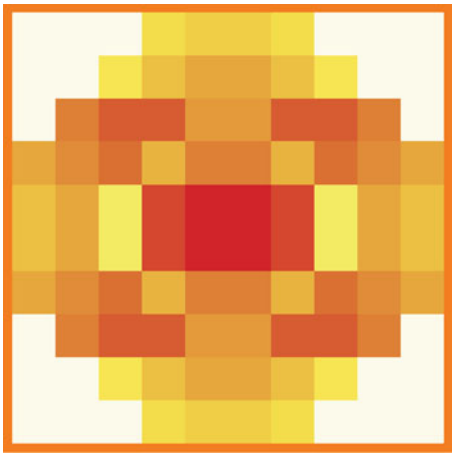

resulting as the superposition $1 + r + h + v$ of the elements in the D_2 orbit

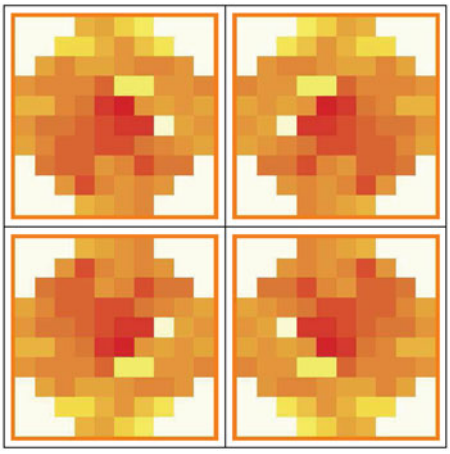

remains *the same* for all D_2 transformations, whereas the superposition $1 - r - h + v$

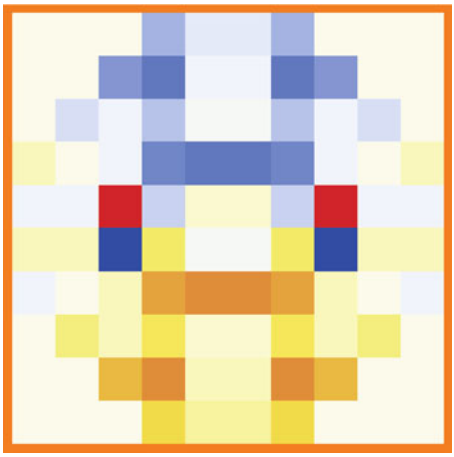

either stays the same, when transformed by 1 or v, or becomes color-*reversed* when transformed by r or h.

Every orbit $\mathscr{O}$ is to be understood, in the present data-analytic context, as a framework, a set of labels for experimental observations, so that the analysis of any data indexed by a dihedral orbit consists of systematically determining the summaries of the data allowed by the orbit invariants, suggesting their statistical analysis, and proposing eventual broad-range interpretations.

The points in the data space for any dihedral analysis will often be expressed as the symbolic linear combinations

$$x = \sum_{\tau} x_\tau \tau, \tau \in D_n$$

in which the $2n$ coefficients x_τ are the data of interest along the orbit. The x_τ are naturally real $(\mathbb{R})$ scalar measurements, eventually extracted from complex coefficients. In a few cases, the x_τ will be points in the ring $\mathscr{R}$ of $n \times n$ real data matrices. We write, respectively, $\mathbb{C}D_n$ or $\mathscr{R}D_n$ to indicate the dihedral (group) algebra and the dihedral (group) rings. They are complex vector spaces endowed with a multiplication induced by the dihedral multiplication. Details will be presented in Chap. 2.

As it will turn out, every dihedral algebra shall correspond to a direct sum of irreducible (matrix) linear subspaces

$$M_{n_1}(\mathbb{C}) \oplus \ldots \oplus M_{n_m}(\mathbb{C}) \simeq \mathbb{C}D_n$$

of dimensions $n_1^2, \ldots, n_m^2$ that is isomorphic to the original data vector space $\mathbb{C}D_n$, in dimension equal to the order $(2n)$ of D_n. In the dihedral ring case, the points in the linear subspaces are matrices over the ring $\mathscr{R}$.

The linear subspaces are stable under the different choices of orbit generators or initial conditions and are indexed by the set $(\widehat{D}_n)$ of irreducible representations (ξ) of D_n. For statistical inference, a sample of these orbital data would then be obtained.

The explicit formulation of the orbit invariants, sometimes referred to as analytical properties, is the result of evaluating the dihedral Fourier transforms, to be defined as the linearizations

$$< x, \xi >= \sum_{\tau \in D_n} x_\tau \xi_\tau \in M_{n_\xi}(\mathbb{C})$$

of x that appear as the components in the direct-sum factorization of $\mathbb{C}D_n$, one for each irreducible representation ξ in dimension of n_ξ. The isomorphic property of the factorization ensures the existence of the Fourier-inverse relation. The formulation of the Fourier transforms as direct-sum components of $\mathbb{C}D_n$ is developed in Chap. 2. In that same chapter we will show that from the full spectral information

$$\{< x, \xi >:\ \xi \in \widehat{D}_n\}$$

on x, a unitary basis $\mathscr{F}$ for $\mathbb{C}D_n$ can always be constructed, relative to which the analysis of the dihedral decomposition of $||x||^2$ becomes (theoretically and computationally) simplified, so that the analysis of variance

$$||x||^2 = \sum_{\xi} \frac{n_\xi}{2n} || < x, \xi > ||^2,$$

can be obtained directly from the Fourier transforms as Parseval's equalities for the dihedral groups.

Finally, we remark that when the dihedral multiplication is replaced by the additive structure of $\mathbb{R}^n$ then

$$< x, \lambda >= \int x_r \xi_r^\lambda dr,$$

where $\xi_r^\lambda = \exp(2\pi i \lambda \cdot r)$, for $r, \lambda \in \mathbb{R}^n$, is the usual Fourier transform of $x \in \mathbb{C}^{\mathbb{R}^n}$ evaluated at the irreducible representations ξ^λ. As suggested in [1], it is then natural to refer to the space of $\widehat{D}_n$ as the dual space of D_n.

These lecture notes are divided as follows: Chap. 1 is an overview of the theory and methods of dihedral analysis. It introduces data sets and examples defining and connecting the algebraic notions of symmetry with those of statistical summaries and inference. Chapter 2 includes the required algebraic aspects and data-analytic results. Applications are developed in Chaps. 3–6.

Chicago, IL — Marlos A.G. Viana
Waterloo, ON — Vasudevan Lakshminarayanan

Acknowledgements

These notes evolved with the constant enthusiasm of many colleagues and students at several institutions where we were given the opportunity to present earlier parts of these lectures, including the universities of Sao Paulo, Porto, Minho, Patras, Complutense de Madrid, Ireland (Galway), the Bauman and St. Petersburg State Universities (Russia), and the Abdus Salam International Centre for Theoretical Physics. Their suggestions and comments were an invaluable contribution to the completion of this project. We also acknowledge the support and encouragement of colleagues in our home institutions (D. Azar and J. Bauman in Chicago, and T. Freddo in Waterloo) throughout the project. This project was initiated under the editorial guidance of John Kimmel and the scientific advising of Ingram Olkin, to whom we extend our continued gratitude. We also express our thankful appreciation to B. Foster, H. Bracken, and the editorial board of the LNS Series for their support and professional assistance. Finally, but certainly not least, our gratitude goes to our families for their constant care and understanding.

Contents

Chapter 1
Symmetry and Experimental Data

1.1 Introduction

This chapter is an overview of the arguments relating symmetry, experimental data, and inference that appear in the theory, methods, and applications of dihedral analysis. The example introduced here is based on the only commutative case $(n = 2)$ and yet it includes all the basic elements present in the non-commutative $(n > 2)$ cases.

1.2 The Flag Ranking Data

Fifteen undergraduate students were individually presented with a printed copy of the set of colored flags shown in Fig. 1.1, and simply asked to rank the flags in each row, according to their preference. The table shown in the Appendix on page 9 shows the resulting 90 rankings (first, second, third and fourth preference) for the flags A,B,C, and D.

Each row in Fig. 1.1 is a distinct symmetry orbit. To see this note that each flag in column B can be obtained from the flag in column A by an horizontal reflection, each flag in column D is the image of flag A by a vertical reflection, and each flag in column C is the double reflection image of flag A.

Flag A is, of course, its own unaltered image, the effect of the identity transformation on itself. In addition, no two flags in distinct rows are image of each other by one of these symmetry transformations. Together, these are the $4! = 24$ possible distinct flags. The symmetries in the set $D_2 = \{1, r, h, v\}$, where 1 indicates the identity transformation leaving the flags unaltered, together with the operation of composition of transformations, form a finite group and multiply according to the table shown in (1.1). That is, the (associative) product $\tau\sigma$ of two symmetries $\tau, \sigma \in D_2$ is a symmetry in D_2; $1\tau = \tau 1 = \tau$, so that 1 is the identity element and

M.A.G. Viana and V. Lakshminarayanan, *Dihedral Fourier Analysis: Data-Analytic Aspects and Applications*, Lecture Notes in Statistics 206,
DOI 10.1007/978-1-4614-5562-2_1,

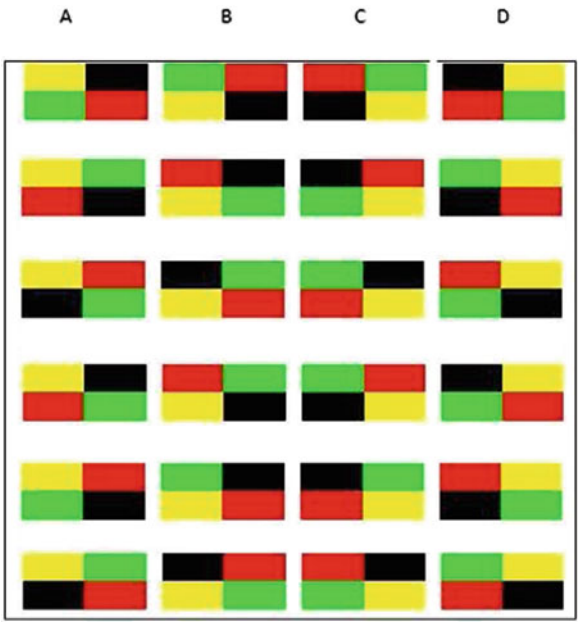

Fig. 1.1 The 24 flags used in the flag ranking experiment

each $\tau \in D_2$ has a corresponding $\tau^{-1} \in D_2$ such that $\tau\tau^{-1} = \tau^{-1}\tau = 1$. Moreover, $\tau\sigma = \sigma\tau$ for all $\tau, \sigma \in D_2$, so that D_2 is a commutative group.

D_2	1	v	h	r
1	1	v	h	r
v	v	1	r	h
h	h	r	1	v
r	r	h	v	1

(1.1)

The table in (1.2) shows the observed joint frequency counts for the first-choice flags (rows) and second-choice flags (columns). For example, in 12 rankings flag A was the first choice and flag D was the second choice. In other words, there were 12 (A, D) transitions.

	A	B	C	D	total
A	0	2	3	12	17
B	4	0	14	4	22
C	6	11	0	10	27
D	16	1	7	0	24
total	26	14	24	26	90

(1.2)

There were also 14 (B, C) transitions and 11 (C, B) transitions, both related by a vertical reflection. Similarly, there were 12 (A, D) and 16 (D, A) transitions, equally

related by a vertical reflection, so that together there were 53 first-to-second choices related to vertical transitions. This set of transitions

$$\mathscr{O}_v = \{(A,D),(D,A),(B,C),(C,B)\},$$

is itself an orbit of D_2, generated by selecting *any* transition $(X,Y) \in \mathscr{O}$ and evaluating $(\tau X, \tau Y)$ for all $\tau \in D_2$. The orbit and its corresponding transition data can be summarized as

$$\mathscr{O}_v = \begin{array}{ccc} (\text{A,D}) & = & (\text{D,A}) \\ \| & & \| \\ (\text{B,C}) & = & (\text{C,B}) \end{array} \mapsto \begin{array}{ccc} 12 & = & 16 \\ \| & & \| \\ 14 & = & 11 \end{array}, \tag{1.3}$$

and, as a point in the group algebra $\mathbb{C}D_2$ is then written as

$$V = 12 + 16\,v + 14\,h + 11\,r.$$

The same reasoning identifies the transitions (A,B), (B,A), (C,D) and (D,C) resulting from horizontal reflections, leading to the orbit and corresponding frequency counts shown in (1.4).

$$\mathscr{O}_h = \begin{array}{ccc} (\text{A,B}) & = & (\text{D,C}) \\ \| & & \| \\ (\text{B,A}) & = & (\text{C,D}) \end{array} \mapsto \begin{array}{ccc} 2 & = & 7 \\ \| & & \| \\ 4 & = & 10 \end{array}. \tag{1.4}$$

The corresponding data are expressed as

$$H = 2 + 7\,v + 4\,h + 10\,r.$$

Similarly, the transitions (A,C), (C,A), (B,D), and (D,B), determined by double reflections, define the orbit

$$\mathscr{O}_o = \begin{array}{ccc} (\text{A,C}) & = & (\text{D,B}) \\ \| & & \| \\ (\text{B,D}) & = & (\text{C,A}) \end{array} \mapsto \begin{array}{ccc} 3 & = & 1 \\ \| & & \| \\ 4 & = & 6 \end{array}, \tag{1.5}$$

with the corresponding data

$$R = 3 + 1\,v + 4\,h + 6\,r.$$

1.3 The Orbit Invariants as Fourier Transforms

We observe that the effect of choosing a different orbit starting point on

$$x = x_1 1 + x_v v + x_r r + x_h h,$$

is equivalent to multiplying x by an element in D_2. For example,

$$hx = x_1(h1) + x_v(hv) + x_r(hr) + x_h(hh) = x_1 h + x_v r + x_r v + x_h 1,$$

thus relabeling the data according to

$$x_1 \leftrightarrow x_h, \quad x_v \leftrightarrow x_r.$$

This is a D_2-shuffle of the original data. The other shuffles are

$$vx: \quad x_1 \leftrightarrow x_v, \quad x_h \leftrightarrow x_r,$$

and

$$rx: \quad x_1 \leftrightarrow x_r, \quad x_v \leftrightarrow x_h.$$

We would like to summarize the orbital data in a way that is independent of the D_2-shuffles, or, equivalently, free of the arbitrariness of the orbit generator choice.

A solution is the set of summaries given by

$$\begin{aligned} &x_1 + x_h + x_v + x_r, \\ &x_1 + x_h - x_v - x_r, \\ &x_1 - x_h + x_v - x_r, \\ &x_1 - x_h - x_v + x_r. \end{aligned}$$

For example,

$$\tau(x_1 + x_h - x_v - x_r) = x_{\tau 1} + x_{\tau h} - x_{\tau v} - x_{\tau r} = \pm(x_1 + x_h - x_v - x_r), \tag{1.6}$$

for all $\tau \in \{1, h, v, r\}$, thus giving rise to a one-dimensional (invariant) subspace. As it will be the case in general, these invariants will be simply the dihedral Fourier transforms of the data x, thus capturing precisely the sets of (orbit) invariants of interest, and, in that process, decomposing the data space $\mathbb{C}D_n$ into (orbit) invariant subspaces. We will return to the analysis of the flag preference data later on in Chap. 5. In the next section we outline the algebraic framework within which the notion of orbit invariance can be better justified.

1.4 The Algebraic Framework

Let x_τ indicate a scalar component of x, indexed by $\tau \in D_2$, and write

$$x = \sum x_\tau \tau \tag{1.7}$$

to denote the symbolic $\mathbb{C}$-linear combination of the dihedral elements with scalar coefficients the components of x. As it is immediately seen, the set

$$\mathbb{C}D_2 = \left\{ \sum_{\tau \in D_2} x_\tau \tau : \; x_\tau \in \mathbb{C} \right\}$$

has a $\mathbb{C}-$vector space structure with a basis indexed by D_2, and is endowed with a multiplication

$$x\, y = \sum_{\tau,\sigma} x_\tau y_\sigma \tau\sigma = \sum_\tau \left(\sum_\sigma x_\sigma y_{\sigma^{-1}\tau} \right) \tau = \sum_\tau (x * y)_\tau \tau = x * y, \tag{1.8}$$

induced by the dihedral multiplication. The resulting structure is called a *dihedral algebra*. If the dihedral coefficients are points in a ring $\mathscr{R}$ with identity, then the resulting structure is indicated by $\mathscr{R}D_2$ and called a *dihedral ring*.

The experimental data of interest for the Fourier analysis over a finite group G are then interpreted simply as points in the group algebra or group ring of G, whereas the Fourier transforms, as we shall see, are certain matrix realizations of the underlying group algebra.

In the D_2 case, there are four linear mappings

	1	h	v	r
ξ^1	1	1	1	1
ξ^h	1	1	−1	−1
ξ^v	1	−1	1	−1
ξ^r	1	−1	−1	1

, (1.9)

that satisfy the homomorphic property $\xi_\tau \xi_\sigma = \xi_{\tau\sigma}$ for all $\tau, \sigma \in D_2$ and lead to the linear combinations

$$< x, \xi >= \sum_{\tau \in D_2} x_\tau \xi_\tau, \tag{1.10}$$

of ξ, with scalar coefficients given by the components of x, one for each

$$\xi \in \widehat{D}_2 = \{\xi^1, \xi^h, \xi^v, \xi^r\}.$$

The linear combinations $< x, \xi >$ will be defined as the Fourier transforms of x evaluated at $\xi \in \widehat{D}_2$, so that the summaries introduced on page 4 follow directly from (1.10). They satisfy the (orbit) invariance property

$$< \tau x, \xi >= \xi_\tau < x, \xi >, \tag{1.11}$$

for all $\tau \in D_2$ and $\xi \in \widehat{D}_2$.

In the present case of D_2, each transform gives rise to a *basis* for an invariant subspace in dimension of one, thus accounting for the dimension of the (data) vector space $\mathbb{C}D_2$. Together, these transforms are exactly two types:

1. An overall sum $< x, \xi^1 >= x_1 + x_h + x_v + x_r$ of responses;
2. And three pairwise comparisons

- $< x, \xi^h >= x_1 + x_h - x_v - x_r$,
- $< x, \xi^v >= x_1 - x_h + x_v - x_r$,
- $< x, \xi^r >= x_1 - x_h - x_v + x_r$.

The pairwise comparisons, we observe, are just sums over the cosets

$$D_2/\{1,v\} = \{\{1,v\},\ \{h,r\}\},$$

$$D_2/\{1,h\} = \{\{1,h\},\ \{v,r\}\},$$

$$D_2/\{1,r\} = \{\{1,r\},\ \{v,h\}\},$$

in a way that when appropriate any probability distribution $(p, 1-p)$ over the cosets is such that a D_2 relabeling will either leave it the same or change it to its complement $(1-p, p)$. In doing so, however, its entropy (Ent) remains constant. This will be particularly useful when the dihedral data are in the form of (multinomial) frequency counts.

1.5 Inference

The flag preference study suggests that we may compare the orbits according to each one of the invariants. When compared with respect to invariant linked to ξ_1, we obtain

$$\xi^1(V,H,O) = (53,23,14),$$

which is a decomposition of the total number (90) of initial rankings into elementary orbit components. Their uniform-prior marginal posterior distributions,

$$\mathscr{L}_v \sim Be(54,38),\ \ \mathscr{L}_h \sim Be(24,68),\ \ \mathscr{L}_r \sim Be(15,77),$$

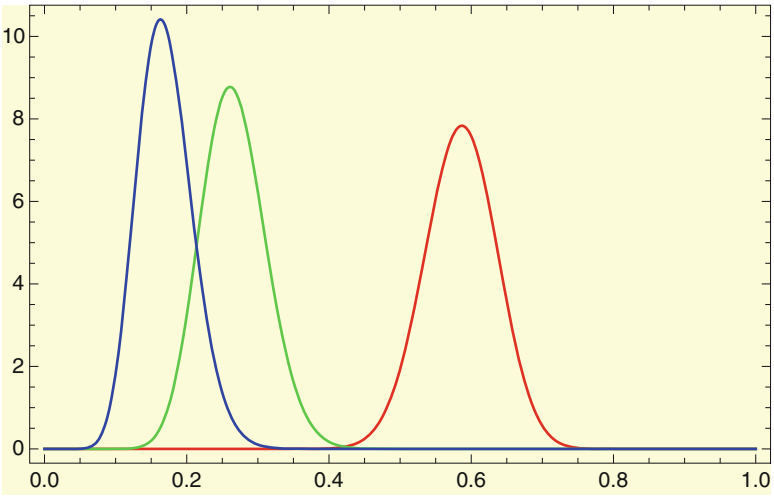

Fig. 1.2 Posterior densities for the probabilities of matching first and second-choice flags by a vertical (*red*), horizontal (*green*), and double-reflection (*blue*) image of each other

are shown in Fig. 1.2, demonstrating a visible preference to matching first and second-choice flags by a vertical reflection image of each other. More on that later on Chap. 5. The pairwise within-orbit invariants determined by ξ^v, ξ^h and ξ^r are informative orbit-invariant components of variability. We may, for example, summarize the within-orbit entropy by their extreme entropy values. The flag data are amenable to broader algebraic formulations, related to the fact that the six four-flag orbits (the rows in Fig. 1.1) are actually points in the quotient group $S_4/D_2 \sim D_3$, so that within D_2-orbit preferences may be studied as points in a D_3 orbit. We will return to that analysis later on in Chap. 5.

Problems

1.1. Verify the D_2-invariance property $< \tau x, \xi >= \xi_\tau < x, \xi >$, for all $\tau \in D_2$ and $\xi \in \widehat{D}_2$.

1.2. Indicating by V the set of all mappings $s : \{1,2,3\} \mapsto \{a,c,t\}$, describe the left $s\tau^{-1}$ and right σs actions of D_3 as a permutation group of $\{a,c,t\}$ and $\{1,2,3\}$ respectively. Show that in one case, the resulting orbits are in one-one correspondence with the non-empty subsets of $\{a,c,t\}$.

1.3. Referring to the transition preference data V,H,R given on page 3, evaluate $\pi_\xi =< X/4, \xi >$ for each $X = V,H,R$ and then show that: (1) $\pi_\xi \pi_\eta = 0$ if $\xi \neq \eta$; (2) $\pi_\xi^2 = \pi_\xi$, and (3) $\sum_{\xi \in \hat{D}_2} \pi_\xi = 1$.

1.4. Referring again to the transition preference data V,H,R given on page 3, evaluate and interpret the pairwise products (as points in the group algebra) among the corresponding relative frequency distributions $X/ < X, \xi_1 >$, for $X = V,H,R$.

1.5. The following matrices summarize the first-to-second transition counts given by the matrix in (1.2), according to the distinct D_3 orbits in the flag preference data.

$$x_1 = \begin{bmatrix} 0\,0\,1\,4 \\ 0\,0\,0\,1 \\ 0\,0\,0\,2 \\ 5\,0\,2\,0 \end{bmatrix}, \; x_r = \begin{bmatrix} 0\,0\,0\,1 \\ 0\,0\,2\,1 \\ 1\,5\,0\,2 \\ 2\,1\,0\,0 \end{bmatrix}, \; x_{r^2} = \begin{bmatrix} 0\,0\,1\,2 \\ 3\,0\,4\,0 \\ 2\,1\,0\,1 \\ 1\,0\,0\,0 \end{bmatrix},$$

$$x_h = \begin{bmatrix} 0\,0\,1\,3 \\ 0\,0\,0\,1 \\ 1\,1\,0\,1 \\ 5\,0\,2\,0 \end{bmatrix}, \; x_{rh} = \begin{bmatrix} 0\,1\,0\,0 \\ 0\,0\,3\,1 \\ 1\,4\,0\,2 \\ 1\,0\,2\,0 \end{bmatrix}, \; x_{r^2h} = \begin{bmatrix} 0\,1\,0\,2 \\ 1\,0\,5\,0 \\ 1\,0\,0\,2 \\ 2\,0\,1\,0 \end{bmatrix}.$$

Refer to Fig. 1.1 on page 2 and show that the orbits are indexed by the dihedral group D_3. Then, re-evaluate the within-orbit posterior distributions for the probabilities of matching first and second-choice flags by reflections and double-reflections.

1.6. Evaluate the frequency distribution of the 24 possible flag rankings, based on the data shown in the Appendix A, on page 9.

1.7. Do the findings suggested by the first-to-second preference transition counts hold for the second-to-third transition counts? Explain.

Appendix A: The Flag Preference Data

Each block gives the six four-flag rankings from one of the 15 subjects.

1st	2nd	3rd	4th	1st	2nd	3rd	4th	1st	2nd	3rd	4th
A	D	B	C	D	A	C	B	A	D	B	C
A	D	B	C	C	B	D	A	D	A	B	C
C	B	D	A	B	C	D	A	C	A	D	B
C	B	A	D	C	D	B	A	C	A	B	D
D	C	A	B	C	D	B	A	A	B	D	C
A	B	C	D	B	C	A	D	A	D	B	C
C	D	B	A	D	C	B	A	D	C	A	B
C	D	B	A	D	A	C	B	B	D	A	C
B	A	C	D	A	D	B	C	B	A	C	D
D	C	B	A	B	D	A	C	D	C	B	A
D	C	B	A	C	A	B	D	C	D	A	B
D	C	B	A	C	D	B	A	C	A	B	D
A	D	C	B	A	C	D	B	D	A	C	B
C	D	A	B	B	C	A	D	C	B	D	A
C	D	A	B	B	A	C	D	B	C	D	A
A	D	C	B	D	A	C	B	D	A	B	C
B	C	D	A	B	C	A	D	C	B	D	A
C	D	A	B	B	C	A	D	B	C	D	A
D	A	C	B	A	D	C	B	D	A	C	B
B	C	A	D	C	B	A	D	C	A	B	D
A	D	B	C	D	A	B	C	B	C	D	A
A	D	B	C	A	D	C	B	D	A	B	C
D	A	C	B	B	C	D	A	C	B	D	A
D	A	C	B	D	A	B	C	B	C	A	D
C	D	A	B	D	A	C	B	B	D	C	A
C	B	D	A	C	B	D	A	D	B	C	A
C	A	B	D	B	C	A	D	A	C	B	D
D	A	C	B	D	A	C	B	A	C	D	B
C	B	D	A	C	B	D	A	B	D	A	C
A	D	C	B	B	C	A	D	B	A	C	D

Chapter 2
Algebraic and Data-Analytic Aspects

2.1 Introduction

As outlined in Chap. 1, the algebraic structure of natural interest for the dihedral analysis is the dihedral group algebra $\mathbb{C}D_n$, defined by the elements

$$x = \sum x_\tau \tau,$$

in one-to-one correspondence with the points x in $\mathbb{C}^{2n}$.

Although the algebraic aspects reviewed in this chapter are focused on the dihedral groups, many related extensions and examples can be found in [2]. Unless stated otherwise, all vector spaces are finite, and their dimensions are assumed to be evaluated over the complex field.

2.2 The Dihedral Groups

The dihedral groups D_n can be objectively introduced as matrix groups of planar rotations and reversals. Specifically, they can be generated by a central counter-clockwise rotation

$$R = \begin{bmatrix} \cos\phi & -\sin\phi \\ \sin\phi & \cos\phi \end{bmatrix}$$

of $\phi = 2\pi/n$ radians and a line reflection (say along the horizontal axis)

$$H = \begin{bmatrix} 1 & 0 \\ 0 & -1 \end{bmatrix},$$

M.A.G. Viana and V. Lakshminarayanan, *Dihedral Fourier Analysis: Data-Analytic Aspects and Applications*, Lecture Notes in Statistics 206,
DOI 10.1007/978-1-4614-5562-2_1, © Springer Science+Business Media New York 2013

by observing that together, the iterated rotation R^j and reversal R^jH matrices for $n \geq 2$ multiply according to the rules

$$R^n = 1, \quad H^2 = 1, \quad HR^j = R^{-j}H, \quad j = 0, \ldots, n-1. \tag{2.1}$$

We observe that the anti-commutativity $HR = R^{-1}H$ of R and H has the effect of producing two equivalent reversal mechanisms distinguished only by the direction of the rotation mechanism.

We briefly recall that an algebraic group is a nonempty set G equipped with an associative binary operation $G \times G \to \sigma\tau \in G$, an (identity) element $1 \in G$, satisfying $1\tau = \tau 1 = \tau$, for all $\tau \in G$ and such that for every $\tau \in G$, there is an (inverse) element $\tau^{-1} \in G$ such that $\tau\tau^{-1} = \tau^{-1}\tau = 1$. The dihedral matrices introduced above, for example, give a non-commutative matrix group of order $2n$ for $n > 2$. The dihedral matrix groups can also be generated by any two reflection matrices along lines with an angular separation of $(2\pi/n)/2$ radians. These angles are often referred to as dihedral angles.

In its abstract formulation, the dihedral group D_n of order $2n$ is the (set) orbit

$$C_n \cup C_n h$$

of

$$C_n = \{1, r, r^2, \ldots, r^{n-1}\}, \quad n \geq 2,$$

by an involution $\{1, h\}$, with multiplication rules given by

$$r^n = 1, \quad h^2 = 1, \quad hr^j = r^{-j}h, \quad j = 0, \ldots, n-1. \tag{2.2}$$

A word about notation: Denoting

$$\alpha : d \in \{1, -1\} \mapsto \alpha(d) = (1-d)/2 \in \{0, 1\},$$

we may occasionally write

$$r^j h^{\alpha(d)} \equiv \begin{cases} r_j & \text{if } \ d = 1 \\ t_j & \text{if } \ d = -1 \end{cases} \tag{2.3}$$

for $j = 0, \ldots, n-1$, to indicate a generic rotation ($d = 1$) or a reversal ($d = -1$) in D_n. We observe that the multiplication in D_n is just the semi-direct product

$$(j, d) \rtimes (j', d') = (j + dj' \mod n, \ dd') \tag{2.4}$$

in $\mathbb{Z}_n \times \mathbb{Z}_2$. Similarly, we shall write

$$\beta_\tau = R^j H^{\alpha(d)}, \ \ j = 0, \ldots, n-1, \, d = \pm 1,$$

to indicated the corresponding rotation and reversal matrices, and their corresponding harmonics

$$\beta_\tau^k = R^{jk} \mod n H^{\alpha(d)} \quad k = 1,2,\ldots,m = \begin{cases} \frac{n}{2} - 1 & \text{if n is even,} \\ \frac{n-1}{2} & \text{if n is odd,} \end{cases} \tag{2.5}$$

understanding that $\beta^1 = \beta$.

2.3 D_n Conjugacy Orbits

Writing

$$[\eta] = \{\tau\eta\tau^{-1},\ \tau \in D_n\}$$

to indicate the conjugacy orbit of $\eta \in D_n$ and using the defining relations h^2=1, $hr^j = r^{-j}h$ for D_n, it directly follows that $r^{j_1}(r^{j_2})r^{-j_1} = r^{j_2}$, and $r^{j_1}h(r^{j_2})hr^{-j_1} = r^{-j_2}$, so that

$$[r^j] = \{r^j, r^{-j}\}$$

is the conjugacy orbit of r^j. In particular, $[1] = \{1\}$. Moreover,

$$r^{j_1}(r^j h)r^{-j_1} = r^{2j_1+j}h, \text{ and } r^{j_1}h(r^j h)hr^{-j_1} = r^{2j_1-j}h,$$

so that one obtains, for n even

$$[r^j h] = \begin{cases} \{r^{2j_1}h:\ j_1 = 0,\ldots,n-1\}, & \text{for } j \text{ even;} \\ \{r^{2j_1+1}h:\ j_1 = 0,\ldots,n-1\}, & \text{for } j \text{ odd,} \end{cases}$$

whereas, for n odd, the reversals are self-conjugate:

$$[r^j h] = \{r^j h:\ j = 0,\ldots,n-1\}.$$

To illustrate, if $n = 6$, the conjugacy orbits are

$$\{1\},\ \{r, r^5\},\ \{r^2, r^4\},\ \{r^3\},\ \{h, r^2h, r^4h\},\ \{rh, r^3h, r^5h\},$$

whereas, if $n = 7$, the orbits are

$$\{1\},\ \{r, r^6\},\ \{r^2, r^5\},\ \{r^3, r^4\},\ \{h, rh, \ldots, r^6h\}.$$

2.4 Dihedral Sets and Modules

We say that a set S is a *dihedral set* if there is a mapping

$$(\tau, s) \in D_n \times S \mapsto \tau s \in S$$

such that $1s = s$ and $\sigma(\tau s) = (\sigma\tau)s$ for all $\sigma, \tau \in D_n$, and $s \in S$. In this case we also say that D_n *acts* on S. We say that the action is *opposite* if $\sigma(\tau s) = (\tau\sigma)s$ for all $\sigma, \tau \in D_n$, and $s \in S$.

If a vector space V is a finite dihedral set and

$$\tau(x+y) = \tau x + \tau y, \;\; \tau(\lambda x) = \lambda(\tau x),$$

for all $x, y \in V$ and scalars λ, then we say that the dihedral action is *linear*, and that V is a dihedral *representation space* or a dihedral *module*. In this case we also say that $x \mapsto \tau x$ is a dihedral *representation*. Its dimension is equal to the dimension of the module V as a complex vector space.

Clearly D_n is itself a dihedral set under the (left) *regular action*

$$\sigma \mapsto \tau\sigma,$$

that extends to an opposite linear action

$$\tau x = \tau \sum_{\sigma} x_\sigma \sigma = \sum_{\sigma} x_{\tau^{-1}\sigma}\sigma \tag{2.6}$$

on $\mathbb{C}D_n$, thus affording the group algebra $\mathbb{C}D_n$ with a (left) module structure of dimension $2n$. We may refer to $\mathbb{C}D_n$ as the dihedral *regular module*. The corresponding facts apply to the right regular action $\sigma \mapsto \sigma\tau^{-1}$, and unless otherwise stated we will assume all modules to be left modules.

From (2.6), with $y, x \in \mathbb{C}D_n$, we have

$$yx = \left(\sum_\tau y_\tau \tau\right)x = \sum_\tau y_\tau(\tau x) = \sum_\tau y_\tau \left(\sum_\sigma x_{\tau^{-1}\sigma}\sigma\right) = \sum_\sigma \left(\sum_\tau y_\tau x_{\tau^{-1}\sigma}\right)\sigma = \sum_\sigma (y*x)_\sigma \sigma,$$

so that the multiplication xy in $\mathbb{C}D_n$ is given by the group convolution $x*y$, allowing us to write

$$xy = x*y.$$

Also from (2.6), the matrix form of the regular representation $x \mapsto \tau x$ is a $2n \times 2n$ permutation matrix, indicated from now on by ϕ, with entries

$$(\phi_\tau)_{\sigma\eta} = 1 \iff \tau\sigma = \eta.$$

Direct calculation then shows that, for all $\tau, \nu \in D_n$,

$$\phi_\tau \phi_\nu = \phi_{\nu\tau}, \tag{2.7}$$

so that ϕ is a dihedral *anti-homomorphism*, whereas its transpose ϕ' gives the corresponding dihedral homomorphism. These notions are equivalent, and will generally be referred as dihedral homomorphisms.

We say that V is a *submodule* of $\mathbb{C}D_n$ to indicate that V is a subspace of $\mathbb{C}D_n$ where D_n acts linearly. Consequently, all submodules are *stable* subspaces in the sense that $\tau x \in V$ for all $x \in V$ and $\tau \in D_n$.

If V is a dihedral submodule in dimension of m, we write ρ_τ to indicate the matrix form (in a given basis) of a generic dihedral (linear) action on V, so that then ρ_τ in a point in the vector space $\in GL_m(\mathbb{C})$ of all invertible $m \times m$ linear mappings over $\mathbb{C}$. By definition, then, ρ is dihedral homomorphism.

If ρ is a dihedral homomorphism then clearly $F\rho F^{-1}$ is also a dihedral homomorphism, for all $F \in GL_m(\mathbb{C})$. In that case we say that the dihedral homomorphisms ρ and $F\rho F^{-1}$ are *equivalent*, and write $\rho \simeq F\rho F^{-1}$ to indicate the equivalence.

Every module has at least two submodules: itself and the zero submodule $\{0\}$. A module with no other submodule is called a *simple* module. Clearly, one-dimensional modules are simple.

Definition 2.1 (Dihedral linearizations). Given a dihedral homomorphism ρ on $GL_m(\mathbb{C})$ and $x \in \mathbb{C}D_n$, the evaluation

$$< x, \rho >= \sum x_\tau \rho_\tau \ \in M_m(\mathbb{C})$$

is called a linearization of $\mathbb{C}D_n$ in $M_m(\mathbb{C})$. In particular, $< x, \phi >$ is called the regular linearization of x.

Proposition 2.1. *For all dihedral homomorphisms ρ, η, ξ, all $x, y \in \mathbb{C}D_n$, and scalars λ, we have:*

1. *If $\rho \simeq \eta \oplus \xi$ then $< x, \rho > \simeq < x, \eta > \oplus < x, \xi >$;*
2. $< x+y, \rho >=< x, \rho > + < y, \rho >$;
3. $\lambda < x, \rho >=< \lambda x, \rho >$;
4. $< xy, \rho >=< x, \rho >< y, \rho >=< x * y, \rho >$.

Proof. The proof is by direct evaluation. For the equalities in 4, we recall that

$$x\,y = \sum_{\tau,\sigma} x_\tau y_\sigma \tau\sigma = \sum_\tau \left(\sum_\sigma x_\sigma y_{\sigma^{-1}\tau} \right) \tau = \sum_\tau (x * y)_\tau \tau = x * y,$$

as introduced earlier on page 14. □

Decompositions such as $< x, \rho > \simeq < x, \eta > \oplus < x, \xi >$ appearing in Proposition 2.1 are often referred to as product of matrix algebras, e.g. [3, p.79], [4, p.48].

We also remark that, more generally, the notation $\rho \simeq m\eta \oplus \ldots \oplus n\xi$ indicates that there is a basis in the representation space of ρ relative to which

$$\rho_\tau = \text{Diag}\,(I_m \otimes \eta_\tau, \ldots, I_n \otimes \xi_\tau), \quad \tau \in G,$$

where I_r indicates the $r \times r$ identity matrix.

Proposition 2.2. *Let, for $n \geq 2$, and $(j,d) \equiv \tau \in D_n$,*

- $1 : (j,d) \mapsto 1$;
- $\alpha : (j,d) \mapsto d$;
- $\gamma_+ : (j,d) \mapsto (-1)^j$, *for n even;*
- $\gamma_- : (j,d) \mapsto d(-1)^j$, *for n even.*

Then, for $\xi \in \{1, \alpha, \gamma_+, \gamma_-\}$ and x in $\mathbb{C}D_n$, the linearizations $< x, \xi >$ are simple dihedral submodules of $\mathbb{C}D_n$.

Proof. The result follows by directly showing that each $\xi \in \{1, \alpha, \gamma_+, \gamma_-\}$ is a one-dimensional dihedral homomorphism, so that $< x, \xi >$ is simple. □

Example 2.1. The simple D_3 submodules described in Proposition 2.2:

- $< x, 1 > = \sum_\tau 1_\tau x_\tau = x_1 + x_r + x_{r^2} + x_h + x_{rh} + x_{r^2h}$;
- $< x, \alpha > = \sum_\tau \alpha_\tau x_\tau = x_1 + x_r + x_{r^2} - x_h - x_{rh} - x_{r^2h}$.

Example 2.2. The simple D_4 submodules described in Proposition 2.2:

- $< x, 1 > = \sum_\tau 1_\tau x_\tau = x_1 + x_r + x_{r^2} + x_{r^3} + x_h + x_{rh} + x_{r^2h} + x_{r^3h}$;
- $< x, \alpha > = \sum_\tau \alpha_\tau x_\tau = x_1 + x_r + x_{r^2} + x_{r^3} - x_h - x_{rh} - x_{r^2h} - x_{r^3h}$;
- $< x, \gamma_+ > = \sum_\tau \gamma_\tau^+ x_\tau = x_1 - x_r + x_{r^2} - x_{r^3} + x_h - x_{rh} + x_{r^2h} - x_{r^3h}$;
- $< x, \gamma_- > = \sum_\tau \gamma_\tau^- x_\tau = x_1 - x_r + x_{r^2} - x_{r^3} - x_h + x_{rh} - x_{r^2h} + x_{r^3h}$.

Example 2.3. Simple one-dimensional modules are constant over conjugacy orbits. The following is the evaluation of the simple dihedral modules described in Proposition 2.2 over the conjugacy orbits

$$\{1\}, \{r, r^5\}, \{r^2, r^4\}, \{r^3\}, \{h, r^2h, r^4h\}, \{rh, r^3h, r^5h\},$$

of D_6, from Sect. 2.3:

$$1 : \{+\}, \{+\}, \{+\}, \{+\}, \{+\}, \{+\},$$

$$\alpha : \{+\}, \{+\}, \{+\}, \{+\}, \{-\}, \{-\},$$

$$\gamma_+ : \{+\}, \{-\}, \{+\}, \{-\}, \{+\}, \{-\},$$

$$\gamma_- : \{+\}, \{-\}, \{+\}, \{-\}, \{-\}, \{+\}.$$

Similarly, over the conjugacy orbits

$$\{1\},\ \{r,r^6\},\ \{r^2,r^5\},\ \{r^3,r^4\},\ \{h,rh,\ldots,r^6h\}.$$

of D_7, we obtain:

$$1:\{+\},\ \{+\},\ \{+\},\ \{+\},\ \{+\},$$
$$\alpha:\{+\},\ \{+\},\ \{+\},\ \{+\},\ \{-\}.$$

Proposition 2.3 (Orbit invariance). *If ρ is a dihedral homomorphism and $x \in \mathbb{C}D_n$ then, for all $\tau,\sigma \in D_n$,*

$$< \tau x,\rho >= \rho_\tau < x,\rho >,\quad < x\sigma,\rho >=< x,\rho > \rho_\sigma.$$

Proof. From (2.6), we have,

$$< \tau x,\rho >= \sum_\sigma x_{\tau^{-1}\sigma}\rho_\sigma = \sum_\gamma x_\gamma \rho_{\tau\gamma} = \sum_\gamma x_\gamma \rho_\tau \rho_\gamma = \rho_\tau < x,\rho >,$$

and, similarly, $< x\sigma,\rho >= \sum_\tau x_{\tau\sigma^{-1}}\rho_\tau = \sum_\gamma x_\gamma \rho_{\gamma\sigma} =< x,\rho > \rho_\sigma$. □

In particular

$$< \tau x\tau^{-1},\rho >= \rho_\tau < x,\rho > \rho_{\tau^{-1}}.$$

Proposition 2.4. *The row (column) spaces of the linearizations $< x,\rho >$ are dihedral left (right) submodules of $\mathbb{C}D_n$.*

Proof. Observing that the row (column) j of a matrix product AB is a linear combination of the rows (columns) of B (A), with coefficients the row (column) j of A (B), the result follows from Proposition 2.3, which defines the actions

$$y\sigma = y\rho_\sigma,\quad \sigma \in D_n,$$

on the right for every y in the column space of $< x,\rho >$, and

$$\tau y = \rho_\tau y,\quad \tau \in D_n$$

on the left, for every y in the row space of $< x,\rho >$. □

It then follows, from Proposition 2.4 that the column (row) space of the regular linearization $< x,\phi >$ is a dihedral left (right) submodule of $\mathbb{C}D_n$.

Proposition 2.5. *$\mathbb{C}D_n$ allows for $m = n/2-1$ distinct two-dimensional submodules for n even and $m = (n-1)/2$ submodules for n odd, $n \geq 2$.*

Proof. Direct verification shows that the β^k defined in (2.5) are dihedral homomorphisms, so that the corresponding linearizations

$$< x, \beta^k >, \quad k = 1, 2, \ldots, m = \begin{cases} \frac{n}{2} - 1 & \text{if n is even,} \\ \frac{n-1}{2} & \text{if n is odd,} \quad x \in \mathbb{C}D_n, \end{cases}$$

give two-dimensional submodules according to Proposition 2.4. □

Proposition 2.6. *The two-dimensional submodules* $< x, \beta^1 >, \ldots, < x, \beta^m >$ *are simple.*

Proof. Since $< \tau x, \beta^k >$ reduces as $\beta_\tau^k < x, \beta^k >$, it is sufficient to study the $\mathbb{C}$-reducibility of β^k in D_n. Since the eigenvectors for (all) the rotation components of β^k in D_n are $(i, 1)$ and $(-i, 1)$ for all k, n, it then follows that the only proper subspace of the (column) spaces of $< x, \beta^k >$ is the null space, completing the proof. □

As a consequence, referring to Proposition 2.2 on page 16, the sum of the squares of the corresponding dimensions in

$$\widehat{D}_n = \{1, \alpha, \gamma_+, \gamma_-, \beta_1, \ldots, \beta_m\} \tag{2.8}$$

is equal to $4 + (n/2 - 1)2^2 = 2n$ when n is even, and is equal to $2 + ((n-1)/2)2^2 = 2n$ in

$$\widehat{D}_n = \{1, \alpha, \beta_1, \ldots, \beta_m\} \tag{2.9}$$

when n is odd. Therefore, e.g. [2, Prop. 4.2], these are exactly the simple modules of $\mathbb{C}D_n$. As a result, we have:

Proposition 2.7. $\mathbb{C}D_n$ *as a semi-simple module factors as*

$$\mathbb{C}D_n \simeq < x, 1 > \oplus < x, \alpha > \oplus < x, \gamma_+ > \oplus < x, \gamma_- > \bigoplus_{k=1}^{n/2-1} < x, \beta_k >$$

when n is even and as

$$\mathbb{C}D_n \simeq < x, 1 > \oplus < x, \alpha > \bigoplus_{k=1}^{(n-1)/2} < x, \beta_k >$$

when n is odd, $n \geq 2$. □

Definition 2.2 (Dihedral Fourier Transforms). Each simple module $< x, \xi >$ in the decomposition of $\mathbb{C}D_n$ given by Proposition 2.7 is called the Fourier transform of x at the corresponding representation ξ.

Additional Notation: From now on we assume that, for $n \geq 2$,

$$m = \begin{cases} \frac{n}{2} - 1 & \text{if n is even,} \\ \frac{n-1}{2} & \text{if n is odd.} \end{cases}$$

Here are a few examples of dihedral decompositions, following Proposition 2.7.

Example 2.4. $\mathbb{C}D_2$ gives four simple modules all in dimension of 1:

$$\begin{aligned}
< x, 1 > &= x_1 + x_r + x_h + x_{rh};\\
< x, \alpha > &= x_1 + x_r - x_h - x_{rh};\\
< x, \gamma_+ > &= x_1 - x_r + x_h - x_{rh};\\
< x, \gamma_- > &= x_1 - x_r - x_h + x_{rh}.
\end{aligned}$$

Example 2.5. $\mathbb{C}D_3$ has two simple modules in dimension of 1:

$$\begin{aligned}
< x, 1 > &= x_1 + x_r + x_{r^2} + x_h + x_{rh} + x_{r^2h};\\
< x, \alpha > &= x_1 + x_r + x_{r^2} - x_h - x_{rh} - x_{r^2h};
\end{aligned}$$

and one in dimension of 2:

$$< x, \beta >= \frac{1}{2}\begin{bmatrix} 2x_1 - x_r - x_{r^2} + 2x_h - x_{rh} - x_{r^2h} & \sqrt{3}\,(-x_r + x_{r^2} + x_{rh} - x_{r^2h}) \\ \sqrt{3}\,(x_r - x_{r^2} + x_{rh} - x_{r^2h}) & 2x_1 - x_r - x_{r^2} - 2x_h + x_{rh} + x_{r^2h} \end{bmatrix}.$$

Example 2.6. $\mathbb{C}D_4$ gives four simple modules in dimension of 1 and one in dimension of 2:

$$\begin{aligned}
< x, 1 > &= x_1 + x_r + x_{r^2} + x_{r^3} + x_h + x_{rh} + x_{r^2h} + x_{r^3h};\\
< x, \alpha > &= x_1 + x_r + x_{r^2} + x_{r^3} - x_h - x_{rh} - x_{r^2h} - x_{r^3h};\\
< x, \gamma_+ > &= x_1 - x_r + x_{r^2} - x_{r^3} + x_h - x_{rh} + x_{r^2h} - x_{r^3h};\\
< x, \gamma_- > &= x_1 - x_r + x_{r^2} - x_{r^3} - x_h + x_{rh} - x_{r^2h} + x_{r^3h};\\
< x, \beta > &= \begin{bmatrix} x_1 - x_{r^2} + x_h - x_{r^2h} & -x_r + x_{r^3} + x_{rh} - x_{r^3h} \\ x_r - x_{r^3} + x_{rh} - x_{r^3h} & x_1 - x_{r^2} - x_h + x_{r^2h} \end{bmatrix}.
\end{aligned}$$

Example 2.7. $\mathbb{C}D_6$ allows for four simple modules in dimension of 1:

$$\begin{aligned}
< x, 1 > &= x_1 + x_r + x_{r^2} + x_{r^3} + x_{r^4} + x_{r^5} + x_h + x_{rh} + x_{r^2h} + x_{r^3h} + x_{r^4h} + x_{r^5h}\\
< x, \alpha > &= x_1 + x_r + x_{r^2} + x_{r^3} + x_{r^4} + x_{r^5} - x_h - x_{rh} - x_{r^2h} - x_{r^3h} - x_{r^4h} - x_{r^5h}\\
< x, \gamma_+ > &= x_1 - x_r + x_{r^2} - x_{r^3} + x_{r^4} - x_{r^5} + x_h - x_{rh} + x_{r^2h} - x_{r^3h} + x_{r^4h} - x_{r^5h}\\
< x, \gamma_- > &= x_1 - x_r + x_{r^2} - x_{r^3} + x_{r^4} - x_{r^5} - x_h + x_{rh} - x_{r^2h} + x_{r^3h} - x_{r^4h} + x_{r^5h};
\end{aligned}$$

and two simple modules in dimension of 2. The matrix entries of $< x, \beta_1 >$ are:

$$< x,\beta_1 >_{1,1} = \frac{1}{2}\,(2x_1 + x_r - x_{r^2} - 2x_{r^3} - x_{r^4} + x_{r^5} + 2x_h + x_{rh} - x_{r^2h} - 2x_{r^3h} - x_{r^4h} + x_{r^5h})$$

$$< x,\beta_1 >_{2,1} = \frac{1}{2}\sqrt{3}\,(-x_r - x_{r^2} + x_{r^4} + x_{r^5} + x_{rh} + x_{r^2h} - x_{r^4h} - x_{r^5h})$$

$$< x,\beta_1 >_{1,2} = \frac{1}{2}\sqrt{3}\,(x_r + x_{r^2} - x_{r^4} - x_{r^5} + x_{rh} + x_{r^2h} - x_{r^4h} - x_{r^5h})$$

$$< x,\beta_1 >_{2,2} = \frac{1}{2}\,(2x_1 + x_r - x_{r^2} - 2x_{r^3} - x_{r^4} + x_{r^5} - 2x_h - x_{rh} + x_{r^2h} + 2x_{r^3h} + x_{r^4h} - x_{r^5h})\,,$$

whereas the matrix entries of $< x,\beta_2 >$ are given by

$$< x,\beta_2 >_{1,1} = \frac{1}{2}\,(2x_1 - x_r - x_{r^2} + 2x_{r^3} - x_{r^4} - x_{r^5} + 2x_h - x_{rh} - x_{r^2h} + 2x_{r^3h} - x_{r^4h} - x_{r^5h})$$

$$< x,\beta_2 >_{2,1} = \frac{1}{2}\sqrt{3}\,(-x_r + x_{r^2} - x_{r^4} + x_{r^5} + x_{rh} - x_{r^2h} + x_{r^4h} - x_{r^5h})$$

$$< x,\beta_2 >_{1,2} = \frac{1}{2}\sqrt{3}\,(x_r - x_{r^2} + x_{r^4} - x_{r^5} + x_{rh} - x_{r^2h} + x_{r^4h} - x_{r^5h})$$

$$< x,\beta_2 >_{2,2} = \frac{1}{2}\,(2x_1 - x_r - x_{r^2} + 2x_{r^3} - x_{r^4} - x_{r^5} - 2x_h + x_{rh} + x_{r^2h} - 2x_{r^3h} + x_{r^4h} + x_{r^5h})\,.$$

2.5 Class Functions

A point $x \in \mathbb{C}D_n$ that is constant on the components of a dihedral conjugacy orbit is called a dihedral *class function*. More precisely, x is such that $x_{\tau\sigma\tau^{-1}} = x_\sigma$, for all $\sigma, \tau \in D_n$.

Proposition 2.8. *If $x \in \mathbb{C}D_n$ is a class function then the dihedral linearizations $< x,\rho >$ commute with ρ_τ for all $\tau \in D_n$.*

Proof. In fact,

$$\rho_\tau < x,\rho > \rho_{\tau^{-1}} = < x,\rho_\tau\rho\rho_{\tau^{-1}} > = \sum_\sigma x_\sigma \rho_{\tau\sigma\tau^{-1}} = \sum_\sigma x_{\tau\sigma\tau^{-1}}\rho_{\tau\sigma\tau^{-1}} = < x,\rho >,$$

completing the proof. □

Definition 2.3 (Dihedral characters). The character of $\xi \in \widehat{D}_n$ is the point $\chi^\xi = \mathrm{tr}\,\xi = \sum_\tau (\mathrm{tr}\,\xi_\tau)\tau \in \mathbb{C}D_n$.

Therefore, given $\xi, \eta \in \widehat{D}_n$, and since χ^ξ is a class function, Schur's Lemma implies that

$$< \chi^\xi, \eta > = \lambda I_{n_\eta},$$

so that taking the trace in each side of the equality and solving for λ we obtain

$$< \chi^{\xi}, \eta >= \frac{1}{n_\eta} < \chi^{\xi}, \chi^{\eta} > I_{n_\eta}. \tag{2.10}$$

Clearly, the dihedral characters are simply

$$\chi^{\xi} = \xi, \quad \text{if } n_\xi = 1$$

or else, when $\xi = \beta^k$,

$$\chi^k_{j,d} = \operatorname{tr} \beta^k_{j,d} = (1+d)\cos\frac{2\pi jk}{n}, \ \ k = 1, \ldots, m.$$

It immediately follows that

Proposition 2.9 (Orthogonality of dihedral characters). *For all χ, η in $\widehat{D}_n$ we have*

$$\frac{1}{2n}\sum_{\tau} \chi^{\xi}_{\tau}\chi^{\eta}_{\tau} = \delta_{\chi,\eta},$$

and, moreover,

$$\frac{1}{2n}\sum_{\xi} \chi^{\xi}_{1}\chi^{\xi}_{\tau} = \begin{cases} \sum_{\xi} \frac{n_\xi^2}{2n} = 1, & \text{if } \tau = 1, \\ 0, & \text{if } \tau \neq 1. \end{cases}$$

2.6 Dihedral Projections

Define, for $\xi \in \widehat{D}_n$,

$$\pi_\xi = \frac{n_\xi}{2n}\chi^{\xi} \in \mathbb{C}D_n.$$

Proposition 2.10. *For all $\xi, \eta \in \widehat{D}_n$, the following properties hold:*

1. $\pi_\xi^2 = \pi_\xi$ *(projection);*
2. $\pi_\xi \pi_\eta = 0, \ \ \eta \neq \xi$ *(algebraic orthogonal);*
3. $\sum_\xi \pi_\xi = 1$ *(partition of unity).*

Proof. To verify the above properties we recall that, for $x, y \in \mathbb{C}D_n$,

$$x\,y = \sum_{\tau,\sigma} x_\tau y_\sigma \tau\sigma = \sum_{\tau}\left(\sum_{\sigma} x_\sigma y_{\sigma^{-1}\tau}\right)\tau = \sum_{\tau}(x * y)_\tau \tau = x * y,$$

as introduced earlier on page 14. In each case, it is then sufficient to evaluate the convolution components $\sum_\sigma x_\sigma y_{\sigma^{-1}\tau}$. *With the semi-direct product (2.4) notation*

$$(j,d) \rtimes (j',d') = (j + dj' \mod n,\ dd')$$

in mind, we identify $(j,d)_\xi \equiv \pi_\tau^\xi$ *and write*

- $(j,d)_1 = 1/2n$;
- $(j,d)_\alpha = d/2n$;
- $(j,d)_{\gamma_+} = (-1)^j/2n$, *for n even;*
- $(j,d)_{\gamma_-} = d(-1)^j/2n$, *for n even;*
- $(j,d)_{\beta^k} = 2Cos\left[\frac{2jk\pi}{n}\right]/n$; *if* $d = 1$, *and* $(j,d)_{\beta^k} = 0$, *if* $d = -1$; $k = 1,\ldots m$.

Therefore

$$\begin{aligned} x_\sigma y_{\sigma^{-1}\tau} &= (j,d)_x[(j,d)_y^{-1} \rtimes (j',d')_y] = (j,d)_x[(-j/d,d)_y \rtimes (j',d')_y] \\ &= (j,d)_x(-j/d + dj' \mod n, dd')_y, \end{aligned}$$

and

$$\sum_\sigma x_\sigma y_{\sigma^{-1}\tau} = \sum_{j,d} (j,d)_x(-j/d + dj' \mod n, dd')_y \tag{2.11}$$

then gives the $\tau = (j',d')$ *component of* $x * y$. *The proof of the three properties follows from directly evaluating (2.11) in each of the cases. For the projection property we have:*

$$(j',d')_{\pi_1^2} = \sum_{j,d} (j,d)_1(-j/d + dj' \mod n, dd')_1 = \sum_{j,d} \frac{1}{2n}\frac{1}{2n} = \frac{1}{2n} = (j',d')_{\pi_1},$$

for all (j',d'), *that is,* $\pi_1^2 = \pi_1$. *Similarly,*

$$\begin{aligned} (j',d')_{\pi_\alpha^2} &= \sum_{j,d} (j,d)_\alpha(-j/d + dj' \mod n, dd')_\alpha \\ &= \sum_{j,d} \frac{d}{2n}\frac{dd'}{2n} = \sum_{j,d} \frac{d'}{4n^2} = \frac{d'}{2n} = (j',d')_{\pi_\alpha}, \end{aligned}$$

for all (j',d'), *that is,* $\pi_\alpha^2 = \pi_\alpha$;

$$\begin{aligned} (j',d')_{\pi_{\gamma_+}^2} &= \sum_{j,d} (j,d)_{\gamma_+}(-j/d + dj' \mod n, dd')_{\gamma_+} \\ &= \sum_{j,d} \frac{(-1)^j}{2n}\frac{(-1)^{j/d+dj'}}{2n} \\ &= \frac{1}{4n^2}\left[\sum_j (-1)^{j'} + \sum_j (-1)^{2j-j'}\right] \end{aligned}$$

$$= \frac{1}{4n^2}[n(-1)^{j'} + n(-1)^{-j' \mod n}]$$
$$= \frac{2n(-1)^{j'}}{2n^2} = \frac{(-1)^{j'}}{2n} = (j',d')_{\pi_{\gamma_+}};$$

for all (j',d')*, that is,* $\pi^2_{\gamma_+} = \pi_{\gamma_+}$*;*

$$(j',d')_{\pi^2_{\gamma_-}} = \sum_{j,d}(j,d)_{\gamma_-}(-j/d + dj' \mod n, dd')_{\gamma_-}$$
$$= \sum_{j,d}\frac{d(-1)^j}{2n}\frac{dd'(-1)^{j/d+dj'}}{2n}$$
$$= d'\sum_{j,d}\frac{(-1)^j}{2n}\frac{(-1)^{j/d+dj'}}{2n} = \frac{d'(-1)^{j'}}{2n} = (j',d')_{\pi_{\gamma_-}};$$

for all (j',d')*, that is,* $\pi^2_{\gamma_-} = \pi_{\gamma_-}$*, and similarly, noting that* $(j,-1)_{\pi_{\beta^k}} = 0$ *for all* $j = 0,\ldots,n-1$*,*

$$(j',d')_{\pi^2_{\beta^k}} = \sum_j (j,1)_{\beta^k}(-j + j' \mod n, 1)_{\beta^k}$$
$$= \sum_j \frac{4}{n^2} Cos\left[\frac{2jk\pi}{n}\right] Cos\left[\frac{2(j-j')k\pi}{n}\right]$$
$$= \frac{2}{n} Cos\left[\frac{2j'k\pi}{n}\right] = (j',1)_{\pi_{\beta^k}},$$

and $(j',d')_{\pi^2_{\beta^k}} = 0$ *if* $d' = 0$*, so that* $(j',d')_{\pi^2_{\beta^k}} = (j',d')_{\pi_{\beta^k}}$ *for all* j',d'*. The derivations proving the orthogonality property are similar and are left as an exercise. To prove the partition of unit property* $\sum_\xi \pi_\xi$ *we first assume that* n *is odd. Then, if* $(j,d) = (0,1)$*, we have:*

$$(0,1)_1 + (0,1)_\alpha + \sum_{k=1}^{m}(0,1)_{\beta^k} = \frac{1}{2n} + \frac{1}{2n} + \frac{n-1}{n} = 1,$$

that is $(\sum_\xi \pi_\xi)_1 = 1$*. If* $j > 1$ *and* $d = 1$ *we have,*

$$(j,1)_1 + (j,1)_\alpha + \sum_{k=1}^{m}(j,1)_{\beta^k} = \frac{2}{2n} - \frac{1}{n} = 0,$$

whereas if $j > 1$ *and* $d = -1$ *we have,*

$$(j,-1)_1 + (j,-1)_\alpha + \sum_{k=1}^{m}(j,-1)_{\beta^k} = \frac{1}{2n} - \frac{1}{2n} + 0 = 0,$$

that is, $(\sum_\xi \pi_\xi)_j = 0$*, if* $j \neq 1$*, and hence* $\sum_\xi \pi_\xi = 1$*. If n is even, we have the additional terms*

$$(j,d)_{\gamma_+} + (j,d)_{\gamma_-} = \begin{cases} \frac{2}{2n},\ \textit{if}\ (j,d) = (0,1); \\ \frac{2}{2n}(-1)^j,\ \textit{if}\ j > 1,\ d = 1; \\ 0\ \textit{if}\ j > 1,\ d = -1, \end{cases}$$

whereas, for n even,

$$\sum_{k=1}^{m} (j,1)_{\beta^k} = \begin{cases} \frac{n-2}{n}\ \textit{if}\ j = 0; \\ -\frac{2}{n}\ \textit{if}\ j > 1\ \textit{is even}\ ; \\ 0\ \textit{if}\ j > 1\ \textit{is odd}\ . \end{cases}$$

Therefore, if $(j,d) = (0,1)$*, we have:*

$$\begin{aligned} \sum_\xi (0,1)_\xi &= (0,1)_1 + (0,1)_\alpha + (j,d)_{\gamma_+} + (j,d)_{\gamma_-} + \sum_{k=1}^{m} (0,1)_{\beta^k} \\ &= \frac{4}{2n} + \frac{n-2}{n} = 1, \end{aligned}$$

so that $(\sum_\xi \pi_\xi)_1 = 1$*; If* $j > 1$ *is even, we have*

$$\sum_\xi (j,1)_\xi = \frac{4}{2n} - \frac{2}{n} = 0;$$

whereas if $j > 1$ *is odd,*

$$\sum_\xi (j,1)_\xi = \frac{2}{2n} - \frac{2}{2n} = 0.$$

Therefore, $(\sum_\xi \pi_\xi)_j = 0$ *for all* $j > 1$ *and* $d = 1$*. Finally, if* $d = -1$*,*

$$\sum_\xi (j,-1)_\xi = \frac{1}{2n} - \frac{1}{2n} + \frac{(-1)^j}{2n} - \frac{(-1)^j}{2n} = 0,$$

and hence $\sum_\xi \pi_\xi = 1$*, concluding the proof.* □

Proposition 2.11 (Canonical Projections). *Let* $\mathscr{P}_\xi =< \pi_\xi, \phi >$*, where* ϕ *is the dihedral* (D_n) *regular homomorphism. Then, for all* $\xi, \eta \in \widehat{D}_n$*, we have:*

1. $\mathscr{P}_\xi^2 = \mathscr{P}_\xi$*;*
2. $\mathscr{P}_\xi \mathscr{P}_\eta = 0,\ \xi \neq \eta$*;*
3. $\sum_\xi \mathscr{P}_\xi = 1$.

Proof. Equalities 1 and 2 follow from equality 4 in Proposition 2.1 on page 15 and equalities 1 and 2 of Proposition 2.10. Equality 3 follows from equality 1 in Proposition 2.1 on page 15 and equality 3 in Proposition 2.10. □

Proposition 2.11 gives a decomposition of the identity element in $GL_m(\mathbb{C})$ into an algebraically orthogonal sum of projection matrices that decompose the identity matrix of the corresponding dimension. The many applications and interpretations of the canonical projections decomposition are presented in detail in [2].

Proposition 2.12. *The (algebra) homomorphism*

$$\varphi : x \in \mathbb{C}D_n \mapsto \bigoplus_{\xi} < x, \xi > \in \prod_{\xi} M_{n_\xi}(\mathbb{C})$$

in an isomorphism.

Proof. First note that $\varphi(1) = \bigoplus_\xi < 1, \xi > = \bigoplus_\xi \xi_1 = \bigoplus_\xi I_{n_\xi}$. Suppose that $\varphi(x) = \bigoplus_\xi I_{n_\xi}$ for some non-null $x \in \mathbb{C}D_n$. Then $< x, \xi > = I_{n_\xi}$ for all $\xi \in \widehat{D}_n$, so that, from Proposition 2.3 on page 17,

$$< \tau x, \xi > = \xi_\tau < x, \xi > = \xi_\tau I_{n_\xi} = \xi_\tau,$$

so that

$$\frac{n_\xi}{2n} < \tau x, \xi > = \frac{n_\xi}{2n} \xi_\tau.$$

Taking the trace on both sides, we have,

$$< \tau x, \pi^\xi > = \frac{n_\xi}{2n} \chi_\tau^\xi = \frac{1}{2n} \chi_1^\xi \chi_\tau^\xi.$$

Summing over $\widehat{D}_n$ we obtain, from Proposition 2.9 on page 21,

$$\sum_\xi < \tau x, \pi^\xi > = < \tau x, \sum_\xi \pi^\xi > = \frac{1}{2n} \sum_\xi \chi_1^\xi \chi_\tau^\xi = \begin{cases} \sum_\xi \frac{n_\xi^2}{2n} = 1, & \text{if } \tau = 1 \\ 0, & \text{if } \tau \neq 1. \end{cases}$$

From Proposition 2.10 we know that $\sum_\xi \pi^\xi = 1$, so that then $< \tau x, 1 > = \delta_{\tau 1}$, or $x = 1$, concluding the proof. □

Proposition 2.13 (Inversion Formula).

$$x_\tau = \sum_\xi \frac{n_\xi}{2n} tr\,[\xi_\tau < x, \xi >].$$

Proof. From Proposition 2.3 on page 17, we have

$$\frac{n_\xi}{2n} < \tau x, \xi > = \frac{n_\xi}{2n} \xi_\tau < x, \xi >,$$

so that, taking the trace on both sides,

$$< \tau x, \pi^{\xi} >= \frac{n_{\xi}}{2n} \mathrm{tr}\, [\xi_{\tau} < x, \xi >],$$

summing over $\widehat{D}_n$, and applying Proposition 2.10, gives

$$< \tau x, 1 >= \sum_{\xi} \frac{n_{\xi}}{2n} \mathrm{tr}\, [\xi_{\tau} < x, \xi >],$$

or

$$x_{\tau} = \sum_{\xi} \frac{n_{\xi}}{2n} \mathrm{tr}\, [\xi_{\tau} < x, \xi >],$$

which is the inversion formula. □

2.7 Fourier Bases

In data analytical applications it is often useful to have a $\mathbb{C}^{2n}$ interpretation of Proposition 2.12, in a way that the algebra isomorphism and the resulting inversion formula appear in terms of a non-singular matrix transformation. To illustrate, consider the $\mathbb{C}D_4$ decomposition, and write

$$\mathscr{X} = \begin{bmatrix} < x, 1 > \\ < x, \alpha > \\ < x, \gamma_{+} > \\ < x, \gamma_{-} > \\ < x, \beta >_{11} \\ < x, \beta >_{21} \\ < x, \beta >_{12} \\ < x, \beta >_{22} \end{bmatrix} \in \mathbb{C}^8.$$

The Fourier basis for this space is defined as the normalized rows of the matrix F satisfying

$$\mathscr{X} = Fx,$$

with normalizing (row) constants $\sqrt{n_{\xi}/2n}$. In the present example, the constants are, respectively, $\sqrt{2}/4$ for the representations in dimension of one and $1/2$ for the representation in dimension of two. The matrix F is shown in (2.12), where the horizontal line separates the rows corresponding to the one-dimensional representations from the rows associated with (the columns of) the two-dimensional representation β.

$$F = \left[\begin{array}{cccc|cccc} 1 & 1 & 1 & 1 & 1 & 1 & 1 & 1 \\ 1 & 1 & 1 & 1 & -1 & -1 & -1 & -1 \\ 1 & -1 & 1 & -1 & 1 & -1 & 1 & -1 \\ 1 & -1 & 1 & -1 & -1 & 1 & -1 & 1 \\ \hline 1 & 0 & -1 & 0 & 1 & 0 & -1 & 0 \\ 0 & 1 & 0 & -1 & 0 & 1 & 0 & -1 \\ 0 & -1 & 0 & 1 & 0 & 1 & 0 & -1 \\ 1 & 0 & -1 & 0 & -1 & 0 & 1 & 0 \end{array}\right]. \tag{2.12}$$

In general, we have

$$(\mathscr{F}x)_\xi = \sqrt{\frac{2n}{n_\xi}} < x, \xi >, \quad \xi \in \widehat{D}_n, \tag{2.13}$$

where $(\mathscr{F}x)_\xi$ indicates the partition of $\mathscr{F}x$ corresponding to $\xi \in \widehat{D}_n$, with the understanding that here $< x, \xi >$ is written as a $n_\xi \times 1$ vector with components given by the columns of $< x, \xi >$.

In the D_4 case above, we adjoined 4 blocks in dimension of 1×8 and one block in dimension of $2^2 \times 8$. If $\mathscr{F}$ is the normalized (hence orthogonal) version of F given by (2.12) and ϕ the (left) regular representation of D_4 then direct calculation shows that

$$\mathscr{F}\phi\mathscr{F}' = \text{Diag}\,(1, \alpha, \gamma_+, \gamma_-, I_2 \otimes \beta), \tag{2.14}$$

and, in general, we have:

Proposition 2.14. *If $\mathscr{F}$ indicates the D_n Fourier basis and ϕ the corresponding (left) regular representation, then*

$$\mathscr{F}\phi_\sigma\mathscr{F}' = Diag\,(\ldots, I_{n_\xi} \otimes \xi_\sigma, \ldots)_{\xi \in \widehat{D}_n}.$$

Proof. The columns of $\mathscr{F}\phi_\sigma$ when ϕ is the left regular representation are given by $\{\sigma\tau : \tau \in D_n\}$. Moreover, any row of $\mathscr{F}\phi$ associated with $\xi \in \widehat{D}_n$ is given by $\sqrt{n_\xi/g}\{\xi^{if}_{\sigma\tau} : \tau \in D_n\}$ for some $i, f = 1, \ldots n_\xi$, and a column of $\mathscr{F}'$ is a row of $\mathscr{F}$, or $\sqrt{n_\eta/g}\{\eta^{jk}_\tau : \tau \in D_n\}$, for some $\eta \in \widehat{D}_n$, and $j, k = 1, \ldots, n_\eta$, and if ξ or η are in dimension of one we make $i = f$ or $j = k$, respectively. Therefore, the ξ, η (block) entry of $\mathscr{F}\phi_\sigma\mathscr{F}'$ is given by

$$(\mathscr{F}\phi_\sigma\mathscr{F}')_{if,jk} = \frac{\sqrt{n_\xi n_\eta}}{g} \sum_\tau \xi^{if}_{\sigma\tau}\eta^{jk}_\tau,$$

whereas, writing $\xi^{if}_{\sigma\tau} = \sum_{\ell=1}^{n_\xi} \xi^{i\ell}_\sigma \xi^{\ell f}_\tau$, we obtain

$$(\mathscr{F}\phi_\sigma\mathscr{F}')_{if,jk} = \frac{\sqrt{n_\xi n_\eta}}{g} \sum_{\ell=1}^{n_\xi} \xi^{i\ell}_\sigma \sum_\tau \xi^{\ell f}_\tau \eta^{jk}_\tau = 0$$

when $\xi \neq \eta$ e.g., [4], [2, p.81]. If $\eta = \xi$, then, recalling that $\xi_\tau^{jk} = \xi_{\tau^{-1}}^{kj}$,

$$(\mathscr{F}\phi_\sigma\mathscr{F}')_{if,jk} = \frac{n_\xi}{g}\sum_{\ell=1}^{n_\xi}\xi_\sigma^{i\ell}\sum_\tau \xi_\tau^{\ell f}\xi_{\tau^{-1}}^{kj} = \frac{n_\xi}{g}\sum_{\ell=1}^{n_\xi}\xi_\sigma^{i\ell}\frac{g}{n_\xi}\delta_{\ell j}\delta_{fk} = 0$$

if $\ell \neq j$ or $f \neq k$. Otherwise, when $\ell = j$ and $f = k$, the ξ,ξ (block) entry of $\mathscr{F}\phi_\sigma\mathscr{F}'$ is

$$(\mathscr{F}\phi_\sigma\mathscr{F}')_{ik,jk} = \xi_\sigma^{ij},$$

when $k = 1,\ldots,n_\xi$, thus giving n_ξ copies of ξ_σ. Arranging the rows of $\mathscr{F}$ that correspond to ξ according to $11,\ldots,n_\xi 1,\ldots 1n_\xi,\ldots,n_\xi n_\xi$ expresses the ξ,ξ entry of $\mathscr{F}\phi_\sigma\mathscr{F}'$ as $I_{n_\xi}\otimes\xi_\sigma$, so that, together, $\mathscr{F}\phi_\sigma\mathscr{F}'$ is a block diagonal matrix with the diagonal components given by $I_{n_\xi}\otimes\xi_\sigma$ for the distinct $\xi \in \widehat{D}_n$, concluding the proof. □

Proposition 2.15. *If $\mathscr{F}$ indicates the Fourier basis of D_n and $\mathscr{P}_\xi$ it the left regular canonical projection associated with $\xi \in \widehat{D}_n$, then*

$$\mathscr{F}\mathscr{P}_\xi\mathscr{F}' = Diag\,(0,\ldots,I_{n_\xi}\otimes I_{n_\xi},\ldots,0).$$

Proof. Evaluation of the regular canonical projection for $\xi \in \widehat{D}_n$ using Propositions 2.14 on the preceding page and 2.9 on page 21, and the equality in (2.10), gives

$$\begin{aligned}\mathscr{F}\mathscr{P}_\xi\mathscr{F}' &= \frac{n_\xi}{2n}\sum_{\tau\in D_n}\chi_\tau^\xi\mathscr{F}\phi_\tau\mathscr{F}' = \frac{n_\xi}{2n}I_{n_\xi}\otimes\sum_{\tau\in D_n}\chi_\tau^\xi\xi_\tau \\ &= \frac{n_\xi}{2n}I_{n_\xi}\otimes<\chi^\xi,\xi> = \frac{n_\xi}{2n}I_{n_\xi}\otimes\frac{2n}{n_\xi}I_{n_\xi} = I_{n_\xi}\otimes I_{n_\xi}.\end{aligned}$$

As a consequence, considering (2.13), we obtain the analysis of variance of x in terms of its spectral decomposition;

Corollary 2.1 (Parseval's Equality). *If $x \in \mathbb{C}^{2n}$ then*

$$||x||^2 = \sum_{\xi\in\widehat{D}_n}\frac{n_\xi}{2n}||<x,\xi>||^2.$$

Example 2.8. Consider the following two points x,y in $\mathbb{C}D_4$,

$$\left(\begin{array}{r|cc} \tau & x & y \\ \hline 1 & 1 & 5 \\ r & 2 & 1 \\ r^2 & 1 & 4 \\ r^3 & 1 & 3 \\ h & 5 & 3 \\ rh & 10 & 4 \\ r^2h & 4 & 1 \\ r^3h & 5 & 5 \end{array}\right).$$

From Example 2.6 on page 19, we have,

$$< x,1 >= 29,\ < y,1 >= 26;$$

$$< x,\alpha >= -19,\ < y,\alpha >= 0;$$
$$< x,\gamma_+ >= -7,\ < y,\gamma_+ >= 0;$$
$$< x,\gamma_- >= -5,\ < y,\gamma_- >= 10;$$
$$< x,\beta >= \begin{pmatrix} 1 & 4 \\ 6 & -1 \end{pmatrix},\ < y,\beta >= \begin{pmatrix} 3 & 1 \\ -3 & -1 \end{pmatrix}.$$

Then,

$$x \cdot x = ||x||^2 = \sum_\tau x_\tau^2 = 173,$$

whereas, equally,

$$\sum_{\xi \in \widehat{D}_n} \frac{n_\xi}{2n} || < x,\xi > ||^2 = \frac{1}{8}(29^2 + 19^2 + 7^2 + 5^2) + \frac{2}{8}(1^2 + 4^2 + 6^2 + 1^2) = 173.$$

Moreover,

$$x \cdot y = \sum_\tau x_\tau y_\tau = 98 = \sum_{\xi \in \widehat{D}_n} \frac{n_\xi}{2n} < x,\xi >< y,\xi >,$$

with the understanding that when ξ is of dimension greater than one ξ the products of the two transforms should read as the (Hadamard) inner product $< x,\xi > \cdot < y,\xi >$ two matrices.

More generally, then, Corollary 2.1 read as:

Corollary 2.2. *If $x, y \in \mathbb{C}^G$ then*

$$x \cdot y = \sum_{\xi \in \widehat{D}_n} \frac{n_\rho}{2n} < x,\xi >< y,\xi > .$$

Example 2.9. Given two points

$$x = x_0 + x_1\omega + x_2\omega^2, \quad y = y_0 + y_1\omega + y_2\omega^2$$

in the group algebra of $\mathbb{C}^3$, then

$$< x, \xi_1 > = x_0 + x_1 + x_2, \quad < x, \xi_2 > = x_0 + x_1\omega + x_2\omega^2, \quad < x, \xi_3 > = x_0 + x_1\omega^2 + x_2\omega$$

are the Fourier transforms of x, and similarly for y. Direct calculation then shows that

$$x \cdot y = \sum_{\tau} x_\tau \bar{y}_\tau = \frac{1}{3}\sum_{j=1}^{3} < x, \xi_j > \overline{< y, \xi_j >}.$$

It is understood that in Corollaries 2.1 and 2.2 the inner products are Hermitian products.

2.8 The Center of $\mathbb{C}D_n$

The center of D_n is the subset of D_n whose elements commute with all points in D_n. We write Cent. D_n to indicate the dihedral center. By linearity, the definition extends to $\mathbb{C}D_n$ and all dihedral linearizations, and clearly Cent. D_n = Cent. $\mathbb{C}D_n$. The reader can check that Cent. D_n is an associative algebra. $\mathbb{C}D_n$ is also called the enveloping algebra of D_n [3, p.79].

Example 2.10 (A basis for the center of the regular linearization of D_3). The reader can verify, using the definition of conjugacy classes, that a basis for the center of the D_3 regular linearization algebra, see page 15,

$$\{< x, \phi >; x \in \mathbb{C}D_3\},$$

where ϕ is the (left) regular representation of D_3, is given by the identity I, and the matrices

$$C_1 = \begin{bmatrix} 0&1&1&0&0&0 \\ 1&0&1&0&0&0 \\ 1&1&0&0&0&0 \\ 0&0&0&0&1&1 \\ 0&0&0&1&0&1 \\ 0&0&0&1&1&0 \end{bmatrix}, \quad C_2 = \begin{bmatrix} 0&0&0&1&1&1 \\ 0&0&0&1&1&1 \\ 0&0&0&1&1&1 \\ 1&1&1&0&0&0 \\ 1&1&1&0&0&0 \\ 1&1&1&0&0&0 \end{bmatrix},$$

so that the matrix elements in the center of the regular linearization have the form

$$C = aI + bC_1 + cC_2 = \begin{bmatrix} a & b & b & c & c & c \\ b & a & b & c & c & c \\ b & b & a & c & c & c \\ c & c & c & a & b & b \\ c & c & c & b & a & b \\ c & c & c & b & b & a \end{bmatrix}.$$

Similar argument shows that the canonical projections $\mathscr{P}_1, \mathscr{P}_\alpha, \mathscr{P}_\beta$ for the regular representation of D_3 also form a basis for the center of the regular linearization algebra, with the advantage of being (algebraically) orthogonal. For example, since C is in the center of the algebra, we must have

$$C = \ell_1 \mathscr{P}_1 + \ell_\alpha \mathscr{P}_\alpha + \ell_\beta \mathscr{P}_\beta,$$

so that then

$$C\mathscr{P}_1 = \ell_1 \mathscr{P}_1, \quad C\mathscr{P}_\alpha = \ell_\alpha \mathscr{P}_\alpha, \quad C\mathscr{P}_\beta = \ell_\beta \mathscr{P}_\beta. \tag{2.15}$$

Taking the trace on both sides, we have

$$\ell_1 = \frac{\text{tr}\, C\mathscr{P}_1}{\text{tr}\, \mathscr{P}_1} = a + 2b + 3c, \ \ell_\alpha = \frac{\text{tr}\, C\mathscr{P}_\alpha}{\text{tr}\, \mathscr{P}_\alpha} = a + 2b - 3c, \ \ell_\beta = \frac{\text{tr}\, C\mathscr{P}_\beta}{\text{tr}\, \mathscr{P}_\beta} = a - b. \tag{2.16}$$

The reader may also verify that the characterization of the matrix elements in the center of the regular linearization algebra of D_3 can be obtained by taking an arbitrary matrix

$$H = < a, \phi > = \begin{bmatrix} a & b & c & \alpha & \beta & \gamma \\ c & a & b & \gamma & \alpha & \beta \\ b & c & a & \beta & \gamma & \alpha \\ \alpha & \gamma & \beta & a & c & b \\ \beta & \alpha & \gamma & b & a & c \\ \gamma & \beta & \alpha & c & b & a \end{bmatrix},$$

in the algebra and centralizing it

$$C \simeq \sum_{\tau \in G} \phi_\tau H \phi'_\tau.$$

The matrices C in the center of the regular linearization algebra transform according to

$$\mathscr{F} C \mathscr{F}^{-1} = \mathscr{C} = \text{Diag}\,(\ell_1, \ell_\alpha, \ell_\beta I_4). \tag{2.17}$$

2.9 Group Rings

The following definitions are relevant to the analysis of data indexed by symmetries.

Definition 2.4. Given a ring R and a group G, the set

$$RG = \left\{ \sum_{\tau} r_\tau \tau, \;\; r_\tau \in R, \tau \in G \right\}$$

of all finite formal R-linear combinations of elements of G, together with the operations of addition (component-wise) and multiplication (induced by the group multiplication), is called the group ring of G over R.

Example 2.11 (Visual fields). The matrix

$$F = \begin{bmatrix} 0 & 0 & 0 & 26 & 27 & 24 & 21 & 0 & 0 & 0 \\ 0 & 0 & 23 & 23 & 26 & 28 & 25 & 22 & 0 & 0 \\ 0 & 27 & 29 & 27 & 27 & 28 & 29 & 29 & 28 & 0 \\ 28 & 29 & 29 & 29 & 31 & 20 & 20 & 28 & 28 & 29 \\ 26 & 26 & 29 & 30 & 33 & 34 & 28 & 27 & 28 & 27 \\ 28 & 30 & 30 & 31 & 32 & 33 & 33 & 4 & 27 & 28 \\ 27 & 29 & 31 & 31 & 32 & 32 & 30 & 29 & 28 & 27 \\ 0 & 30 & 31 & 31 & 28 & 29 & 32 & 30 & 30 & 0 \\ 0 & 0 & 28 & 32 & 29 & 28 & 29 & 28 & 0 & 0 \\ 0 & 0 & 0 & 26 & 27 & 28 & 29 & 0 & 0 & 0 \end{bmatrix}$$

describes the output of an automated perimetry test used in the assessment of the visual field. The entries represent the sensitivity of the retina in detecting the light stimulus and is expressed in decibel units, with a maximal possible reading of 50db. A 50db target is the dimmest target the instrument can project. The smaller the reading the lower the sensitivity at that retinal location given by reference to the rows and columns of the matrix.

The set of matrices

$$\{F_1, F_r, F_{r^2}, F_{r^3}, F_h, F_{rh}, F_{r^2h}, F_{r^3h}\}$$

shown below give a dihedral (D_4) orbit on the visual field and each matrix field is a point in the ring of the 10×10 matrices over the reals, indexed by D_4, so that the formal sums

$$\sum_{\tau \in D_4} F_\tau \tau,$$

gives an example of a point in the group ring of D_4 over the ring of the real 10×10 matrices. Each one of the following matrices is obtained from F by applying the corresponding planar (counterclockwise) rotations and reversals to its row-column

indices, in the natural way, with the x (y) axis placed between rows (columns) 5 and 6.

$$F_1 = \begin{bmatrix} 0 & 0 & 0 & 26 & 27 & 24 & 21 & 0 & 0 & 0 \\ 0 & 0 & 23 & 23 & 26 & 28 & 25 & 22 & 0 & 0 \\ 0 & 27 & 29 & 27 & 27 & 28 & 29 & 29 & 28 & 0 \\ 28 & 29 & 29 & 29 & 31 & 20 & 20 & 28 & 28 & 29 \\ 26 & 26 & 29 & 30 & 33 & 34 & 28 & 27 & 28 & 27 \\ 28 & 30 & 30 & 31 & 32 & 33 & 33 & 4 & 27 & 28 \\ 27 & 29 & 31 & 31 & 32 & 32 & 30 & 29 & 28 & 27 \\ 0 & 30 & 31 & 31 & 28 & 29 & 32 & 30 & 30 & 0 \\ 0 & 0 & 28 & 32 & 29 & 28 & 29 & 28 & 0 & 0 \\ 0 & 0 & 0 & 26 & 27 & 28 & 29 & 0 & 0 & 0 \end{bmatrix}, \quad F_r = \begin{bmatrix} 0 & 0 & 0 & 26 & 27 & 24 & 21 & 0 & 0 & 0 \\ 0 & 0 & 23 & 23 & 26 & 28 & 25 & 22 & 0 & 0 \\ 0 & 27 & 29 & 27 & 27 & 28 & 29 & 29 & 28 & 0 \\ 28 & 29 & 29 & 29 & 31 & 20 & 20 & 28 & 28 & 29 \\ 26 & 26 & 29 & 30 & 33 & 34 & 28 & 27 & 28 & 27 \\ 28 & 30 & 30 & 31 & 32 & 33 & 33 & 4 & 27 & 28 \\ 27 & 29 & 31 & 31 & 32 & 32 & 30 & 29 & 28 & 27 \\ 0 & 30 & 31 & 31 & 28 & 29 & 32 & 30 & 30 & 0 \\ 0 & 0 & 28 & 32 & 29 & 28 & 29 & 28 & 0 & 0 \\ 0 & 0 & 0 & 26 & 27 & 28 & 29 & 0 & 0 & 0 \end{bmatrix}$$

$$F_{r^2} = \begin{bmatrix} 0 & 0 & 0 & 29 & 28 & 27 & 26 & 0 & 0 & 0 \\ 0 & 0 & 28 & 29 & 28 & 29 & 32 & 28 & 0 & 0 \\ 0 & 30 & 30 & 32 & 29 & 28 & 31 & 31 & 30 & 0 \\ 27 & 28 & 29 & 30 & 32 & 32 & 31 & 31 & 29 & 27 \\ 28 & 27 & 4 & 33 & 33 & 32 & 31 & 30 & 30 & 28 \\ 27 & 28 & 27 & 28 & 34 & 33 & 30 & 29 & 26 & 26 \\ 29 & 28 & 28 & 20 & 20 & 31 & 29 & 29 & 29 & 28 \\ 0 & 28 & 29 & 29 & 28 & 27 & 27 & 29 & 27 & 0 \\ 0 & 0 & 22 & 25 & 28 & 26 & 23 & 23 & 0 & 0 \\ 0 & 0 & 0 & 21 & 24 & 27 & 26 & 0 & 0 & 0 \end{bmatrix}, \quad F_{r^3} = \begin{bmatrix} 0 & 0 & 0 & 29 & 27 & 28 & 27 & 0 & 0 & 0 \\ 0 & 0 & 28 & 28 & 28 & 27 & 28 & 30 & 0 & 0 \\ 0 & 22 & 29 & 28 & 27 & 4 & 29 & 30 & 28 & 0 \\ 21 & 25 & 29 & 20 & 28 & 33 & 30 & 32 & 29 & 29 \\ 24 & 28 & 28 & 20 & 34 & 33 & 32 & 29 & 28 & 28 \\ 27 & 26 & 27 & 31 & 33 & 32 & 32 & 28 & 29 & 27 \\ 26 & 23 & 27 & 29 & 30 & 31 & 31 & 31 & 32 & 26 \\ 0 & 23 & 29 & 29 & 29 & 30 & 31 & 31 & 28 & 0 \\ 0 & 0 & 27 & 29 & 26 & 30 & 29 & 30 & 0 & 0 \\ 0 & 0 & 0 & 28 & 26 & 28 & 27 & 0 & 0 & 0 \end{bmatrix},$$

$$F_h = \begin{bmatrix} 0 & 0 & 0 & 26 & 27 & 28 & 29 & 0 & 0 & 0 \\ 0 & 0 & 28 & 32 & 29 & 28 & 29 & 28 & 0 & 0 \\ 0 & 30 & 31 & 31 & 28 & 29 & 32 & 30 & 30 & 0 \\ 27 & 29 & 31 & 31 & 32 & 32 & 30 & 29 & 28 & 27 \\ 28 & 30 & 30 & 31 & 32 & 33 & 33 & 4 & 27 & 28 \\ 26 & 26 & 29 & 30 & 33 & 34 & 28 & 27 & 28 & 27 \\ 28 & 29 & 29 & 29 & 31 & 20 & 20 & 28 & 28 & 29 \\ 0 & 27 & 29 & 27 & 27 & 28 & 29 & 29 & 28 & 0 \\ 0 & 0 & 23 & 23 & 26 & 28 & 25 & 22 & 0 & 0 \\ 0 & 0 & 0 & 26 & 27 & 24 & 21 & 0 & 0 & 0 \end{bmatrix}, \quad F_{rh} = \begin{bmatrix} 0 & 0 & 0 & 27 & 28 & 27 & 29 & 0 & 0 & 0 \\ 0 & 0 & 30 & 28 & 27 & 28 & 28 & 28 & 0 & 0 \\ 0 & 28 & 30 & 29 & 4 & 27 & 28 & 29 & 22 & 0 \\ 29 & 29 & 32 & 30 & 33 & 28 & 20 & 29 & 25 & 21 \\ 28 & 28 & 29 & 32 & 33 & 34 & 20 & 28 & 28 & 24 \\ 27 & 29 & 28 & 32 & 32 & 33 & 31 & 27 & 26 & 27 \\ 26 & 32 & 31 & 31 & 31 & 30 & 29 & 27 & 23 & 26 \\ 0 & 28 & 31 & 31 & 30 & 29 & 29 & 29 & 23 & 0 \\ 0 & 0 & 30 & 29 & 30 & 26 & 29 & 27 & 0 & 0 \\ 0 & 0 & 0 & 27 & 28 & 26 & 28 & 0 & 0 & 0 \end{bmatrix},$$

$$F_{r^2h} = \begin{bmatrix} 0 & 0 & 0 & 21 & 24 & 27 & 26 & 0 & 0 & 0 \\ 0 & 0 & 22 & 25 & 28 & 26 & 23 & 23 & 0 & 0 \\ 0 & 28 & 29 & 29 & 28 & 27 & 27 & 29 & 27 & 0 \\ 29 & 28 & 28 & 20 & 20 & 31 & 29 & 29 & 29 & 28 \\ 27 & 28 & 27 & 28 & 34 & 33 & 30 & 29 & 26 & 26 \\ 28 & 27 & 4 & 33 & 33 & 32 & 31 & 30 & 30 & 28 \\ 27 & 28 & 29 & 30 & 32 & 32 & 31 & 31 & 29 & 27 \\ 0 & 30 & 30 & 32 & 29 & 28 & 31 & 31 & 30 & 0 \\ 0 & 0 & 28 & 29 & 28 & 29 & 32 & 28 & 0 & 0 \\ 0 & 0 & 0 & 29 & 28 & 27 & 26 & 0 & 0 & 0 \end{bmatrix}, \quad F_{r^3h} = \begin{bmatrix} 0 & 0 & 0 & 28 & 26 & 28 & 27 & 0 & 0 & 0 \\ 0 & 0 & 27 & 29 & 26 & 30 & 29 & 30 & 0 & 0 \\ 0 & 23 & 29 & 29 & 29 & 30 & 31 & 31 & 28 & 0 \\ 26 & 23 & 27 & 29 & 30 & 31 & 31 & 31 & 32 & 26 \\ 27 & 26 & 27 & 31 & 33 & 32 & 32 & 28 & 29 & 27 \\ 24 & 28 & 28 & 20 & 34 & 33 & 32 & 29 & 28 & 28 \\ 21 & 25 & 29 & 20 & 28 & 33 & 30 & 32 & 29 & 29 \\ 0 & 22 & 29 & 28 & 27 & 4 & 29 & 30 & 28 & 0 \\ 0 & 0 & 28 & 28 & 28 & 27 & 28 & 30 & 0 & 0 \\ 0 & 0 & 0 & 29 & 27 & 28 & 27 & 0 & 0 & 0 \end{bmatrix}.$$

2.10 Multivariate Normal Data

The following result follows from applying Propositions 2.14 and 2.15.

Proposition 2.16. *Let x be a random vector with components indexed by D_n carrying a multivariate normal distribution with vector of means μ and covariance matrix Λ, or $x \sim N(\mu, \Lambda)$ and assume that Λ is in the center of the (left) regular $\mathbb{C}$-algebra of D_n. Then*

$$\Lambda = \sum_{\xi \in \widehat{D}_n} \lambda_\xi \mathscr{P}_\xi$$

where $\mathscr{P}_\xi$ is the regular canonical projection associated with $\xi \in \widehat{D}_n$, $\lambda_\xi = tr\, \mathscr{P}_\xi \Lambda / tr\, \mathscr{P}_\xi$, and if $\mathscr{F}$ indicates the Fourier basis of D_n,

$$\mathscr{F}x \sim N(\mathscr{F}\mu, Diag\ (\ldots, \lambda_\xi I_{n_\xi^2}, \ldots)_{\xi \in \widehat{D}_n}).$$

Moreover, for each $\xi \in \widehat{D}_n$,

$$(\mathscr{F}x)_\xi \sim N((\mathscr{F}\mu)_\xi, \lambda_\xi I_{n_\xi^2}),$$

is the distribution of the block-component $(\mathscr{F}x)_\xi$ of $\mathscr{F}x$ corresponding to ξ, and these components are independently distributed (and independent) multivariate normal models.

2.11 Selected Dihedral Bases

In this section we derive the element components of Proposition 2.16 for the dihedral groups D_3, D_4, D_5, D_6, and D_7.

Example 2.12 (D_3). The Fourier basis for D_3, following Sect. 2.5, is giving by

$$\mathscr{F}_3 = \left[\begin{array}{cccccc} 0.42 & 0.42 & 0.42 & 0.42 & 0.42 & 0.42 \\ 0.42 & 0.42 & 0.42 & -0.42 & -0.42 & -0.42 \\ \hline 0.59 & -0.30 & -0.30 & 0.59 & -0.30 & -0.30 \\ 0.0 & 0.51 & -0.51 & 0.0 & 0.51 & -0.51 \\ 0.0 & -0.51 & 0.51 & 0.0 & 0.51 & -0.51 \\ 0.59 & -0.30 & -0.30 & -0.59 & 0.30 & 0.30 \end{array}\right],$$

whereas

$$\Lambda_3 = \left[\begin{array}{ccc|ccc} a & b & b & c & c & c \\ b & a & b & c & c & c \\ b & b & a & c & c & c \\ \hline c & c & c & a & b & b \\ c & c & c & b & a & b \\ c & c & c & b & b & a \end{array}\right]$$

is the covariance structure amenable to Proposition 2.16. The first two rows of $\mathscr{F}_3$ account for the two characters of D_3 in dimension of one, and the remaining ones for the single character in dimension of two. The two row blocks correspond to rotations and reversals, respectively, and similarly for the two column blocks. This notation applies to similar matrices in this section. The matrix Λ_3 is in the center of D_3, and hence in the center of its group algebra. Its coefficients in the basis given by the regular canonical projections are,

$$\lambda_1 = a + 2b + 3c,\ \lambda_\alpha = a + 2b - 3c,\ \lambda_\beta = a - b,$$

corresponding to the symmetric, signature and (single) two-dimension characters. From Proposition 2.16, corresponding to the symmetric and alternating characters, respectively,

$$(\mathscr{F}x)_1 \sim N((\mathscr{F}\mu)_1, a + 2b + 3c),\quad (\mathscr{F}x)_\alpha \sim N((\mathscr{F}\mu)_\alpha, a + 2b - 3c),$$

whereas, corresponding to the single character in dimension of two,

$$(\mathscr{F}x)_\beta \sim N((\mathscr{F}x)_\beta, (a-b)I_4).$$

Example 2.13 (D_4). Similarly,

$$\mathscr{F}_4 = \left[\begin{array}{cccccccc}
0.36 & 0.36 & 0.36 & 0.36 & 0.36 & 0.36 & 0.36 & 0.36 \\
0.36 & 0.36 & 0.36 & 0.36 & -0.36 & -0.36 & -0.36 & -0.36 \\
0.36 & -0.36 & 0.36 & -0.36 & 0.36 & -0.36 & 0.36 & -0.36 \\
0.36 & -0.36 & 0.36 & -0.36 & -0.36 & 0.36 & -0.36 & 0.36 \\
\hline
0.50 & 0 & -0.50 & 0 & 0.50 & 0 & -0.50 & 0 \\
0 & 0.50 & 0 & -0.50 & 0 & 0.50 & 0 & -0.50 \\
0 & -0.50 & 0 & 0.50 & 0 & 0.50 & 0 & -0.50 \\
0.50 & 0 & -0.50 & 0 & -0.50 & 0 & 0.50 & 0
\end{array}\right]$$

is the Fourier basis for D_4, where the first four rows are indexed by the symmetric (1), anti-symmetric (α), γ^+, and γ^- characters, all in dimension of one (their interpretation is discussed later on in Sect. 2.7). The remaining four rows account for the single character in dimension of two (β). The covariance structure in the center of D_4 has the pattern of

$$\Lambda_4 = \left[\begin{array}{cccc|cccc}
a & b & c & b & d & e & d & e \\
b & a & b & c & e & d & e & d \\
c & b & a & b & d & e & d & e \\
b & c & b & a & e & d & e & d \\
\hline
d & e & d & e & a & b & c & b \\
e & d & e & d & b & a & b & c \\
d & e & d & e & c & b & a & b \\
e & d & e & d & b & c & b & a
\end{array}\right],$$

and

$$\lambda_1 = a+2b+c+2d+2e,\ \lambda_\alpha = a+2b+c-2d-2e$$
$$\lambda_{\gamma^+} = a-2b+c+2d-2e,\ \lambda_{\gamma^-} = a-2b+c-2d+2e,\ \lambda_\beta = a-c$$

are its coefficients in the regular canonical projection basis.

Example 2.14 (D_5). Its Fourier basis

$$\mathscr{F}_5 = \left[\begin{array}{rrrrrrrrrr}
0.31 & 0.31 & 0.31 & 0.31 & 0.31 & 0.31 & 0.31 & 0.31 & 0.31 & 0.31 \\
0.31 & 0.31 & 0.31 & 0.31 & 0.31 & -0.31 & -0.31 & -0.31 & -0.31 & -0.31 \\
\hline
0.45 & 0.16 & -0.36 & -0.36 & 0.16 & 0.45 & 0.16 & -0.36 & -0.36 & 0.16 \\
0.0 & 0.42 & 0.26 & -0.26 & -0.42 & 0.0 & 0.42 & 0.26 & -0.26 & -0.42 \\
0.0 & -0.42 & -0.26 & 0.26 & 0.42 & 0.0 & 0.42 & 0.26 & -0.26 & -0.42 \\
0.45 & 0.16 & -0.36 & -0.36 & 0.16 & -0.45 & -0.16 & 0.36 & 0.36 & -0.16 \\
\hline
0.45 & -0.36 & 0.16 & 0.16 & -0.36 & 0.45 & -0.36 & 0.16 & 0.16 & -0.36 \\
0.0 & 0.26 & -0.42 & 0.42 & -0.26 & 0.0 & 0.26 & -0.42 & 0.42 & -0.26 \\
0.0 & -0.26 & 0.42 & -0.42 & 0.26 & 0.0 & 0.26 & -0.42 & 0.42 & -0.26 \\
0.45 & -0.36 & 0.16 & 0.16 & -0.36 & -0.45 & 0.36 & -0.16 & -0.16 & 0.36
\end{array}\right]$$

is indexed by the symmetric and alternating characters, one fundamental character in dimension of two (β) and its first harmonic (β^1), also in dimension of two. The covariance structure with the symmetry of D_5 has the pattern of

$$\Lambda_5 = \left[\begin{array}{ccccc|ccccc}
a & b & c & c & b & d & d & d & d & d \\
b & a & b & c & c & d & d & d & d & d \\
c & b & a & b & c & d & d & d & d & d \\
c & c & b & a & b & d & d & d & d & d \\
b & c & c & b & a & d & d & d & d & d \\
\hline
d & d & d & d & d & a & b & c & c & b \\
d & d & d & d & d & b & a & b & c & c \\
d & d & d & d & d & c & b & a & b & c \\
d & d & d & d & d & c & c & b & a & b \\
d & d & d & d & d & b & c & c & b & a
\end{array}\right],$$

and is expressed, in the canonical projection basis, in terms of the coefficients

$$\lambda_1 = a+2b+2c+5d,\ \lambda_\alpha = a+2b+2c-5d$$
$$\lambda_\beta = a+2\cos(2/5\,\pi)b-2\cos(1/5\,\pi)c,\ \lambda_{\beta^1} = a-2\cos(1/5\,\pi)b+2\cos(2/5\,\pi)c.$$

Example 2.15 (D_6). With similar interpretations, we have:

$$\Lambda_6 = \left[\begin{array}{cccccc|cccccc} a & b & c & d & c & b & e & f & e & f & e & f \\ b & a & b & c & d & c & f & e & f & e & f & e \\ c & b & a & b & c & d & e & f & e & f & e & f \\ d & c & b & a & b & c & f & e & f & e & f & e \\ c & d & c & b & a & b & e & f & e & f & e & f \\ b & c & d & c & b & a & f & e & f & e & f & e \\ \hline e & f & e & f & e & f & a & b & c & d & c & b \\ f & e & f & e & f & e & b & a & b & c & d & c \\ e & f & e & f & e & f & c & b & a & b & c & d \\ f & e & f & e & f & e & d & c & b & a & b & c \\ e & f & e & f & e & f & c & d & c & b & a & b \\ f & e & f & e & f & e & b & c & d & c & b & a \end{array}\right],$$

with coefficients

$$\lambda_1 = a+2b+2c+d+3e+3f,\ \lambda_\alpha = a+2b+2c+d-3e-3f$$
$$\lambda_{\gamma^+} = a-2b+2c-d+3e-3f,\ \lambda_{\gamma^-} = a-2b+2c-d-3e+3f$$
$$\lambda_\beta = b+a-c-d,\ \lambda_{\beta^1} = a-c+d-b.$$

Example 2.16 (D_7). The matrices in its center have the form

$$\Lambda_7 = \left[\begin{array}{cccccc|cccccc} a & b & c & d & d & c & b & e & e & e & e & e & e \\ b & a & b & c & d & d & c & e & e & e & e & e & e \\ c & b & a & b & c & d & d & e & e & e & e & e & e \\ d & c & b & a & b & c & d & e & e & e & e & e & e \\ d & d & c & b & a & b & c & e & e & e & e & e & e \\ c & d & d & c & b & a & b & e & e & e & e & e & e \\ b & c & d & d & c & b & a & e & e & e & e & e & e \\ \hline e & e & e & e & e & e & e & a & b & c & d & d & c & b \\ e & e & e & e & e & e & e & b & a & b & c & d & d & c \\ e & e & e & e & e & e & e & c & b & a & b & c & d & d \\ e & e & e & e & e & e & e & d & c & b & a & b & c & d \\ e & e & e & e & e & e & e & d & d & c & b & a & b & c \\ e & e & e & e & e & e & e & c & d & d & c & b & a & b \\ e & e & e & e & e & e & e & b & c & d & d & c & b & a \end{array}\right].$$

Its coefficients are indexed by the symmetric, alternating, the fundamental two harmonics, specifically,

$$\lambda_1 = a+2b+2c+2d+7e,\ \lambda_\alpha = a+2b+2c+2d-7e,$$
$$\lambda_\beta = a+2\cos(2/7\,\pi)b-2\cos(3/7\,\pi)c-2\cos(1/7\,\pi)d,$$
$$\lambda_{\beta^1} = a-2\cos(3/7\,\pi)b-2\cos(1/7\,\pi)c+2\cos(2/7\,\pi)d,$$
$$\lambda_{\beta^2} = a-2\cos(3/7\,\pi)d+2\cos(2/7\,\pi)c-2\cos(1/7\,\pi)b.$$

2.12 Log-Transformed Multinomial Data

Here the dihedral data x is such that the underlying dihedral group is also the support for a multinomial distribution with probability parameters p based on $N =< 1, x >$ observations. Let ℓ indicate the corresponding log count data, with components $\ell_\tau = \log(x_\tau/N)$, for $\tau \in D_n$, and $D_p = \text{Diag}\,(\ldots, p_\tau, \ldots)$. Then, e.g., [5, p.494],

Proposition 2.17.

$$\mathscr{L}[\sqrt{N}\mathscr{F}(\ell - \lambda)] \to \mathscr{N}(0, \mathscr{F}D_p^{-1}\mathscr{F}^* - \mathscr{F}ee'\mathscr{F}^*),$$

where $\lambda_\tau = \log p_\tau$ *are the components of* λ.

In particular, here,

$$\mathscr{F}ee'\mathscr{F}^* = \text{Diag}\,(g^2, 0, \ldots, 0).$$

2.13 Additional Remarks

1. Most of the definitions introduced in this chapter are, more precisely, definitions *on the left*, with corresponding definitions obtained by dihedral actions defined on the right;
2. The regular linearizations $< x, \phi >$ are particular types of *linearizations* in the sense of [1]. Specifically, if a finite group G acts on a set S and $x \in \mathbb{C}^S$, then

   $$[T(\tau)x](s) = x(\tau^{-1}s)$$

   gives a linear representation of G in $\mathbb{C}^S$, so that when $S = G$ the regular linearization is

   $$\phi_\tau(x)\sigma = x_{\tau^{-1}\sigma};$$

3. Proposition 2.10 on page 21 is a general result for finite groups and depends essentially of the orthogonality relations among irreducible characters, e.g., [4, p.50], [6, p.473].
4. Proposition 2.12 on page 25 is the central result underlying the algebraic aspects presented in these notes and a general property of semisimple algebras e.g., [4, Sect. 6.2].

Problems

2.1. Describe (1) the action of the dihedral group D_3 on the distinct vertices $\{a, b, c\}$ of a regular triangle and (2) its action on the oriented edges

$$\{(a,b),(b,c),(c,a),(b,a),(a,c),(c,b)\}$$

of the triangle. Re-evaluate (1) and (2) above when a and b are indistinguishable.

2.2. Describe the distinct dihedral groups D_2 as permutation subgroups of S_4. For example D_2 can be generated both by $\{(12),(34)\}$ and by $\{(12)(34),(13)(24)\}$.

2.3. Describe the distinct dihedral groups D_3 as permutation subgroups of S_3.

2.4. Describe the distinct dihedral groups D_4 as permutation subgroups of S_4.

2.5. Verify that rotations and reversals have opposite parity.

2.6. Describe the D_4 trace indexing $x_\tau = \text{tr}\,[\beta_\tau \Sigma]$ of a an arbitrary 2×2 covariance matrix.

2.7. Describe the D_4 trace indexing $x_\tau = \text{tr}\,[(\beta_\tau \otimes \beta_\tau)\Sigma]$ of a an arbitrary 4×4 covariance matrix.

2.8. Functional invariance can be characterized by its commutativity with a given symmetry operator. Show that when the two-dimensional Laplace operator $\Delta f = \partial_{xx} f + \partial_{yy} f$ is applied to a function $f(p)$ subject to rotation $r(p)$ of its argument, then $\Delta f(r(p)) = r(\Delta f(p))$. That is, $(\Delta f)r = r(\Delta f)$.

2.9. Referring to Problem 1.2 on page 7, study the correspondence between the power set of n objects and the set of all n-ary words in length of n. Endowing the power set with the inclusion-exclusion multiplication turns it into an Abelian group. Carry on the Fourier analysis and evaluate the canonical projections.

2.10. Determine the dihedral invariants of D_n acting (by permutation) on the power set of $n = 2,3,4,5,6$ objects. Study how the invariants depend on the chosen realization of D_n.

2.11. Determine the dihedral linearizations $< x,\rho >$ of the permutation representations ρ of D_n acting on $\{1,\ldots,n\}$, for $n = 2,3,4,5,6$. Specify the particular realization of D_n adopted in the linearization.

2.12. Following with the definitions introduced on page 12, show that $\beta^k_{\sigma\times\tau} = \beta^k_\sigma \beta^k_\tau$.

2.13. Starting with the D_4 linearization

$$< x,\beta >= \begin{bmatrix} 1+h-r^2-r^2h & -r+rh+r^3-r^3h \\ r+rh-r^3-r^3h & 1-h-r^2+r^2h \end{bmatrix}$$

of x at β, using the short notation $x_\tau \equiv \tau$, let each entry (B^+_{ij}, B^-_{ij}) of

$$B = \begin{bmatrix} (1+h,\ r^2+r^2h) & (rh+r^3,\ r+r^3h) \\ (r+rh,\ r^3+r^3h) & (1+r^2h,\ h+r^2) \end{bmatrix}$$

indicate the *signed* components of $< x, \beta >$. Show that B transforms as

$$rB = \begin{bmatrix} B_{21} & B_{22} \\ B_{11}^{\perp} & B_{12}^{\perp} \end{bmatrix}, \quad r^2B = \begin{bmatrix} B_{11}^{\perp} & B_{12}^{\perp} \\ B_{21}^{\perp} & B_{22}^{\perp} \end{bmatrix},$$

$$r^3B = \begin{bmatrix} B_{21}^{\perp} & B_{22}^{\perp} \\ B_{11} & B_{12} \end{bmatrix}, \quad hB = \begin{bmatrix} B_{11} & B_{12} \\ B_{21}^{\perp} & B_{22}^{\perp} \end{bmatrix},$$

$$rhB = \begin{bmatrix} B_{21} & B_{22} \\ B_{11} & B_{12} \end{bmatrix}, \quad r^2hB = \begin{bmatrix} B_{11}^{\perp} & B_{12}^{\perp} \\ B_{21} & B_{22} \end{bmatrix}, \quad r^3hB = \begin{bmatrix} B_{21}^{\perp} & B_{22}^{\perp} \\ B_{11}^{\perp} & B_{12}^{\perp} \end{bmatrix},$$

where $B_{ij}^{\perp}$ indicates the transposed entry (B_{ij}^{-}, B_{ij}^{+}) of B_{ij}. Argue that the signed components of B and their complements are stable within each column space of $< x, \beta >$.

2.14. Prove the algebraic orthogonal property in Proposition 2.10 on page 21.

Chapter 3
Curvature and Refraction Data

3.1 Introduction

The cornea is the main refracting surface of the human eye. Its front (anterior) surface is approximately $1.3\,\text{cm}^2$ with an average radius of curvature of about 7.8 mm. Typical computer algorithms for corneal curvature measurement (known as keratometry) are based on projecting a pattern of concentric rings of light onto the anterior surface of the cornea and numerically determining the relative separation between the images of these reflected rings of light. This models the anterior surface of the cornea as a highly polished spherical mirror. By sampling the curvature at specific circularly equidistant points, a numerical model for the surface curvature may be obtained.

The corneal curvature, κ, and its refractive index, η, contribute to determining the surface's optical refractive power $\kappa(\eta - \eta')$, where $\eta' = 1$ is the reference refractive index of the air. Most of the light takes place at the surface of the cornea, which has refractive index $\eta = 1.3376$. Light then passes through the aqueous humor ($\eta = 1.336$, close to the refractive index of water) to the lens ($\eta = 1.386$–1.406, where it is refracted further) and through the vitreous humor to the retina at the back of the eye.

The standard unit of refractive optical power is the diopter (D) and is defined as the inverse of the radius of curvature. One diopter equals one inverse meter (m^{-1}). For example, using the standard keratometric index $\eta = 1.3375$, a cornea with a curvature of 7.50 mm at 0° has power $(1/0.0075) \times 0.3375 = 45\text{D}$, whereas if the curvature at 90° is 7.25 mm, the power is 46.50 D. The difference between these steep (maximum) and the flat (minimum) curvatures is the amount of regular astigmatism present in the optics of the eye, which interferes with a sharp formation of the image on the retina. In the present example, the regular astigmatism is 1.50 D.

Figure 3.1 shows the optical power contours for two fellow eyes. In this chapter we will develop the dihedral spectral analysis for refraction power contours and related optical applications.

M.A.G. Viana and V. Lakshminarayanan, *Dihedral Fourier Analysis: Data-Analytic Aspects and Applications*, Lecture Notes in Statistics 206,
DOI 10.1007/978-1-4614-5562-2_1,

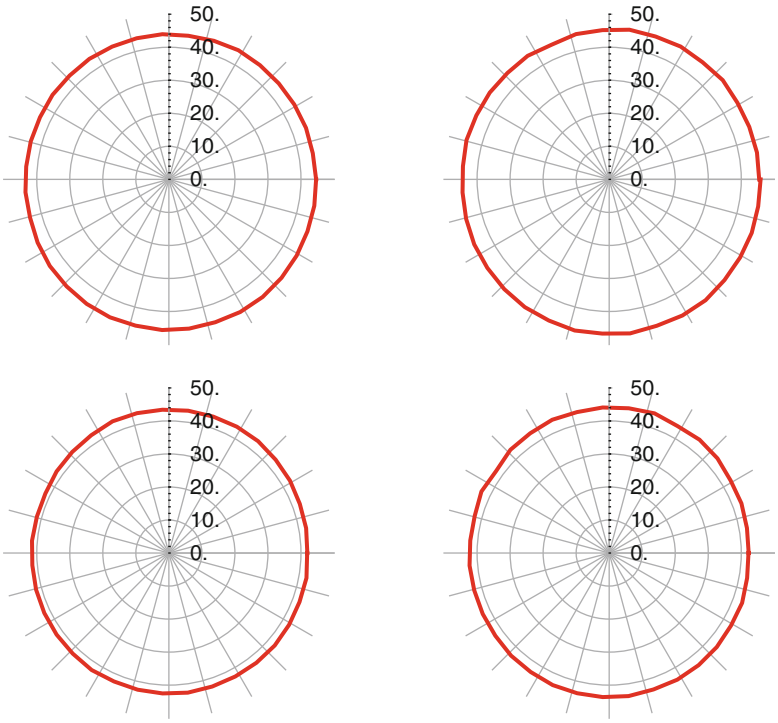

Fig. 3.1 36-point optical power for two fellow eyes. Left eyes on the left column

3.2 Dihedral Analysis of Optical Power

We will illustrate the assessment of the dihedral data with a numerical, shorter random contour

$$y = \{-2.04877, 1.42571, 0.552724, -1.23325\}.$$

of length 4.

The rotational symmetry data extracted from the original contour are defined as the (usual Pearson) correlations between y and its zero-, one-, two-, and threefold rotated contours. In our illustration, we computed the correlation between y and, respectively,

$$\{-2.04877, 1.42571, 0.552724, -1.23325\},$$

$$\{1.42571, 0.552724, -1.23325, -2.04877\},$$

$$\{0.552724, -1.23325, -2.04877, 1.42571\},$$

and

$$\{-1.23325, -2.04877, 1.42571, 0.552724\},$$

thus producing the rotation data

$$\{1,-0.0933946,-0.813211,-0.0933946\}.$$

The reversal symmetries extracted from the contour are defined as the correlations between y and the *reversed* images

$$\{-1.23325,0.552724,1.42571,-2.04877\},$$

$$\{-2.04877,-1.23325,0.552724,1.42571\},$$

$$\{1.42571,-2.04877,-1.23325,0.552724\},$$

and

$$\{0.552724,1.42571,-2.04877,-1.23325\},$$

of the originally rotated contours, thus producing the reversal data

$$\{0.812994,0.0735885,-0.999784,0.113201\}.$$

The dihedral data extracted from the original contour is then the joint data

$$x=\{1,-0.0933946,-0.813211,-0.0933946,0.812994,0.0735885,-0.999784,0.113201\},$$

indexed by D_4.

Specifically, given a contour y in length of n, its D_n indexing is given by

$$x_\tau = \text{Corr}\,(y, H^{\alpha(d)}R^j y),\ \ j=0,1,\ldots n-1,\ d=-1,1, \tag{3.1}$$

where, here, R is the $n\times n$ cyclic permutation matrix for $(12\ldots n)$, and H is corresponding permutation matrix with all ones along the transverse $(i,n-i)$ diagonal. We also observe that

Clearly, the mapping

$$\tau = h^{\alpha(d)}r^j \in D_n \mapsto \rho_\tau = H^{\alpha(d)}R^j \in GL_n(\mathbb{R})$$

is simply the representation of D_n acting naturally on the index set $\{1,\ldots n\}$, so that

$$x_\tau = \text{Corr}\,(y,\rho_\tau y) = \frac{y'\rho_\tau y - n\overline{y}^2}{||y-\overline{y}||^2}.$$

As a direct consequence of the Canonical Projections Theorem we have,

Proposition 3.1. *If $x_\tau = Corr\,(y,\rho_\tau y)$ for $\tau\in D_n$ then*

$$1=\sum_\xi \frac{n_\xi}{2n} < x,\chi^\xi >, \tag{3.2}$$

where the sum is over all irreducible representations of D_n.

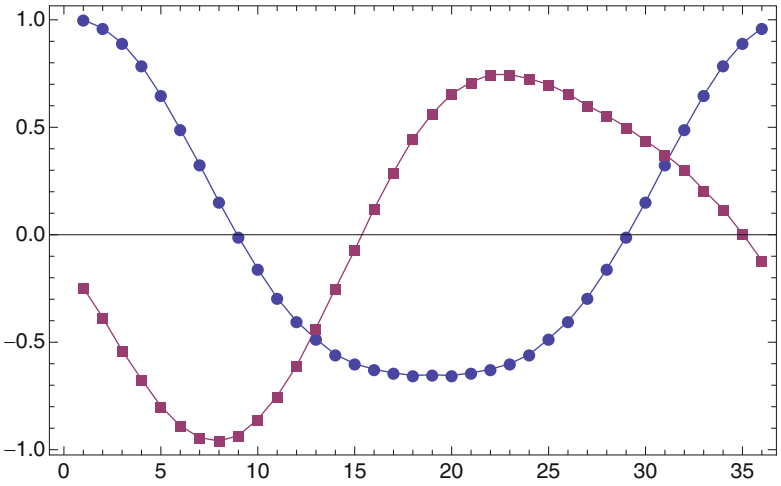

Fig. 3.2 Rotation (*dots*) and reversal (*squares*) data for the L_1 contour

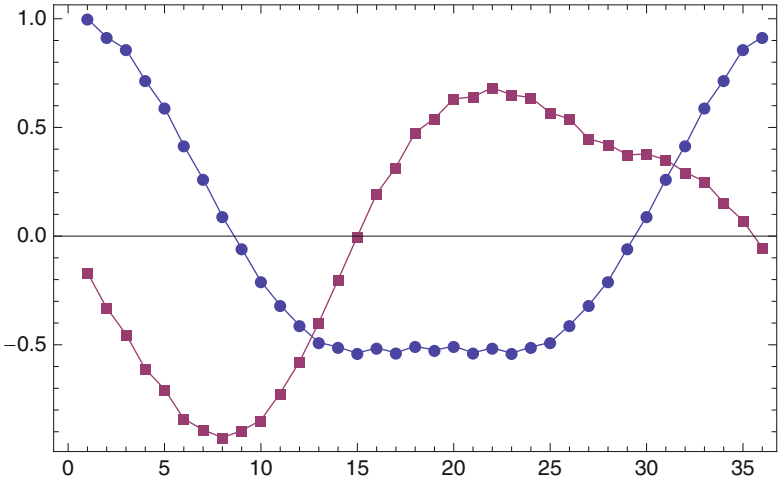

Fig. 3.3 Rotation (*dots*) and reversal (*squares*) data for the R_1 contour

The dihedral indexing based on the correlation coefficients is, of course, bound to the interval $(-1, 1)$.

We conclude this section with the detailed spectral analysis of the power contours shown in Fig. 3.1. For simple reference we will denote the contours for the fellow eyes on the top row by L_1 and R_1. Similarly, for the second row, L_2 and R_2.

Figures 3.2–3.5 show the rotation and reversal data extracted from the indicated contours, as introduced in (3.1) above. It is apparent that the dihedral indexing can reveal or at least amplify seemingly miniscule asymmetries in the power profiles, thus enhancing their distinctive aspects.

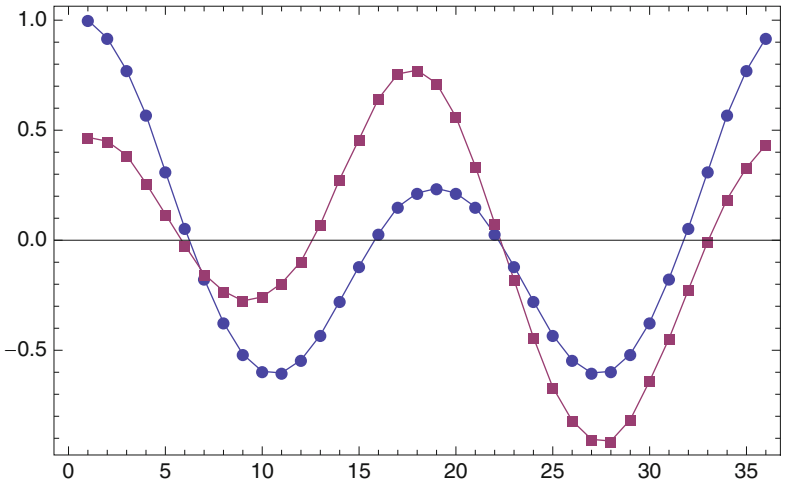

Fig. 3.4 Rotation (*dots*) and reversal (*squares*) data for the L_2 contour

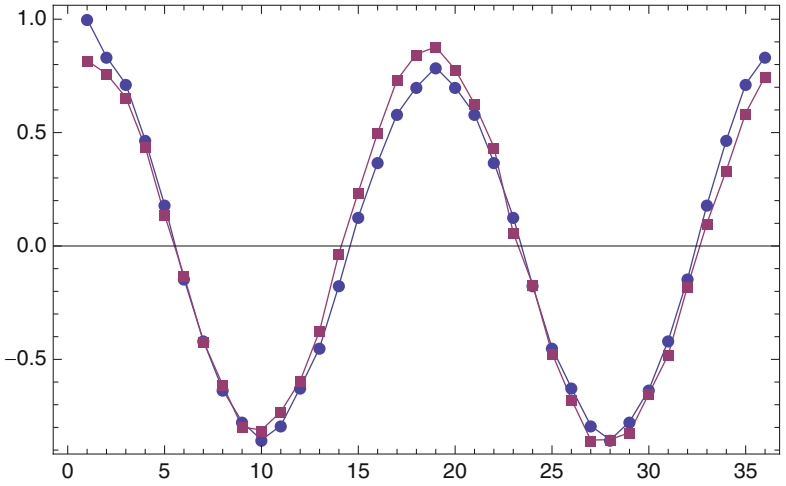

Fig. 3.5 Rotation (*dots*) and reversal (*squares*) data for the R_2 contour

These data can be interpreted against known power profiles. For example, the theoretical power profile

$$t \mapsto \begin{bmatrix} \cos t & \sin t \end{bmatrix} \begin{bmatrix} s + c\sin^2(\alpha) & -c\sin(2\alpha)/2 \\ -c\sin(2\alpha)/2 & s + c\cos^2(\alpha) \end{bmatrix} \begin{bmatrix} \cos t \\ \sin t \end{bmatrix}, \quad t \in (0, 2\pi)$$

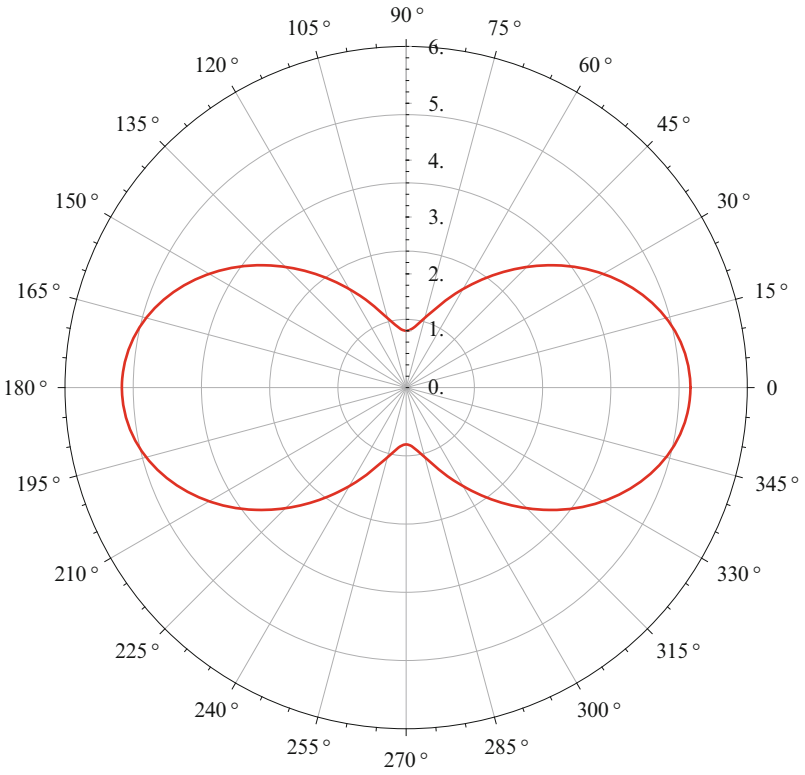

Fig. 3.6 Power profile of a $(s,c,\alpha) = (5,-4,0)$ sphero-cylindrical lens

for a $(s,c,\alpha) = (5,-4,0)$ sphero-cylindrical lens, shown in Fig. 3.6, corresponds to the 36-point, or D_{36}, dihedral profile shown in Fig. 3.7, with features that are compatible with those shown for the observed profile shown in Fig. 3.5.

3.2.1 The Spectral Decomposition

For each profile y, we evaluate the Parseval's decomposition

$$||x||^2 = \sum_{\xi} \frac{n_\xi}{2n} || < x, \xi > ||^2,$$

for the extracted data x over D_{36}, which allows for 4 irreducible representations in dimension of one and 17 representations in dimension of two, thus accounting for the $4+4\times 17 = 72$ data points indexed by D_{36} (Fig. 3.8). The tables in (3.3)

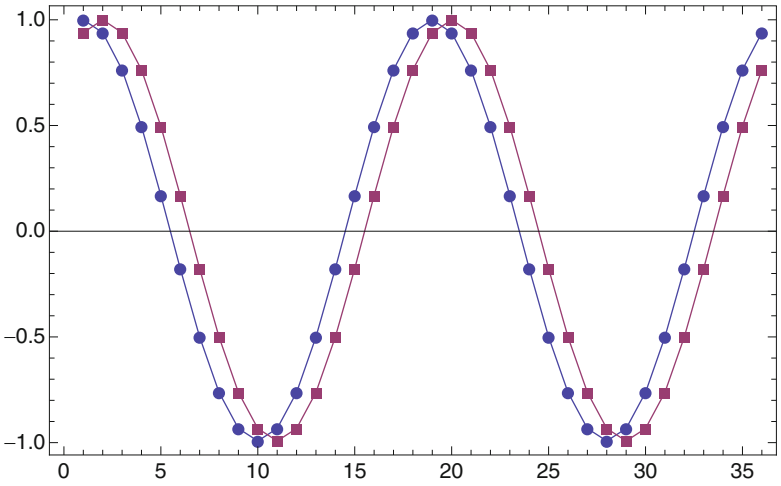

Fig. 3.7 D_{36} data extracted from the power profile of a $(s, c, \alpha) = (5, -4, 0)$ sphero-cylindrical lens

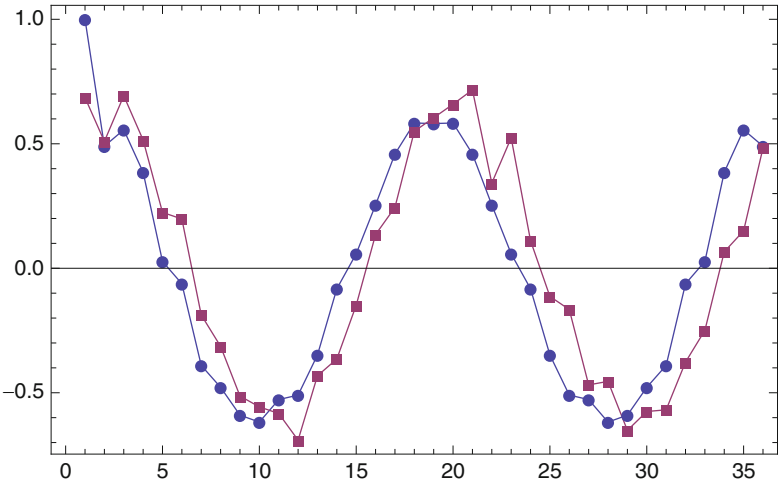

Fig. 3.8 D_{36} data extracted from the power profile of a $(s, c, \alpha) = (5, -4, 0)$ sphero-cylindrical lens with added white noise

show the D_{36} dihedral spectral decomposition for the fellows eyes corresponding to the contours L_1, R_1, L_2, R_2 introduced above, and the tables in (3.4) show the D_{36} spectral decomposition for a purely spherical power contour $(s, c, \alpha) = (5, 0, 0)$, for the contour of $(s, c, \alpha) = (5, -4, 0)$ shown above in Fig. 3.6, and for the same contour with white noise added.

$$
\begin{bmatrix}
1 & 0 \\
\alpha & 0 \\
\gamma_+ & 0 \\
\gamma_- & 0.0000810 \\
\beta_1 & 24.1 \\
\beta_2 & 0.959 \\
\beta_3 & 0.000294 \\
\beta_4 & 0.000455 \\
\beta_5 & 0.000070 \\
\beta_6 & 0.000063 \\
\beta_7 & 0.000031 \\
\beta_8 & 0.000008 \\
\beta_9 & 0.000081 \\
\beta_{10} & 0.0000241 \\
\beta_{11} & 0.0000021 \\
\beta_{12} & 0.000312 \\
\beta_{13} & 0.0000148 \\
\beta_{14} & 0.0000025 \\
\beta_{15} & 0.0000119 \\
\beta_{16} & 0.0000256 \\
\beta_{17} & 0.00000007 \\
\text{------} & \text{----------} \\
||x||\text{\^{}}2 & 25.0
\end{bmatrix},
\begin{bmatrix}
1 & 0 \\
\alpha & 0 \\
\gamma_+ & 0 \\
\gamma_- & 0.000108 \\
\beta_1 & 19.3 \\
\beta_2 & 1.63 \\
\beta_3 & 0.0000246 \\
\beta_4 & 0.00509 \\
\beta_5 & 0.00154 \\
\beta_6 & 0.000105 \\
\beta_7 & 0.000398 \\
\beta_8 & 0.0000655 \\
\beta_9 & 0.0000100 \\
\beta_{10} & 0.000478 \\
\beta_{11} & 0.0000316 \\
\beta_{12} & 0.0000283 \\
\beta_{13} & 0.0000472 \\
\beta_{14} & 0.000537 \\
\beta_{15} & 0.000180 \\
\beta_{16} & 0.000008 \\
\beta_{17} & 0.00711 \\
\text{------} & \text{----------} \\
||x||\text{\^{}}2 & 21.0
\end{bmatrix}
\begin{bmatrix}
1 & 0 \\
\alpha & 0 \\
\gamma_+ & 0 \\
\gamma_- & 0.0000299 \\
\beta_1 & 3.67 \\
\beta_2 & 13.0 \\
\beta_3 & 0.0557 \\
\beta_4 & 0.00173 \\
\beta_5 & 0.00454 \\
\beta_6 & 0.0000197 \\
\beta_7 & 0.000171 \\
\beta_8 & 0.000001 \\
\beta_9 & 0.000189 \\
\beta_{10} & 0.0000605 \\
\beta_{11} & 0.000704 \\
\beta_{12} & 0.000181 \\
\beta_{13} & 0.000276 \\
\beta_{14} & 0.000164 \\
\beta_{15} & 0.000006 \\
\beta_{16} & 0.0000773 \\
\beta_{17} & 0.000009 \\
\text{------} & \text{----------} \\
||x||\text{\^{}}2 & 16.8
\end{bmatrix},
\begin{bmatrix}
1 & 0 \\
\alpha & 0 \\
\gamma_+ & 0 \\
\gamma_- & 0.00352 \\
\beta_1 & 0.122 \\
\beta_2 & 25.5 \\
\beta_3 & 0.0183 \\
\beta_4 & 0.000827 \\
\beta_5 & 0.000844 \\
\beta_6 & 0.0000151 \\
\beta_7 & 0.0000506 \\
\beta_8 & 0.0000205 \\
\beta_9 & 0.0000790 \\
\beta_{10} & 0.00886 \\
\beta_{11} & 0.000170 \\
\beta_{12} & 0.0000518 \\
\beta_{13} & 0.00284 \\
\beta_{14} & 0.00271 \\
\beta_{15} & 0.0000260 \\
\beta_{16} & 0.00544 \\
\beta_{17} & 0.00155 \\
\text{------} & \text{----------} \\
||x||\text{\^{}}2 & 25.7
\end{bmatrix}
\tag{3.3}
$$

$$
\begin{bmatrix}
1 & 0 \\
\alpha & 0 \\
\gamma_+ & 0 \\
\gamma_- & 0 \\
\beta_1 & 0 \\
\beta_2 & 0 \\
\beta_3 & 0 \\
\beta_4 & 36.0 \\
\beta_5 & 0 \\
\beta_6 & 0 \\
\beta_7 & 0 \\
\beta_8 & 0 \\
\beta_9 & 0 \\
\beta_{10} & 0 \\
\beta_{11} & 0 \\
\beta_{12} & 0 \\
\beta_{13} & 0 \\
\beta_{14} & 0 \\
\beta_{15} & 0 \\
\beta_{16} & 0 \\
\beta_{17} & 0 \\
\text{------} & \text{----------} \\
||x||\text{\^{}}2 & 36.0
\end{bmatrix},
\begin{bmatrix}
1 & 0 \\
\alpha & 0 \\
\gamma_+ & 0 \\
\gamma_- & 0 \\
\beta_1 & 0 \\
\beta_2 & 35.7 \\
\beta_3 & 0 \\
\beta_4 & 0.000545 \\
\beta_5 & 0 \\
\beta_6 & 0 \\
\beta_7 & 0 \\
\beta_8 & 0 \\
\beta_9 & 0 \\
\beta_{10} & 0 \\
\beta_{11} & 0 \\
\beta_{12} & 0 \\
\beta_{13} & 0 \\
\beta_{14} & 0 \\
\beta_{15} & 0 \\
\beta_{16} & 0 \\
\beta_{17} & 0 \\
\text{------} & \text{----------} \\
||x||\text{\^{}}2 & 35.7
\end{bmatrix},
\begin{bmatrix}
1 & 0 \\
\alpha & 0 \\
\gamma_+ & 0 \\
\gamma_- & 0.00206 \\
\beta_1 & 0.0000894 \\
\beta_2 & 21.8 \\
\beta_3 & 0.0297 \\
\beta_4 & 0.0312 \\
\beta_5 & 0.0209 \\
\beta_6 & 0.000662 \\
\beta_7 & 0.0533 \\
\beta_8 & 0.00970 \\
\beta_9 & 0.0318 \\
\beta_{10} & 0.000699 \\
\beta_{11} & 0.0000391 \\
\beta_{12} & 0.000004 \\
\beta_{13} & 0.00538 \\
\beta_{14} & 0.00609 \\
\beta_{15} & 0.0000667 \\
\beta_{16} & 0.00199 \\
\beta_{17} & 0.000660 \\
\text{------} & \text{----------} \\
||x||\text{\^{}}2 & 22.0
\end{bmatrix}
\tag{3.4}
$$

3.3 Dihedral Analysis of Wavefront Aberration Polynomials

Consider, to illustrate, the following estimated wavefront aberration radial polynomials, shown in Fig. 3.9:

$$W_2(r,t) = 0.264861\left(-1+2r^2\right) - 0.106237r^2\text{Cos}[2t] - 0.228447r^2\text{Sin}[2t];$$

$$\begin{aligned} W_3(r,t) = {} & -0.0328445r\left(-2+3r^2\right)\text{Cos}[t] + 0.179979r^3\text{Cos}[3t] \\ & + 0.014439r\left(-2+3r^2\right)\text{Sin}[t] - 0.0865721r^3\text{Sin}[3t]; \end{aligned}$$

$$\begin{aligned} W_4(r,t) = {} & -0.0230155\left(1-6r^2+6r^4\right) - 0.00927528r^2\left(-3+4r^2\right)\text{Cos}[2t] \\ & + 0.0326643r^4\text{Cos}[4t] - 0.00361759r^2\left(-3+4r^2\right)\text{Sin}[2t] \\ & + 0.0613639r^4\text{Sin}[4t]; \end{aligned}$$

$$\begin{aligned} W_5(r,t) = {} & 0.0527403r\left(3-12r^2+10r^4\right)\text{Cos}[t] - 0.0534837r^3\left(-4+5r^2\right)\text{Cos}[3t] \\ & - 0.0143293r^5\text{Cos}[5t] + 0.0434211r\left(3-12r^2+10r^4\right)\text{Sin}[t] \\ & - 0.0380357r^3\left(-4+5r^2\right)\text{Sin}[3t] + 0.0457845r^5\text{Sin}[5t]. \end{aligned}$$

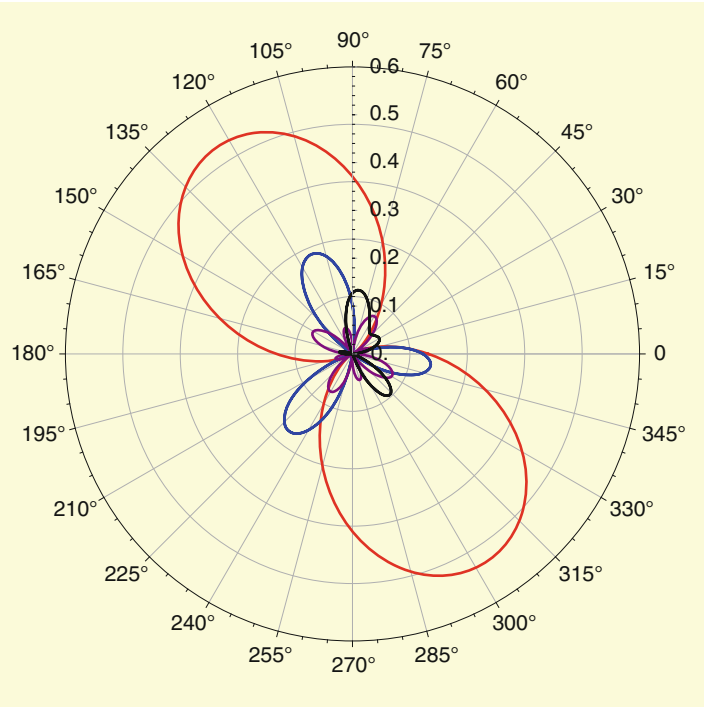

Fig. 3.9 Single mode contours ($r = 1$) for the polynomials W_2 (*red*, two-foil), W_3 (*blue*, trefoil), W_4 (*purple*, tetrafoil), and W_5 (*black*, pentafoil)

Their superposition $W = W_2 + W_3 + W_4 + W_5$ is shown in Fig. 3.10, whereas its associated rotations-reversals data is shown in Fig. 3.11.

The dihedral D_{12} decompositions for the elementary modes W_2, W_3, W_4, W_5 are shown on (3.5), whereas the decompositions for the joint superposed mode is shown in (3.6). The elementary modes are clearly and distinctly characterized in each case:

$$W_2 : \beta_2, \quad W_3 : \beta_1, \beta_4, \quad W_4 : \beta_2, \beta_4, \quad W_5 : \beta_1, \beta_3, \beta_5,$$

whereas the superposed mode is projected among those individual sets of components

$$\begin{bmatrix} 1 & 0 \\ \alpha & 0 \\ \gamma_+ & 0 \\ \gamma_- & 0 \\ \beta_1 & 0 \\ \beta_2 & 12.0 \\ \beta_3 & 0 \\ \beta_4 & 0 \\ \beta_5 & 0 \\ \text{------} & \text{----------} \\ ||x||\text{\^{}}2 & 12.0 \end{bmatrix}, \begin{bmatrix} 1 & 0 \\ \alpha & 0 \\ \gamma_+ & 0 \\ \gamma_- & 0 \\ \beta_1 & 0.0117 \\ \beta_2 & 0 \\ \beta_3 & 11.3 \\ \beta_4 & 0 \\ \beta_5 & 0 \\ \text{------} & \text{----------} \\ ||x||\text{\^{}}2 & 11.3 \end{bmatrix}, \begin{bmatrix} 1 & 0 \\ \alpha & 0 \\ \gamma_+ & 0 \\ \gamma_- & 0 \\ \beta_1 & 0 \\ \beta_2 & 0.00485 \\ \beta_3 & 0 \\ \beta_4 & 11.5 \\ \beta_5 & 0 \\ \text{------} & \text{----------} \\ ||x||\text{\^{}}2 & 11.5 \end{bmatrix}, \begin{bmatrix} 1 & 0 \\ \alpha & 0 \\ \gamma_+ & 0 \\ \gamma_- & 0 \\ \beta_1 & 2.06 \\ \beta_2 & 0 \\ \beta_3 & 1.75 \\ \beta_4 & 0 \\ \beta_5 & 0.500 \\ \text{------} & \text{----------} \\ ||x||\text{\^{}}2 & 4.31 \end{bmatrix} \tag{3.5}$$

$$\begin{bmatrix} 1 & 0 \\ \alpha & 0 \\ \gamma_+ & 0 \\ \gamma_- & 0 \\ \beta_1 & 0.0140 \\ \beta_2 & 4.51 \\ \beta_3 & 0.993 \\ \beta_4 & 0.0233 \\ \beta_5 & 0.00529 \\ \text{------} & \text{----------} \\ ||x||\text{\^{}}2 & 5.55 \end{bmatrix} \tag{3.6}$$

3.4 Dihedral Spatial Filters

The basic theoretical framework, borrowed from earlier developments in filter theory, describes the intensity of an elementary image, e.g., [8], as a linear superposition, or convolution,

$$\mathscr{I}(u) = \int \mathscr{S}(u - v)\mathscr{O}(v)dv,$$

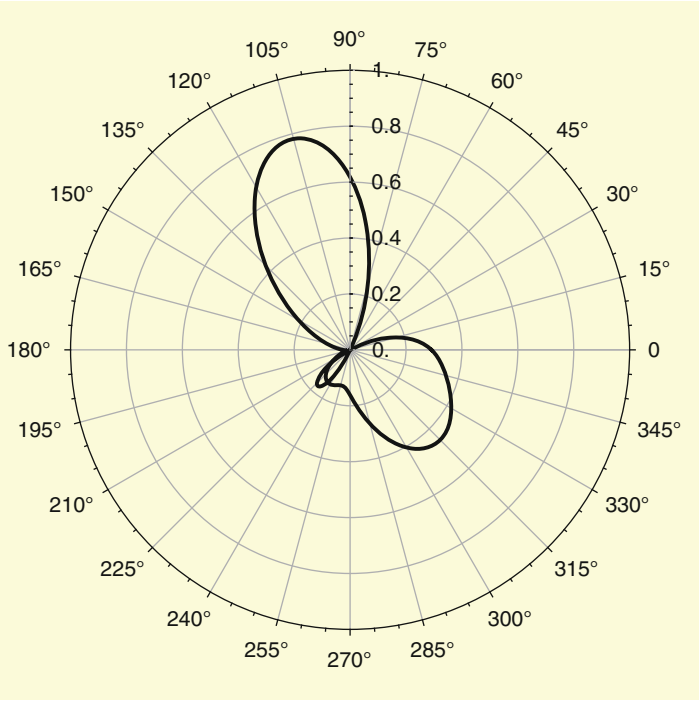

Fig. 3.10 Superposition $W_2 + W_3 + W_4 + W_5$ of the single modes shown in Fig. 3.9

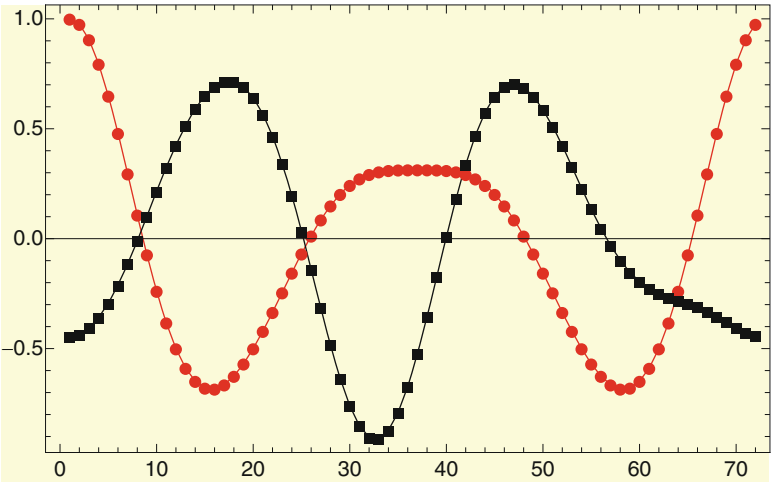

Fig. 3.11 Rotations (*red dots*) and Reversals (*black squares*) for the joint mode W of Fig. 3.10

over the object plane ($\mathbb{R}^2$), of a spread function or impulse response $\mathscr{S}$ and the source image $\mathscr{O}$ in the object plane ($\mathbb{R}^2$). This is conveniently arranged so that, in turn,

$$\widehat{\mathscr{I}} = \widehat{\mathscr{S}}\widehat{\mathscr{O}} \tag{3.7}$$

is the corresponding spectral distribution $\hat{\mathscr{I}}$ of $\mathscr{I}$ (its Fourier transform), where

$$\hat{\mathscr{S}}(\omega) = \int \mathscr{S}(u)\exp[-i\omega\cdot u]du$$

is the optical transfer function or frequency response. Equality (3.7) corresponds to equality 4 in Proposition 2.1 on page 15 in the dihedral analysis formulation.

The Dihedral Filters

From Sect. 3.4, we now study the (first-order) dihedral bases

$$b_\tau(x) = x'\beta_\tau x$$

as spatial filters (or point spread functions) for the power contours

$$p(x) = x'Fx = \frac{1}{2}\{(2s+c)(x_1^2+x_2^2) - c\cos(2\alpha)(x_1^2-x_2^2) - 2c\sin(2\alpha)x_1x_2\}.$$

Evaluation of their convolution

$$m_\tau(y) = [b_\tau * p](y) = \int_B b_\tau(y-x)p(x)dx,\ \ \tau\in D_n,$$

over a window B in polar coordinates gives

$$m_\tau(\theta) = \left(2(1+d)(c+2s)\mathrm{Cos}\left[\frac{2j\pi}{n}\right] + c(-1+d)\mathrm{Cos}\left[2\left(\alpha+\frac{j\pi}{n}-\theta\right)\right]\right),$$

up to a proportionality constant due to integrating out the polar radius, and where (j,d) indicates the element $\tau\in D_n$. That is, $j=0,\ldots,n-1$ are the step rotations $(d=1)$ and reversals $(d=-1)$. In the above expression, the window is $\pm\pi/2$. We also note that, clearly, the resulting discrete convolution is embedded in the continuous (unconnected) D_∞ case,

$$\mu_\tau(\theta) = 2(1+d)(c+2s)\mathrm{Cos}[\phi] + c(-1+d)\mathrm{Cos}[\phi+2(\alpha-\theta)],$$

up to a proportionality constant.

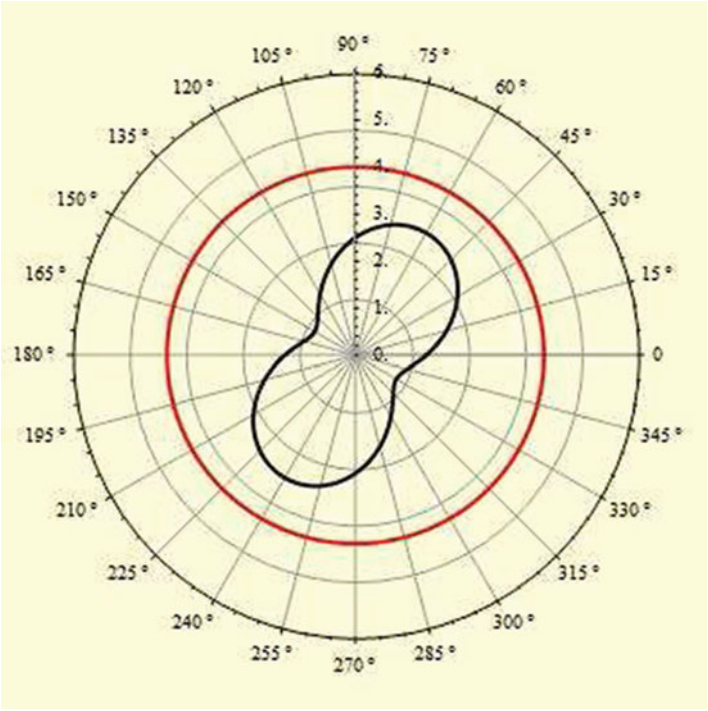

Fig. 3.12 Profile contour for $(s, c, \alpha) = (3, -2, \pi/3)$, in *black*, and extracted spherical-equivalent component contour, in *red color*, using a dihedral D_4 rotational (even) filter

Extracting the Attributes of the Power Profiles

Figures 3.12–3.14 show the original profile (in black color) of a power matrix with spherical power $s = 3D$, cylindrical power $c = -2D$ and major orientation $\alpha = \pi/3$.

The contours in red color are the resulting extracted contours μ_τ after the convolution with the D_4 filters for rotations (Fig. 3.12) and reversals (Figs. 3.13 and 3.14). The two even filters $j = 0, 2$ for rotations are equivalent, and the odd ones $j = 1, 3$ are null. The reversal filters give two sets of filters $j = 0, 2$ and $j = 1, 3$, each one with two equivalent filters.

Specifically, the rotation filters evaluate

$$m_{0,1}(0) = m_{2,1}(0) = \pm 2(s + c/2) = \pm 2M, \tag{3.8}$$

thus extracting Humphrey's spherical equivalent (M). The even reversals evaluate

$$m_{0,-1}(0) = m_{2,-1}(0) = \pm(c/2)\cos(2\alpha) = \pm C_+, \tag{3.9}$$

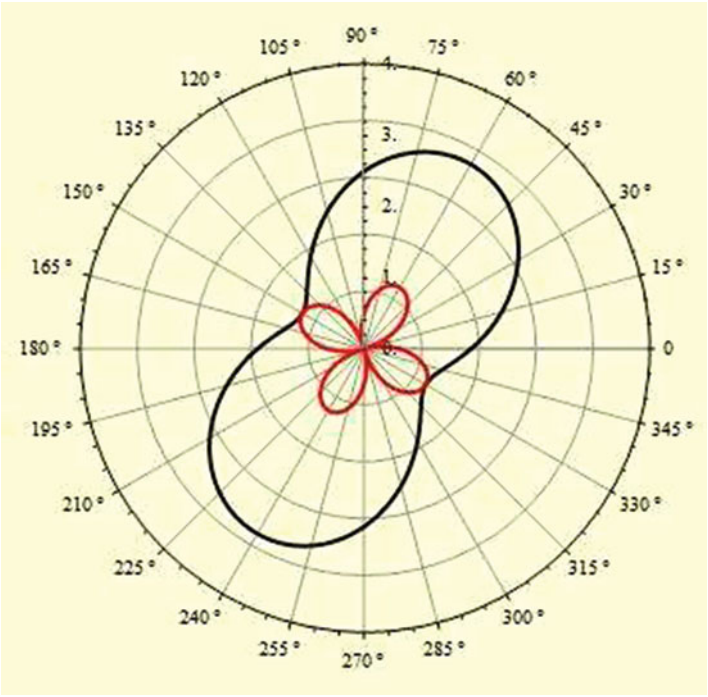

Fig. 3.13 Profile contour for $(s, c, \alpha) = (3, -2, \pi/3)$, in *black*, and extracted orthogonal astigmatism C_+ component contour, in *red color*, using a dihedral D_4 reversal (even) filter

thus extracting the orthogonal astigmatism component C_+, whereas the odd reversals extract

$$m_{1,-1}(0) = m_{3,-1}(0) = \pm(c/2)\sin(2\alpha) = \pm C_\times \tag{3.10}$$

the oblique astigmatism component $C_\times$. Clearly, the ratio of these two components determines the orientation α. Therefore, all features of the contour are recovered by the dihedral (D_4) filters.

Figure 3.15 shows, similarly, the corresponding extracted component features for a $(s, c, \alpha) = (0.5, 3, \pi/3)$ power profile.

A Direct Evaluation of the Profile Features

As shown earlier, the power matrix decomposes as a dihedral linearization

$$F = M\begin{bmatrix}1 & 0\\ 0 & 1\end{bmatrix} + C_+\begin{bmatrix}1 & 0\\ 0 & -1\end{bmatrix} + C_\times\begin{bmatrix}0 & 1\\ 1 & 0\end{bmatrix} = M\beta_{0,0} + C_+\beta_{0,-1} + C_\times\beta_{1,-1},$$

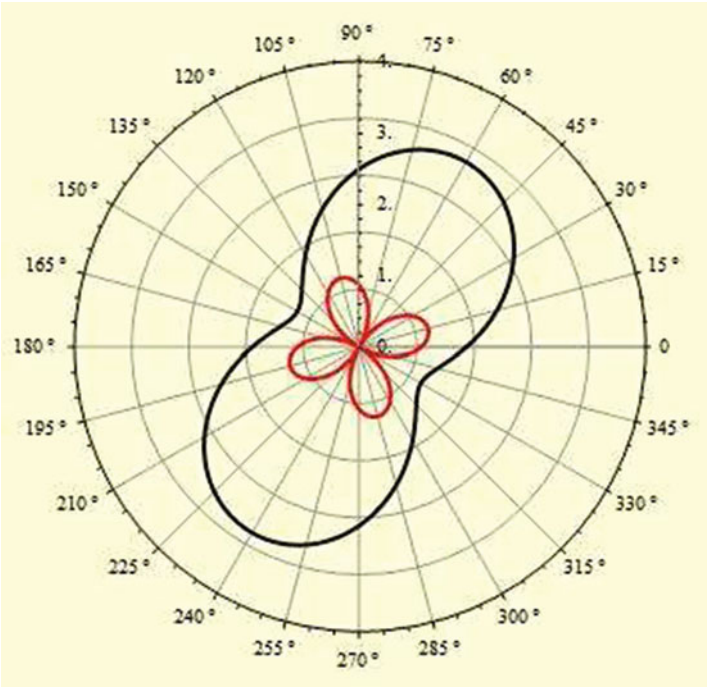

Fig. 3.14 Profile contour for $(s, c, \alpha) = (3, -2, \pi/3)$, in *black*, and extracted oblique astigmatism $C_\times$ component contour, in *red color*, using a dihedral D_4 reversal (odd) filter

so that the convolution of $p(x) = x'Rx$ with $b_\tau(x) = x'\beta_\tau x$ depends only on the convolutions $b_\tau * b_\sigma$, for $\tau, \sigma \in D_n$. Direct evaluation up to a constant of proportionality then shows that in D_4, we have for all $j, k = 0, 1, 2, 3$,

$$[b_{1,j} * b_{1,k}](\theta) = \mathrm{Cos}\left[\frac{j\pi}{2}\right] \mathrm{Cos}\left[\frac{k\pi}{2}\right],$$

independent of θ, and

$$[b_{-1,j} * b_{-1,k}](\theta) = \mathrm{Cos}\left[\frac{(j+k)\pi}{2} - 2\theta\right],$$

whereas $b_{1,j} * b_{-1,k} = 0$. These relations then directly determine the power profile features (3.8)–(3.10).

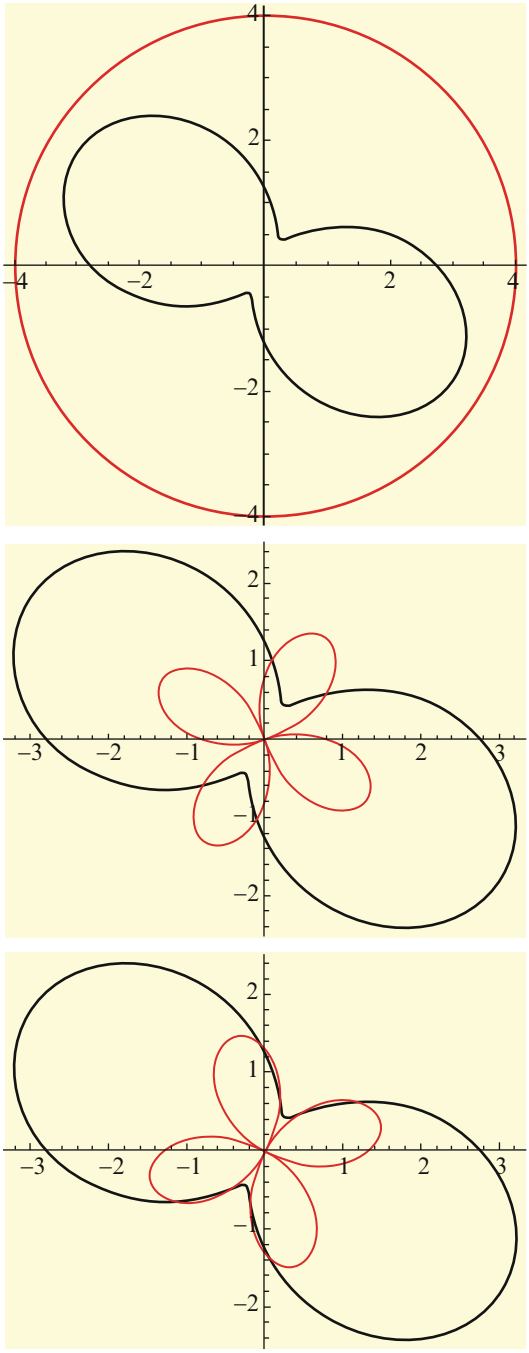

Fig. 3.15 Profile contour for $(s, c, \alpha) = (0.5, 3, \pi/3)$, in *black*, and extracted spherical equivalent (*top*), orthogonal astigmatism (*center*) and oblique astigmatism (*bottom*) component contours, in *red color*, using a dihedral D_4 rotational (even), reversal (even), and reversal (odd) filters, respectively

3.5 The Algebraic Structure of Dioptric Power Matrices

We recall that a ring $(R,+,\cdot)$ is a set R together with two binary operations $+$ and $\cdot$ in R such that

- $(R,+)$ is an Abelian group;
- $a\cdot(b\cdot c)=(a\cdot b)\cdot c$;
- $a\cdot(b+c)=a\cdot b+a\cdot c,(b+c)\cdot a=b\cdot a+c\cdot a.$

We often simply write ab to indicate $a\cdot b$. The identity element in $(R,+)$ is indicated by 0, and if there is an element $1\in R\neq\{0\}$ such that $1a=a1=a$ for all $a\in R$ then R is said to be a ring with unit. We say that $a\in R$ is a unit if there is an element $b\in R$ such that $ab=ba=1$. The set of units in R is a group called the group of units of R.

Consider the dioptric power matrices

$$R(s,c,\alpha)=\begin{bmatrix} s+c\sin^2(\alpha) & -c\sin(2\alpha)/2 \\ -c\sin(2\alpha)/2 & s+c\cos^2(\alpha)\end{bmatrix},$$

defined here for $s,c,\in\mathbb{R}$ and $0\leq\alpha\leq 2\pi$. In what follows we will construct a ring structure for the dioptric power matrices under the usual sum and multiplication of matrices. This requires showing that, under certain conditions, the power matrices are closed under addition and multiplication. The remaining properties will follow from the fact that these matrices are a subset of the ring of all real 2×2 matrices under addition and multiplication, that $R(1,0,0)$ gives the multiplicative identity, and $R(0,0,0)=0$ gives the additive identity in R.

To verify the additive closure, first note that

$$R(s,c,\alpha)=(s+c/2)\begin{bmatrix}1&0\\0&1\end{bmatrix}-(c/2)\cos(2\alpha)\begin{bmatrix}1&0\\0&-1\end{bmatrix}-(c/2)\sin(2\alpha)\begin{bmatrix}0&1\\1&0\end{bmatrix},$$

where the matrix components are elements in the matrix group of D_4. It is then easier to see that

$$R(s_1,c_1,\alpha_1)+R(s_2,c_2,\alpha_2)=R(s_1+s_2,c_1+c_2,\alpha^*),$$

where

$$\alpha^*=\frac{1}{2}\arctan\frac{c_1\sin(2\alpha_1)+c_2\sin(2\alpha_2)}{c_1\cos(2\alpha_1)+c_2\cos(2\alpha_2)},$$

for $c_1\cos(2\alpha_1)+c_2\cos(2\alpha_2)\neq 0$, and otherwise $\alpha^*=\pi/2$. Of course, $\alpha^*+\pi$ is the other optically equivalent solution. Therefore, we have the Abelian structure for $(R,+)$, thus endowing $(R,+,\cdot)$ with the structure of a ring with unit.

To illustrate, numerically,

$$R(5,4,\pi/6)+R(3,2,\pi/8)=R(8,6,\alpha^*),$$

where

$$\alpha^* = \frac{1}{2}\arctan\frac{4\sin(\pi/3)+2\sin(\pi/4)}{4\cos(\pi/3)+2\cos(\pi/4)} = \frac{0.96}{2} = 0.48.$$

To conclude this section we add that the group of units of the dioptric power ring is determined by those matrices such that $\det R(s,c,\alpha) = s(s+c) \neq 0$.

Problems

3.1. Show that $\sum_\tau x_\tau = 0$, where x_τ is given by (3.2) on page 43.

3.2. Verify the multiplicative closure of the dioptric power matrix ring.

3.3. Referring to (3.1), study the probability law of

$$x_\tau = \text{Corr}\,(y, H^{\alpha(d)}R^j y), \quad j = 0,1,\ldots n-1,\ d = -1,1,$$

under a bivariate Gaussian structure for x, y.

3.4. Following with Problem 3.3 above, study the covariance structure for the resulting dihedral orbit under the same Gaussian structure. This is the broad set up for inference when the unit of analysis is a given symmetry orbit, and a sample of such orbits is then obtained experimentally. The algebraic mechanism for introducing an (analysis of variance) error component is detailed in [2, e.g., Standard Decomposition].

Chapter 4
Symbolic Sequences

4.1 Introduction

In this chapter we discuss in detail a dihedral analysis of multinomial data indexed by D_4. Specifically, we consider the analysis of data indexed by the rotations and reversals orbit

$$\{\text{AGCT}, \text{GCTA}, \text{CTAG}, \text{TAGC}, \text{TCGA}, \text{CGAT}, \text{GATC}, \text{ATCG}\}$$

of the DNA word AGCT under D_4 that, together with the non-equivalent DNA orbits

$$\{\text{ACGT}, \text{CGTA}, \text{GTAC}, \text{TACG}, \text{TGCA}, \text{GCAT}, \text{CATG}, \text{ATGC}\},$$

$$\{\text{GACT}, \text{ACTG}, \text{CTGA}, \text{TGAC}, \text{TCAG}, \text{CAGT}, \text{AGTC}, \text{GTCA}\},$$

of, respectively ACGT and GACT, describe the full symmetric group S_4 orbit of AGCT.

The data are frequency counts along 6 adjacent equal-length regions of the complete HIV1 genome.[1] For related examples see [9–11].

The matrices shown in (4.1)

[1]Human immunodeficiency virus type 1, isolate BRU, complete genome (LAV-1), Accession number K02013.1 (HIVBRUCG), http://www.ncbi.nlm.nih.gov/nucleotide/. The complete BRU isolate is 9,229 BP-long

M.A.G. Viana and V. Lakshminarayanan, *Dihedral Fourier Analysis: Data-Analytic Aspects and Applications*, Lecture Notes in Statistics 206,
DOI 10.1007/978-1-4614-5562-2_1, © Springer Science+Business Media New York 2013

τ	$\mathscr{O}_{D_4}$						$\mathscr{O}_{D_4}$						$\mathscr{O}_{D_4}$					
1	AGCT	11	6	5	4	6	16	ACGT	0	0	1	0	2	1	GACT	7	6	6	6	0	6
r	GCTA	7	3	3	6	7	11	CGTA	0	0	0	0	1	0	ACTG	3	7	3	5	8	7
r^2	CTAG	9	3	4	11	3	5	GTAC	3	9	7	6	9	6	CTGA	3	5	5	2	6	6
r^3	TAGC	5	1	9	9	5	7,	TACG	1	0	1	1	1	0,	TGAC	7	5	3	4	4	6
r^3h	TCGA	2	0	0	1	0	3	TGCA	10	4	6	5	8	3	TCAG	14	14	6	10	6	6
r^2h	CGAT	2	1	0	0	1	2	GCAT	8	5	5	9	5	5	CAGT	8	12	13	6	7	4
rh	GATC	4	5	3	4	3	6	CATG	6	2	7	8	5	3	AGTC	1	2	4	4	3	2
h	ATCG	1	0	0	0	0	3	ATGC	6	1	3	6	7	3	GTCA	4	4	6	4	4	4

. (4.1)

give the frequency counts along the dihedral orbits described above, where each column corresponds to one of 6 equal-length adjacent regions in the genome. Each region is approximately 1,500 base pairs. A program used to generate the frequency counts is given in Appendix A on page 75.

4.2 The Dihedral Orbit Display

Given a set of dihedral D_4 frequency counts x_τ, the field orbit

$$X_\tau = \beta_\tau q + x_\tau \beta_\tau e_j, \tag{4.2}$$

where $e'_j = (\delta_{1j}, \delta_{2j})$, scales each direction vector $\beta_\tau e_j$ positioned at $\beta_\tau q$ according to the corresponding frequency count x_τ, thus producing a dihedral D_4 orbit scaled by the observed dihedral (frequency count) data. Figure 4.1 shows the dihedral display of the GACT orbit in region 4 of the HIV1 genome, corresponding to the frequency counts shown in (4.1). It jointly displays all points in the orbit, highlighting the rotations

$$\begin{array}{ccc} r\uparrow \bullet & = & \bullet \rightarrow 1 \\ \| & & \| \\ r^2 \leftarrow \bullet & = & \bullet \downarrow r^3 \end{array},$$

shown in black color arrows, and reversals

$$\begin{array}{ccc} r^2h \leftarrow \bullet & = & \bullet \uparrow rh \\ \| & & \| \\ r^3h \downarrow \bullet & = & \bullet \rightarrow h \end{array},$$

shown in red color arrows. The frequency counts are scaled, for plotting purposes, by $2/\sum_\tau x_\tau$, so that the magnitude of an arrow has an ordinal character only, proportional to its relative frequency in the orbit.

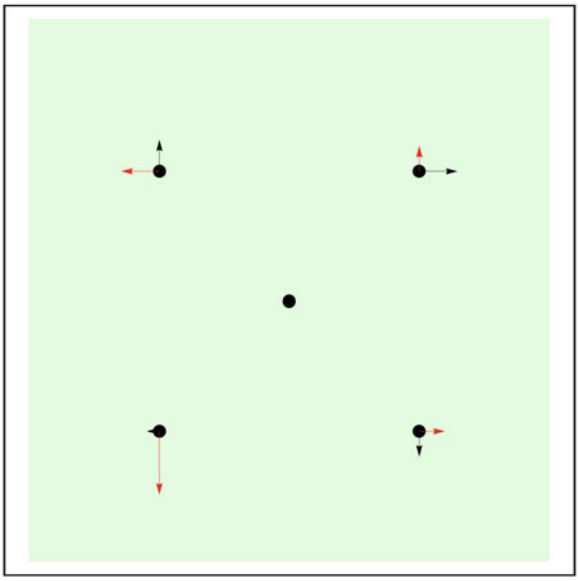

Fig. 4.1 Dihedral display of the GACT orbit in region 4 of the HIV1 genome

4.3 A Center of Mass Display

The resultant effect of the scaled orbit in the center of mass is then proportional to

$$\mathscr{C}_j(X) = \sum_\tau X_\tau = \left(\sum_\tau \beta_\tau\right) q + \left(\sum_\tau x_\tau \beta_\tau\right) e_j.$$

Since β is irreducible, we have $\sum_\tau \beta_\tau = 0$, whereas $\sum_\tau x_\tau \beta_\tau$ is the Fourier transform of x at β, so that

$$\mathscr{C}_j(X) = < x, \beta > e_j.$$

Conversely, we have then the following useful interpretation:

Proposition 4.1. *The column spaces of the dihedral two-dimensional D_4 Fourier transform of the orbit displacement data are center of mass displacements corresponding to elementary displacements dx and dy.*

That is,

$$dx \mapsto \mathscr{C}_1(X) = < x, \beta > e_1 = \begin{bmatrix} 1 - r^2 + h - r^2 h \\ r - r^3 + rh - r^3 h \end{bmatrix} \equiv \mathscr{C}_1,$$

$$dy \mapsto \mathscr{C}_2(X) = < x, \beta > e_2 = \begin{bmatrix} -r + r^3 + rh - r^3 h \\ 1 - r^2 - h + r^2 h \end{bmatrix} \equiv \mathscr{C}_2.$$

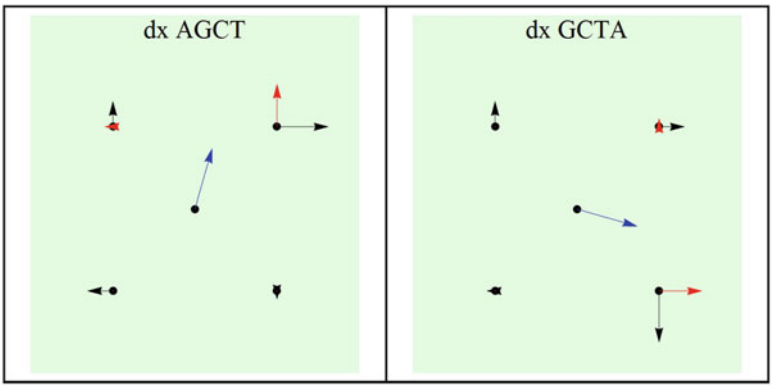

Fig. 4.2 The AGCT and GCTA orbits for the HIV1 genome in region 2

The orbit invariance at the center of mass, from (2.3), is simply

$$\mathscr{C}_j(\tau X) = < \tau x, \beta > e_j = \beta_{\tau^{-1}} \mathscr{C}_j, \tag{4.3}$$

and the unitary character of β guarantees that

$$||\mathscr{C}_j(\tau X)|| = ||\mathscr{C}_j(X)||,$$

for all $\tau \in D_4$. Figure 4.2 shows the equivalent orbits AGCT and GCTA in region 2 of the HIV1 genome. Here the relabeling AGCT $\mapsto$ GCTA is effected by the 90° counterclockwise rotation, or $\tau = r$. Consequently, as illustrated, the center of mass is rotated by 270° (τ^{-1}).

A generic interpretation of components of $\mathscr{C}_1$ can be visualized in the diagrams (4.4) and (4.5), both or which, under homogeneous weights, are $\pm$ translations

$$\begin{array}{cccc} -r^2h \rightarrow \bullet & = & \bullet \rightarrow 1 & \qquad r^2h \leftarrow \bullet = \bullet \leftarrow -1 \\ \| & & \| & \qquad \| \quad \| \\ -r^2 \rightarrow \bullet & = & \bullet \rightarrow h & \qquad r^2 \rightarrow \bullet = \bullet \leftarrow -h \end{array} \quad ; \tag{4.4}$$

along the x-axis and $\pm$ translations

$$\begin{array}{cccc} r\uparrow \bullet & = & \bullet\uparrow rh & \qquad -r\downarrow\bullet = \bullet\downarrow -rh \\ \| & & \| & \qquad \| \quad \| \\ -r^3h\uparrow\bullet & = & \bullet\uparrow -r^3 & \qquad r^3h\downarrow\bullet = \bullet\downarrow r^3 \end{array} \tag{4.5}$$

along the y-axis. Similarly, the components of $\mathscr{C}_2$, visualized in (4.6) and (4.7), under homogeneous weights, also give $\pm$ translations

$$\begin{array}{ccc} -r\downarrow \bullet & = & \bullet\uparrow rh \\ \| & & \| \\ -r^3h\uparrow\bullet & = & \bullet\downarrow r^3 \end{array} \qquad \begin{array}{ccc} r\uparrow \bullet & = & \bullet\downarrow -rh \\ \| & & \| \\ r^3h\downarrow\bullet & = & \bullet\uparrow -r^3 \end{array} ; \tag{4.6}$$

along the x-axis and ± translations

$$\begin{array}{ccc} r^2h\leftarrow\bullet & = & \bullet\rightarrow 1 \\ \| & & \| \\ -r^2\rightarrow\bullet & = & \bullet\leftarrow -h \end{array} \qquad \begin{array}{ccc} -r^2h\rightarrow\bullet & = & \bullet\leftarrow -1 \\ \| & & \| \\ r^2\leftarrow\bullet & = & \bullet\rightarrow h \end{array} \tag{4.7}$$

along the y-axis. In terms of the symbolic sequences, the resultant of $\mathscr{C}_1$ is a superposition of the *modes*

$$\begin{array}{ccc} -\text{cgat}\rightarrow\bullet & = & \bullet\rightarrow\text{agct} \\ \| & & \| \\ -\text{ctag}\rightarrow\bullet & = & \bullet\rightarrow\text{atcg} \end{array} \qquad \begin{array}{ccc} \text{cgat}\leftarrow\bullet & = & \bullet\leftarrow -\text{agct} \\ \| & & \| \\ \text{ctag}\rightarrow\bullet & = & \bullet\leftarrow -\text{atcg} \end{array} ; \tag{4.8}$$

and

$$\begin{array}{ccc} \text{gcta}\uparrow\bullet & = & \bullet\uparrow\text{gatc} \\ \| & & \| \\ -\text{tcga}\uparrow\bullet & = & \bullet\uparrow -\text{tagc} \end{array} \qquad \begin{array}{ccc} -\text{gcta}\downarrow\bullet & = & \bullet\downarrow -\text{gatc} \\ \| & & \| \\ \text{tcga}\downarrow\bullet & = & \bullet\downarrow\text{tagc} \end{array} , \tag{4.9}$$

whereas $\mathscr{C}_2$ gives a superposition of

$$\begin{array}{ccc} -\text{gcta}\downarrow\bullet & = & \bullet\uparrow\text{gatc} \\ \| & & \| \\ -\text{tcga}\uparrow\bullet & = & \bullet\downarrow\text{tagc} \end{array} \qquad \begin{array}{ccc} \text{gcta}\uparrow\bullet & = & \bullet\downarrow -\text{gatc} \\ \| & & \| \\ \text{tcga}\downarrow\bullet & = & \bullet\uparrow -\text{tagc} \end{array} ; \tag{4.10}$$

and

$$\begin{array}{ccc} \text{cgat}\leftarrow\bullet & = & \bullet\rightarrow\text{agct} \\ \| & & \| \\ -\text{ctag}\rightarrow\bullet & = & \bullet\leftarrow -\text{atcg} \end{array} \qquad \begin{array}{ccc} -\text{cgat}\rightarrow\bullet & = & \bullet\leftarrow -\text{agct} \\ \| & & \| \\ \text{ctag}\leftarrow\bullet & = & \bullet\rightarrow\text{atcg} \end{array} . \tag{4.11}$$

Figure 4.3 shows the dx and dy components of the two-dimensional dihedral D_4 Fourier transform for the frequency counts along the AGCT orbit in region 2 for the HIV1 genome.

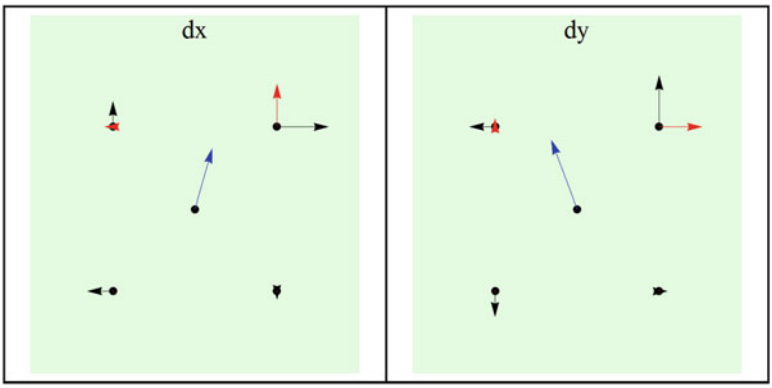

Fig. 4.3 The *dx* and *dy* components of the two-dimensional dihedral D_4 Fourier transform for the frequency counts along the AGCT orbit in region 2 for the HIV1 genome

4.4 Invariant Displays

From (4.3), the irreducibility of β implies that

$$\sum_{\sigma} \xi_\sigma \mathscr{C}_j(\sigma X) = \left(\sum_{\sigma} \xi_\sigma \beta_{\sigma^{-1}} \right) \mathscr{C}_j = 0,$$

for the $\xi = 1, \alpha, \gamma_+$ and γ_-. The corresponding invariant profiles are obtained as the superpositions of

$$\sigma X_\tau = \beta_{\sigma^{-1}\tau} q + x_\tau \beta_{\sigma^{-1}\tau} e_j = \beta_\gamma q + x_{\sigma\gamma} e_j$$

relative to $\xi = 1, \alpha, \gamma_+$ and γ_-. That is,

$$X_\gamma^\xi = \beta_\gamma q + (\sum_{\sigma} \xi_\sigma x_{\sigma\gamma}) \beta_\gamma e_j, \quad \gamma \in D_4.$$

The resulting invariant orbits for the original AGCT orbit, based on the frequency counts introduced in (4.1), are shown in (4.12)–(4.15) and corresponding Figs. 4.4–4.7. These summaries are in analogy to the visual field summaries, mentioned earlier in the Preface and Example 2.11 on page 32. Each rotated or reversed viewing of vector fields composing the image either leaves the field the same or changes the sign (direction) of the vector fields.

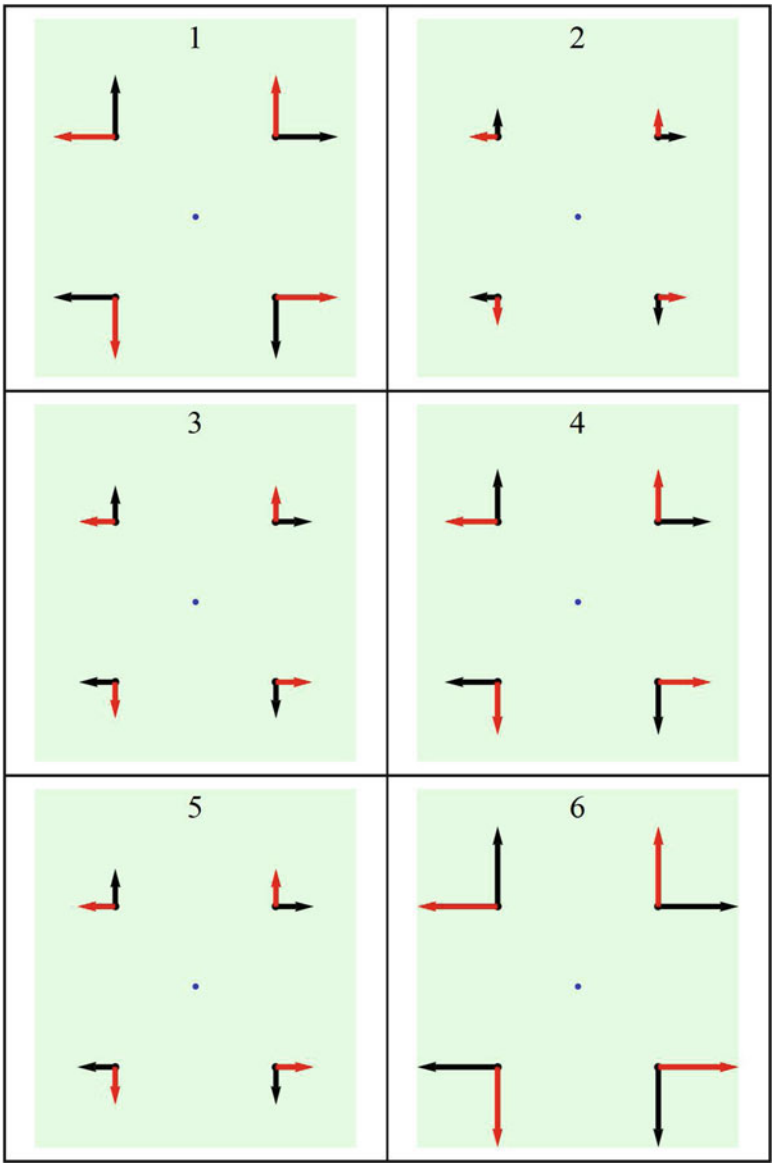

Fig. 4.4 The invariant X^1 profile for the AGCT orbit, along the six regions of the HIV genome

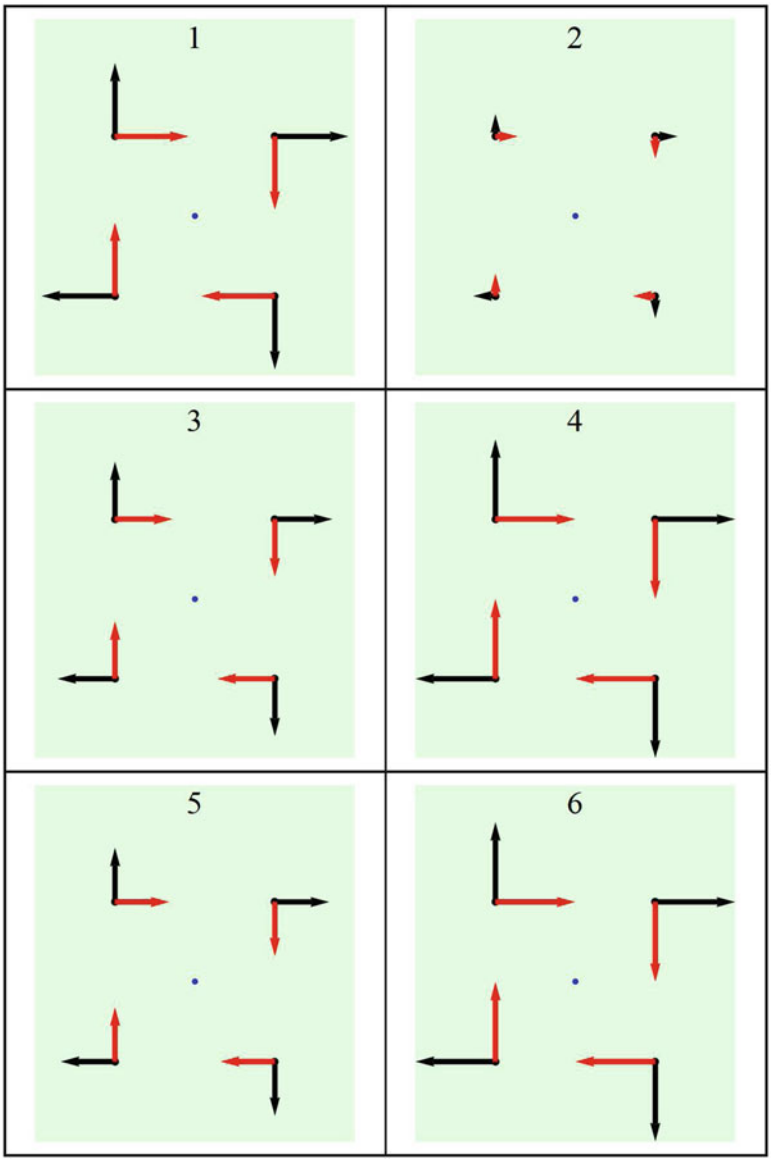

Fig. 4.5 The invariant X^{α} profile for the AGCT orbit, along the six regions of the HIV genome

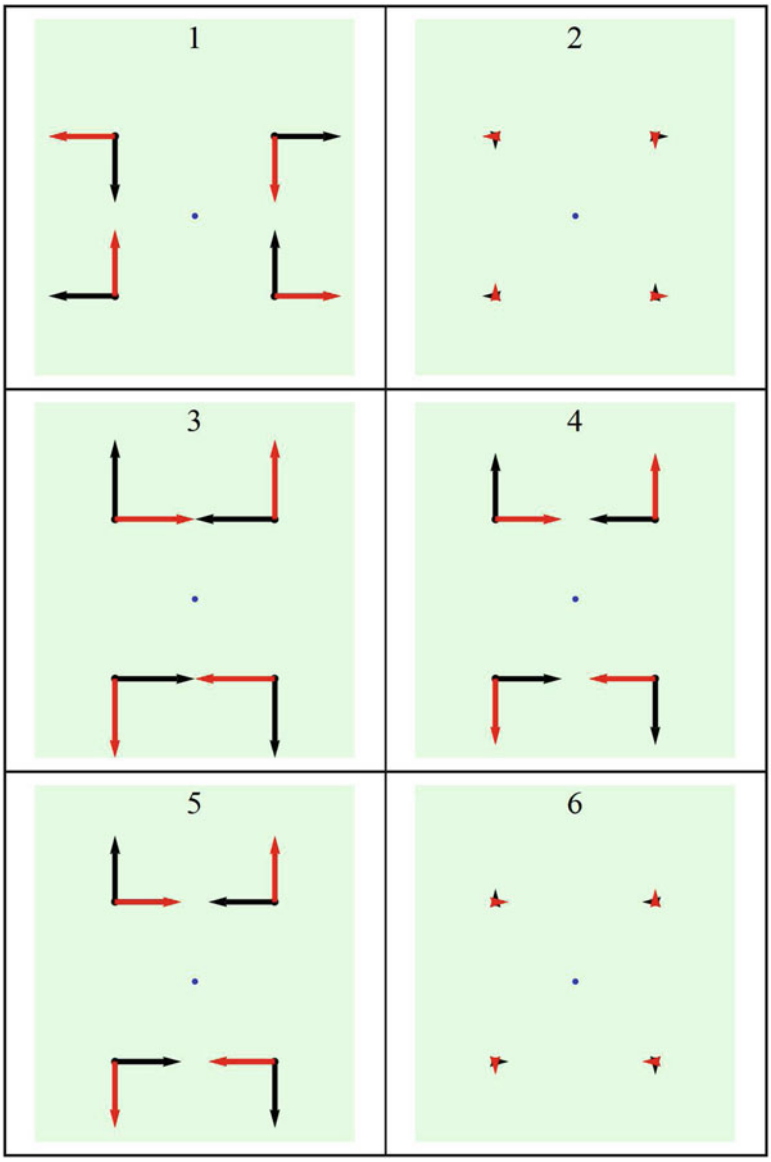

Fig. 4.6 The invariant X^{γ_+} profile for the AGCT orbit, along the six regions of the HIV genome

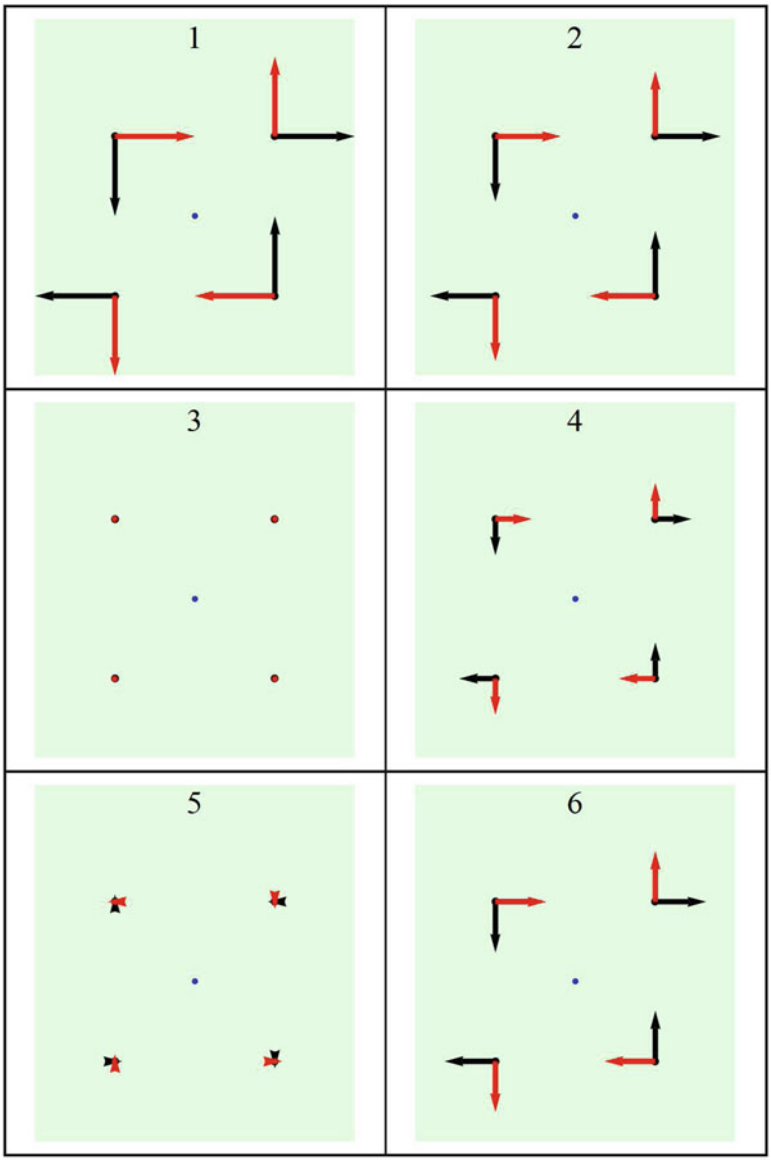

Fig. 4.7 The invariant $X^{\gamma-}$ profile for the AGCT orbit, along the six regions of the HIV genome

τ	X^1	1	2	3	4	5	6
1	$1+h+r^2h+r^2+rh+r+r^3+r^3h$	41	19	24	35	25	53
r	$1+h+r^2h+r^2+rh+r+r^3+r^3h$	41	19	24	35	25	53
r^2	$1+h+r^2h+r^2+rh+r+r^3+r^3h$	41	19	24	35	25	53
r^3	$1+h+r^2h+r^2+rh+r+r^3+r^3h$	41	19	24	35	25	53
h	$1+h+r^2h+r^2+rh+r+r^3+r^3h$	41	19	24	35	25	53
rh	$1+h+r^2h+r^2+rh+r+r^3+r^3h$	41	19	24	35	25	53
r^2h	$1+h+r^2h+r^2+rh+r+r^3+r^3h$	41	19	24	35	25	53
r^3h	$1+h+r^2h+r^2+rh+r+r^3+r^3h$	41	19	24	35	25	53

(4.12)

τ	X^α	1	2	3	4	5	6
1	$1-h-r^2h+r^2-rh+r+r^3-r^3h$	23	7	18	25	17	25
r	$1-h-r^2h+r^2-rh+r+r^3-r^3h$	23	7	18	25	17	25
r^2	$1-h-r^2h+r^2-rh+r+r^3-r^3h$	23	7	18	25	17	25
r^3	$1-h-r^2h+r^2-rh+r+r^3-r^3h$	23	7	18	25	17	25
h	$-1+h+r^2h-r^2+rh-r-r^3+r^3h$	−23	−7	−18	−25	−17	−25
rh	$-1+h+r^2h-r^2+rh-r-r^3+r^3h$	−23	−7	−18	−25	−17	−25
r^2h	$-1+h+r^2h-r^2+rh-r-r^3+r^3h$	−23	−7	−18	−25	−17	−25
r^3h	$-1+h+r^2h-r^2+rh-r-r^3+r^3h$	−23	−7	−18	−25	−17	−25

(4.13)

τ	X^{γ_+}	1	2	3	4	5	6
1	$1+h+r^2h+r^2-rh-r-r^3-r^3h$	5	1	−6	−5	−5	−1
r	$-1-h-r^2h-r^2+rh+r+r^3+r^3h$	−5	−1	6	5	5	1
r^2	$1+h+r^2h+r^2-rh-r-r^3-r^3h$	5	1	−6	−5	−5	−1
r^3	$-1-h-r^2h-r^2+rh+r+r^3+r^3h$	−5	−1	6	5	5	1
h	$1+h+r^2h+r^2-rh-r-r^3-r^3h$	5	1	−6	−5	−5	−1
rh	$-1-h-r^2h-r^2+rh+r+r^3+r^3h$	−5	−1	6	5	5	1
r^2h	$1+h+r^2h+r^2-rh-r-r^3-r^3h$	5	1	−6	−5	−5	−1
r^3h	$-1-h-r^2h-r^2+rh+r+r^3+r^3h$	−5	−1	6	5	5	1

(4.14)

τ	X^{γ_-}	1	2	3	4	5	6
1	$1-h-r^2h+r^2+rh-r-r^3+r^3h$	11	9	0	5	−1	7
r	$-1+h+r^2h-r^2-rh+r+r^3-r^3h$	−11	−9	0	−5	1	−7
r^2	$1-h-r^2h+r^2+rh-r-r^3+r^3h$	11	9	0	5	−1	7
r^3	$-1+h+r^2h-r^2-rh+r+r^3-r^3h$	−11	−9	0	−5	1	−7
h	$-1+h+r^2h-r^2-rh+r+r^3-r^3h$	−11	−9	0	−5	1	−7
rh	$1-h-r^2h+r^2+rh-r-r^3+r^3h$	11	9	0	5	−1	7
r^2h	$-1+h+r^2h-r^2-rh+r+r^3-r^3h$	−11	−9	0	−5	1	−7
r^3h	$1-h-r^2h+r^2+rh-r-r^3+r^3h$	11	9	0	5	−1	7

(4.15)

4.5 A Class of D_4 Orbit Invariants

We recall that the $H = -\sum_j p_j \log p_j$ of a finite set of n mutually exclusive events with corresponding probabilities $p_1, \ldots, p_n$ is a measure of the amount of uncertainty associated with those events [12, p. 3]. Its value is zero when any of the events is certain, it is positive otherwise, and attains its maximum value ($\log n$) when the events are equally likely, that is, $p_1 = \ldots = p_n = 1/n$, or the uniform distribution case. Alternatively [13, p.7], H is the mean value of the quantities $-\log p_j$ and can be interpreted as the mean information in an observation obtained to ascertain the mutually exclusive and exhaustive (hypotheses defined by those) events.

The orbit invariants, from Example 2.6 on page 19, are just the Fourier transforms, written here in short notation ($\tau \equiv x_\tau$):

- $< x, 1 >= 1 + r + r^2 + r^3 + h + rh + r^2h + r^3h$;
- $< x, \alpha >= 1 + r + r^2 + r^3 - h - rh - r^2h - r^3h$;
- $< x, \gamma_+ >= 1 - r + r^2 - r^3 + h - rh + r^2h - r^3h$;
- $< x, \gamma_- >= 1 - r + r^2 - r^3 - h + rh - r^2h + r^3h$;
- $< x, \beta >= \begin{bmatrix} 1 - r^2 + h - r^2h & -r + r^3 + rh - r^3h \\ r - r^3 + rh - r^3h & 1 - r^2 - h + r^2h \end{bmatrix}$.

To properly summarize the frequency counts, avoiding eventual negative sums, we evaluate the *signed* two-component transforms

$$\mathscr{L}_\alpha = \left(1 + r + r^2 + r^3, h + rh + r^2h + r^3h\right),$$

$$\mathscr{L}_{\gamma_+} = \left(1 + h + r^2 + r^2h,\ r + r^3 + rh + r^3h\right),$$

$$\mathscr{L}_{\gamma_-} = \left(1 + r^2 + rh + r^3h,\ h + r + r^3 + r^2h\right),$$

by summing the positive ($\xi = 1$) and negative-signed ($\xi = -1$) counts as a two-component distribution $\mathscr{L}_\xi = (f_+^\xi, f_-^\xi)$. Similarly, the entries of $< x, \beta >$ lead to the two-component transform $\mathscr{L}_\beta$ with entries

$$\mathscr{L}_{11} = \left(1 + h,\ r^2 + r^2h\right),\ \ \mathscr{L}_{12} = \left(r^3 + rh,\ r + r^3h\right),$$

$$\mathscr{L}_{21} = \left(r + rh,\ r^3 + r^3h\right),\ \ \mathscr{L}_{22} = \left(1 + r^2h,\ h + r^2\right).$$

Then, defining

$$-\mathscr{L} = (f_-, f_+) \equiv \mathscr{L}^\perp,$$

direct verification shows that

$$\tau \mathscr{L}_\xi = \xi_{\tau^{-1}} \mathscr{L}_\xi,$$

for all $\tau \in D_4$ and $\xi = \alpha, \gamma_+, \gamma_-, \beta$. Moreover, indicating by Ent $\mathscr{L}$ the entropy of $\mathscr{L}$ (as a properly normalized relative frequency distribution), we have

$$\text{Ent } \mathscr{L}_\xi = \text{Ent } \mathscr{L}_\xi^\perp, \tag{4.16}$$

for $\xi = \alpha, \gamma_+, \gamma_-$. When $\xi = \beta$, the interpretation of $\tau\mathscr{L}_\xi = \xi_{\tau^{-1}}\mathscr{L}_\xi$ is that the column spaces of $\mathscr{L}_\beta$ are invariant subspaces. However, because β_τ is always one of the matrices

$$\begin{pmatrix} 1 & 0 \\ 0 & 1 \end{pmatrix}, \begin{pmatrix} 0 & -1 \\ 1 & 0 \end{pmatrix}, \begin{pmatrix} -1 & 0 \\ 0 & -1 \end{pmatrix}, \begin{pmatrix} 0 & 1 \\ -1 & 0 \end{pmatrix}, \begin{pmatrix} 1 & 0 \\ 0 & -1 \end{pmatrix}, \begin{pmatrix} 0 & 1 \\ 1 & 0 \end{pmatrix}, \begin{pmatrix} -1 & 0 \\ 0 & 1 \end{pmatrix}, \begin{pmatrix} 0 & -1 \\ -1 & 0 \end{pmatrix},$$

it follows that for all $\tau \in D_4$

$$\text{Ent } \tau\{\mathscr{L}_{1i}, \mathscr{L}_{2i}\} \in \{\text{Ent } \mathscr{L}_{1i}, \text{Ent } \mathscr{L}_{2i}\}, \ \ i = 1, 2,$$

so that the extreme (column) entropies,

$$\max \text{Ent } \{\mathscr{L}_{1i}, \mathscr{L}_{2i}\}, \quad \min \text{Ent } \{\mathscr{L}_{1i}, \mathscr{L}_{2i}\}, \ \ i = 1, 2, \tag{4.17}$$

are dihedral D_4 orbit constants, or invariants. In summary, we have:

Proposition 4.2. *The (relative) frequency count summaries*

$$\textit{Ent } \mathscr{L}_\alpha, \ \textit{Ent } \mathscr{L}_{\gamma_+}, \ \textit{Ent } \mathscr{L}_{\gamma_-},$$

and

$$\max \textit{Ent } \{\mathscr{L}_{1i}, \mathscr{L}_{2i}\}, \ \min \textit{Ent } \{\mathscr{L}_{1i}, \mathscr{L}_{2i}\}, \ \ i = 1, 2,$$

are dihedral D_4 invariants.

4.6 Entropy Displays

Referring to the frequency counts shown in (4.1) we evaluated the invariants in each of the six regions, based on the frequency distributions defined (in the AGCT orbit) by

$$\mathscr{L}_\alpha = \{\text{AGCT} + \text{CTAG} + \text{GCTA} + \text{TAGC}, \ \text{ATCG} + \text{CGAT} + \text{GATC} + \text{TCGA}\},$$

$$\mathscr{L}_{\gamma_+} = \{\text{AGCT} + \text{CTAG} + \text{GATC} + \text{TCGA}, \ \text{ATCG} + \text{CGAT} + \text{GCTA} + \text{TAGC}\},$$

$$\mathscr{L}_{\gamma_-} = \{\text{AGCT} + \text{ATCG} + \text{CGAT} + \text{CTAG}, \ \text{GATC} + \text{GCTA} + \text{TAGC} + \text{TCGA}\},$$

and

$$\mathscr{L}_\beta = \begin{pmatrix} \{\text{AGCT} + \text{TCGA}, \ \text{CTAG} + \text{GATC}\} & \{\text{CGAT} + \text{TAGC}, \ \text{ATCG} + \text{GCTA}\} \\ \{\text{CGAT} + \text{GCTA}, \ \text{ATCG} + \text{TAGC}\} & \{\text{AGCT} + \text{GATC}, \ \text{CTAG} + \text{TCGA}\} \end{pmatrix}.$$

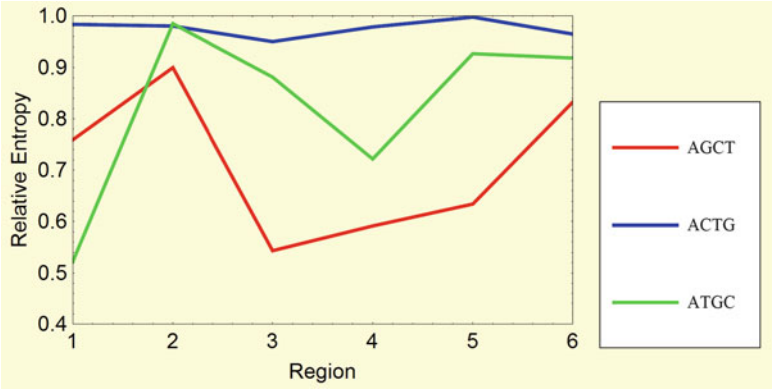

Fig. 4.8 The rotation-reversal Ent $\mathscr{L}_\alpha$ relative entropy profiles for the D_4 orbits of AGCT, ACTG, and ATGC

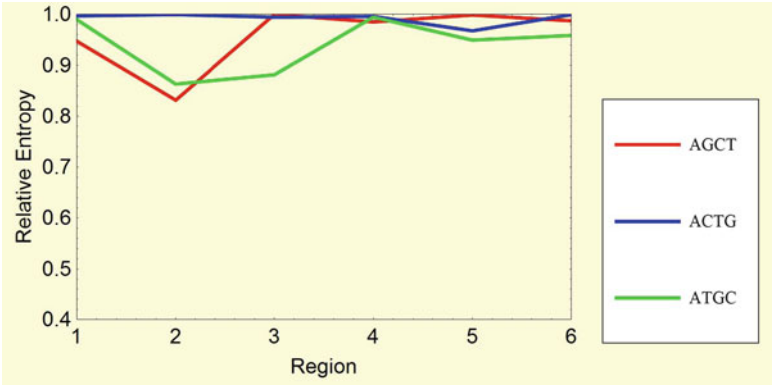

Fig. 4.9 The Ent $\mathscr{L}_{\gamma_+}$ invariant relative entropy profiles for the D_4 orbits of AGCT, ACTG, and ATGC

For example, the total frequency count for rotations in the AGCT orbit in region 1 is

$$1 + r + r^2 + r^3 = 11 + 7 + 9 + 5 = 31,$$

and

$$h + rh + r^2h + r^3h = 2 + 2 + 4 + 1 = 9,$$

for reversals, so that $\mathscr{L}_\alpha = (32, 9)$ and Ent $\mathscr{L}_\alpha = 0.52629$. The maximum entropy for a two-part distribution in 0.693147, so that we evaluated the relative entropy as the fraction of the max entropy. In this case, we have $0.52629/0.693147 = 0.759276$. The same evaluation, along the six consecutive regions, gives the rotation-reversal profile

$$\text{Ent}\,\mathscr{L}_\alpha = \{0.759276, 0.899744, 0.543565, 0.591673, 0.63431, 0.832946\}$$

for the AGCT orbit. Figure 4.8 shows the profiles for the three distinct D_4 orbits, based on the frequency counts in (4.1). The remaining profiles are shown in Figs. 4.9–4.12.

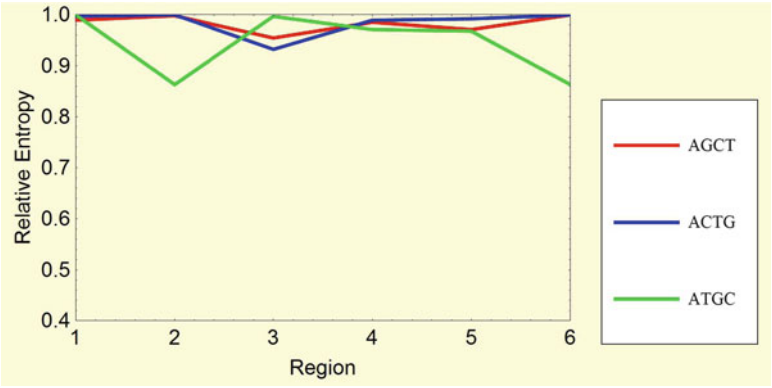

Fig. 4.10 The Ent $\mathscr{L}_{\gamma\_}$ invariant relative entropy profiles for the D_4 orbits of AGCT, ACTG, and ATGC

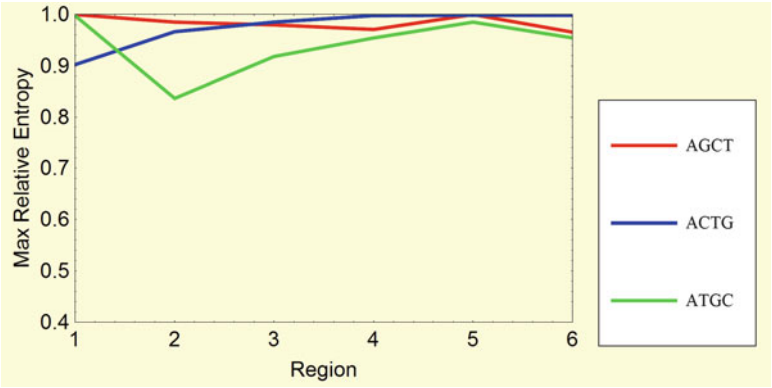

Fig. 4.11 The max Ent $\{\mathscr{L}_{11}, \mathscr{L}_{21}\}$ invariant relative entropy profiles for the D_4 orbits of AGCT, ACTG, and ATGC

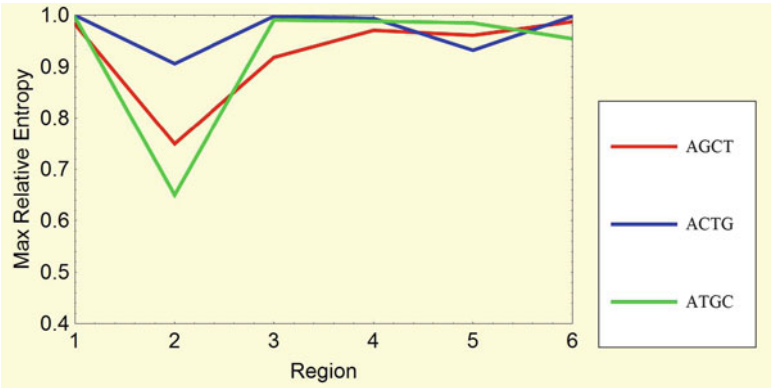

Fig. 4.12 The max Ent $\{\mathscr{L}_{12}, \mathscr{L}_{22}\}$ invariant relative entropy profiles for the D_4 orbits of AGCT, ACTG, and ATGC

Problems

4.1. The following table

$\mathcal{O}$	1	2	3
AGCT	112	92	84
GCTA	54	44	32
CTAG	17	6	4
TAGC	52	34	16
ATCG	84	111	53
GATC	72	89	47
CGAT	65	137	82
TCGA	37	81	46

gives the frequency counts along a D_4 dihedral orbit on three equal-length consecutive regions of the Salmonella virus,[2] spanning the complete $93,877$ BP-long genome. Similarly, the following table

$\mathcal{O}$	1	2	3
AGCT	0	1	4
GCTA	0	2	1
CTAG	0	2	3
TAGC	1	1	2
ATCG	4	1	3
GATC	5	6	3
CGAT	3	1	1
TCGA	5	0	5

gives the corresponding frequency counts for the $2,761$ BP-long Tobbaco virus.[3]

1. Study, in each one of the three regions, the entropy of the dihedral invariants (as Fourier transforms) for the Salmonella virus.
2. Study, in each one of the three regions, the entropy of the dihedral invariants (as Fourier transforms) for the Tobacco virus.
3. Propose a method to statistically assess the chirality hypothesis, as the interpretation of the $< x, \xi_\alpha >$ invariant.
4. Based on the methodology proposed above, study the chirality of both genomes, in each one of the regions.
5. Study the large-sample distribution of the entropy associated with each dihedral invariant (as Fourier transforms).
6. Propose a Monte Carlo method to compare the chirality entropy of the two genomes, in each region.

[2] Accession *NC*_017054.1 Salmonella enterica subsp. enterica serovar Typhimurium str., complete sequence.

[3] Accession *NC*_004654.1 Tobacco leaf curl Japan virus, complete genome.

Appendix A: Selected Computational Tools

The following routines are executable in (Wolfram Research, Champaign, IL) Mathematica.

D_4 Orbit Generation

Auxiliary Cell Expressions

```
myd4 := {Cycles[{}], Cycles[{{1, 4, 3, 2}}],
  Cycles[{{1, 3}, {2, 4}}], Cycles[{{1, 2, 3, 4}}],
  Cycles[{{2, 4}}], Cycles[{{1, 2}, {3, 4}}],
  Cycles[{{1, 3}}],
  Cycles[{{1, 4}, {2, 3}}]} (*auxiliary cell*)
```

Main Cell Expressions

```
d4orbit[s1_, s2_, s3_, s4_] :=
 DeleteDuplicates[
   Table[StringJoin[
     Permute[{SymbolName[s1], SymbolName[s2],
              SymbolName[s3],
       SymbolName[s4]}, myd4[[j]]]], {j, 1, 8}]]
```

Usage

```
In[]:= d4orbit[A,G,C,T]
Out[]= {AGCT,GCTA,CTAG,TAGC,ATCG,GATC,CGAT,TCGA}

In[]:= d4orbit[A,G,A,T]
Out[]= {AGAT,GATA,ATAG,TAGA}

In[]:= d4orbit[A,G,A,G]
Out[]= {AGAG,GAGA}

In[]:= d4orbit[A,A,A,A]
Out[]= {AAAA}
```

D_4 Orbit Generation and Frequency Counts

Auxiliary Cell Expressions

```
length[seq_] := StringLength[seq[Sequence]][[1]]
```

```
unicount[word_, seq_, nr_] :=
 Table[Length[
   StringPosition[
    StringTake[
     seq[Sequence][[1]],
         {1 + (i - 1)*Floor[ length[seq]/nr ],
          i*Floor[ length[seq]/nr ]}],
          SymbolName[word]]], {i, 1, nr}]
```

Main Cell Expressions

```
matd4orbit[s1_, s2_, s3_, s4_, seq_, nr_] :=
 Join[
    Table[{Symbol[d4orbit[s1, s2, s3, s4][[j]]]}, {j, 1,
      Length[d4orbit[s1, s2, s3, s4]]}],
    Table[unicount[Symbol[
          d4orbit[s1, s2, s3, s4][[j]]], seq, nr],
     {j,1, Length[d4orbit[s1, s2, s3, s4]]}], 2]
       // MatrixForm
```

Usage

The cell expression

```
matd4orbit[s1_, s2_, s3_, s4_, seq_, nr_]
```

generates the frequency counts for the D_4 orbit of **s1, s2, s3, s4** in **nr** adjacent equal-length regions in the sequence **seq**, given in FASTA format.

```
In[] matd4orbit[A, G, C, T, hiv1, 2]
```

Out[]:

$$\begin{pmatrix} \text{AGCT} & 22 & 26 \\ \text{GCTA} & 13 & 24 \\ \text{CTAG} & 16 & 19 \\ \text{TAGC} & 16 & 21 \\ \text{ATCG} & 1 & 3 \\ \text{GATC} & 12 & 13 \\ \text{CGAT} & 3 & 3 \\ \text{TCGA} & 2 & 4 \end{pmatrix}$$

Chapter 5
Symmetry Preference and Perception

5.1 Introduction

The human tendency of pairing asymmetrical images in a way that gives preference to stimuli that more closely approach perfection has been observed in more general contexts, e.g., [14]. The flag preference data described in Chap. 1 suggest that hidden in the first-to-second rankings is the preference for matching the two flags in a way that one is a vertical reflection image of the other. This demonstration was repeated again with a second group of 13 subjects, thus producing a total of 78 rankings. In the second demonstration, the flags had the same coloring and were squares in shape instead of rectangular. The results, summarized in (5.1), are strikingly similar to the those introduced in (1.2), on page 2.

	A	B	C	D	total
A	0	4	2	14	20
B	2	0	15	2	19
C	3	17	0	2	22
D	14	2	1	0	17
total	19	23	18	18	78

(5.1)

Subsequently, another set of data was obtained from a modified set of flags, shown in Fig. 5.1, with the same purpose of ranking the flags in each row according to one's preference. Subjects were in the same age group (college students) as in the other rankings. The distribution of the first-to-second transition counts is shown in (5.2).

M.A.G. Viana and V. Lakshminarayanan, *Dihedral Fourier Analysis: Data-Analytic Aspects and Applications*, Lecture Notes in Statistics 206,
DOI 10.1007/978-1-4614-5562-2_1, © Springer Science+Business Media New York 2013

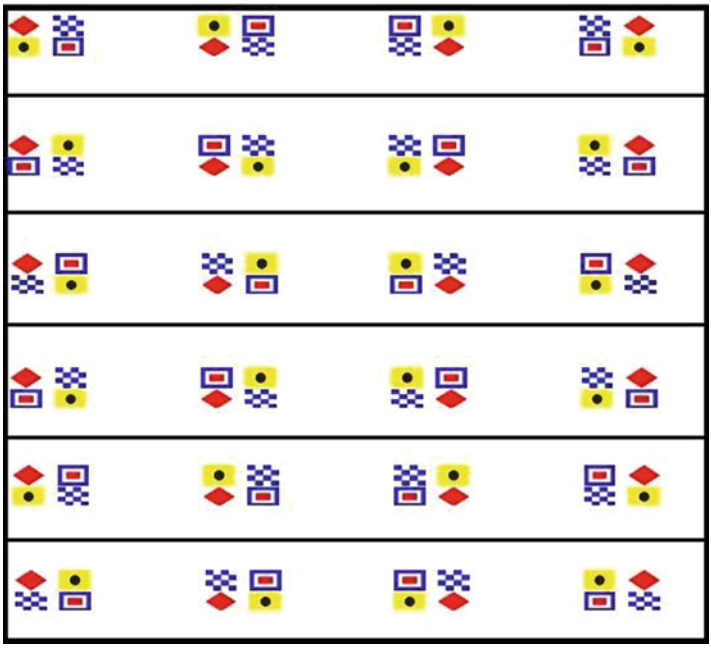

Fig. 5.1 The set of flags for the modified symmetry perception data

	A	*B*	*C*	*D*	total
A	0	37	17	26	80
B	34	0	52	23	109
C	20	35	0	37	92
D	34	15	24	0	73
total	88	87	93	86	354

, (5.2)

The objective of this chapter is describing the orbit structure of the aggregated frequency counts, such as those in (5.1) or (5.2) together with the full set of rankings.

5.2 The D_2 Orbit Structure in S_4

The sets of flags shown in Fig. 1.1 on page 2 or Fig. 5.1 correspond to the 24 distinct permutations of their four colors or patterns, respectively. As mentioned earlier, using the colored (*Y*ellow, *B*lack, *G*reen, and *R*ed) set as a reference, the first row is generated as the D_2 orbit

$$\mathscr{O}_1 = \{\text{YBGR} = \begin{matrix} Y & \!\!=\!\!= & B \\ \| & & \| \\ G & \!\!=\!\!= & R \end{matrix}, \ \text{GRYB}, \text{RGBY}, \text{BYRG}\},$$

and the subsequent ones by letting

$$D_3 = \{1, r, r^2, h, rh, r^2h\}$$

act on the $\{B, G, R\}$ colors while fixing the yellow-colored corner:

$$\mathscr{O}_r = \{\text{YGRB} = \begin{matrix} Y & \!\!=\!\!= & G \\ \| & & \| \\ R & \!\!=\!\!= & B \end{matrix}, \ \text{RBYG}, \text{BRGY}, \text{GYBR}\},$$

$$\mathscr{O}_{r^2} = \{\text{YRBG} = \begin{matrix} Y & \!\!=\!\!= & R \\ \| & & \| \\ B & \!\!=\!\!= & G \end{matrix}, \ \text{BGYR}, \text{GBRY}, \text{RYGB}\},$$

$$\mathscr{O}_h = \{\text{YBRG} = \begin{matrix} Y & \!\!=\!\!= & B \\ \| & & \| \\ R & \!\!=\!\!= & G \end{matrix}, \ \text{RGYB}, \text{GRBY}, \text{BYGR}\},$$

$$\mathscr{O}_{rh} = \{\text{YRGB} = \begin{matrix} Y & \!\!=\!\!= & R \\ \| & & \| \\ G & \!\!=\!\!= & B \end{matrix}, \ \text{GBYR}, \text{BGRY}, \text{RYBG}\},$$

$$\mathscr{O}_{r^2h} = \{\text{YGBR} = \begin{matrix} Y & \!\!=\!\!= & G \\ \| & & \| \\ B & \!\!=\!\!= & R \end{matrix}, \ \text{BRYG}, \text{RBGY}, \text{GYRB}\}.$$

The resulting orbits are then indexed by $D_3 \simeq S_3$ and the elementary structure of the full set of flags is $S_4/D_2 \simeq D_3$. The same structure is present in the set of flags shown in Fig. 5.1.

Correspondingly, the within-orbit first-to-second preference transition counts,

$$\mathscr{T}_1 = \begin{pmatrix} 0 & 7 & 7 & 2 \\ 3 & 0 & 6 & 0 \\ 3 & 8 & 0 & 9 \\ 7 & 2 & 5 & 0 \end{pmatrix}, \ \mathscr{T}_r = \begin{pmatrix} 0 & 6 & 4 & 6 \\ 7 & 0 & 9 & 5 \\ 2 & 10 & 0 & 2 \\ 4 & 2 & 2 & 0 \end{pmatrix}, \ \mathscr{T}_{r^2} = \begin{pmatrix} 0 & 6 & 2 & 5 \\ 4 & 0 & 9 & 4 \\ 4 & 5 & 0 & 7 \\ 3 & 6 & 4 & 0 \end{pmatrix},$$

$$\mathscr{T}_h = \begin{pmatrix} 0 & 2 & 2 & 2 \\ 7 & 0 & 10 & 7 \\ 3 & 3 & 0 & 4 \\ 10 & 4 & 5 & 0 \end{pmatrix}, \quad \mathscr{T}_{rh} = \begin{pmatrix} 0 & 8 & 1 & 4 \\ 6 & 0 & 4 & 5 \\ 3 & 5 & 0 & 11 \\ 10 & 1 & 1 & 0 \end{pmatrix}, \quad \mathscr{T}_{r^2h} = \begin{pmatrix} 0 & 8 & 1 & 7 \\ 7 & 0 & 14 & 2 \\ 5 & 4 & 0 & 4 \\ 0 & 0 & 7 & 0 \end{pmatrix}$$

give a decomposition

$$\begin{pmatrix} 0 & 37 & 17 & 26 \\ 34 & 0 & 52 & 23 \\ 20 & 35 & 0 & 37 \\ 34 & 15 & 24 & 0 \end{pmatrix} = \sum_{\tau} \mathscr{T}_{\tau}$$

of the total count (5.2) that is also indexed by D_3. The first-to-second preference counts are embedded in the distribution $\mathscr{R}$ of the frequency counts for the complete four-flag rankings, that, accordingly, allows for a decomposition $\mathscr{R} = \sum \mathscr{R}_{\tau}$ presented in the table shown in (5.3).

Permutation	$\mathscr{R}_1$	$\mathscr{R}_r$	$\mathscr{R}_{r^2}$	$\mathscr{R}_h$	$\mathscr{R}_{rh}$	$\mathscr{R}_{r^2h}$	$\mathscr{R}$
abcd	6	4	5	1	6	5	27
abdc	1	2	1	1	2	3	10
acbd	6	2	2	1	1	0	12
acdb	1	2	0	1	0	1	5
adbc	2	4	3	1	3	3	16
adcb	0	2	2	1	1	4	10
bacd	0	5	2	2	3	6	18
badc	3	2	2	5	3	1	16
bcad	2	5	4	3	0	8	22
bcda	4	4	5	7	4	6	30
bdac	0	2	3	6	3	2	16
bdca	0	3	1	1	2	0	7
cabd	1	1	2	1	2	2	9
cadb	2	1	2	2	1	3	11
cbad	5	6	3	1	3	3	21
cbda	3	4	2	2	2	1	14
cdab	4	0	3	1	8	1	17
cdba	5	2	4	3	3	3	20
dabc	2	3	2	5	4	0	16
dacb	5	1	1	5	6	0	18
dbac	0	2	3	1	1	0	7
dbca	2	0	3	3	0	0	8
dcab	2	0	4	2	0	3	11
dcba	3	2	0	3	1	4	13

(5.3)

Clearly, each ij entry in the first-to-second preference count matrices is obtained as the sum of the frequency counts for the rankings $ijxy + ijyx$ for the choices x, y complementary to i, j in $\{a, b, c, d\}$. For example, the frequency counts for transitions (A,D), (D,A), (B,C), and (C,B) associated with vertically transformed first-second choices are obtained as the total for the sums of the frequencies for the rankings adbc + adcb, dabc + dacb, bcad + bcda, and cbad + cbda respectively. Given, say,

$$\mathscr{T}_1 = \begin{pmatrix} 0 & 7 & 7 & 2 \\ 3 & 0 & 6 & 0 \\ 3 & 8 & 0 & 9 \\ 7 & 2 & 5 & 0 \end{pmatrix},$$

and $\mathscr{R}_1$ in (5.3), we have $2 = (\text{A,D}) = \text{adbc} + \text{adcb} = 2 + 0$, $7 = (\text{D,A}) = \text{dabc} + \text{dacb} = 2 + 5$, $6 = (\text{B,C}) = \text{bcad} + \text{bcda} = 2 + 4$, and $8 = (\text{C,B}) = \text{cbad} + \text{cbda} = 5 + 3$.

5.3 The Dihedral D_2 Summaries

The D_2 dihedral analysis based on the overall transitions

$$\begin{pmatrix} 0 & 37 & 17 & 26 \\ 34 & 0 & 52 & 23 \\ 20 & 35 & 0 & 37 \\ 34 & 15 & 24 & 0 \end{pmatrix} = \sum_{\tau} \mathscr{T}_{\tau}$$

is the analysis of the $\mathbb{C}D_2$ data, in the same notation of Chap. 1,

$$V = 26 + 34v + 52h + 35r,$$

$$H = 37 + 24v + 34h + 37r,$$

$$R = 17 + 24v + 23h + 20r.$$

$$(< V, \xi_1 >, < H, \xi_1 >, < R, \xi_1 >) = (147, 132, 75),$$

as described earlier in Chap. 1, page 7, gives the posterior (marginal) densities

$$\mathscr{L}_v \sim Be(148, 208),\ \mathscr{L}_h \sim Be(133, 223),\ \mathscr{L}_r \sim Be(76, 280),$$

relative to uniform prior, shown in Fig. 5.2. When compared with the Fig. 1.2, it becomes evident that the preference to matching first and second-choice flags by a vertical reflection image of each other was lessened by the patterned (perhaps distracting) style of the flags in the present data. Furthermore, each orbit gives the additional component summaries $< x, \xi >$ relative to the remaining characters

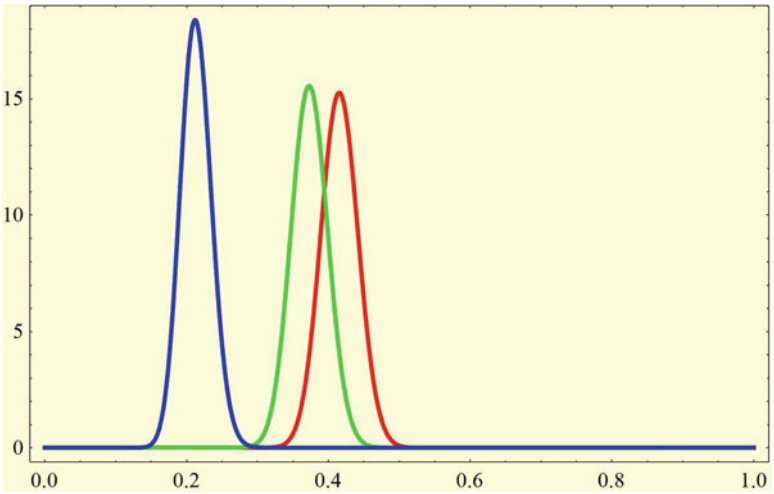

Fig. 5.2 Posterior densities for the probabilities of matching first and second-choice flags by a vertical (*red*), horizontal (*green*), and double-reflection (*blue*) image of each other

	1	h	v	r
ξ^1	1	1	1	1
ξ^h	1	1	−1	−1
ξ^v	1	−1	1	−1
ξ^r	1	−1	−1	1

,

from (1.9), on page 5. Specifically, we obtain, in analogy with the dihedral analysis presented in Chap. 4,

$$< V, \xi > \mapsto \begin{cases} \mathscr{L}_v & = (60, 87) \\ \mathscr{L}_h & = (78, 69) \\ \mathscr{L}_r & = (61, 86) \end{cases},$$

that can be summarized, by Proposition 4.2 on page 71, by their minimum entropy

$$\min\{\text{Ent}\,\mathscr{L}_v, \text{Ent}\,\mathscr{L}_h, \text{Ent}\,\mathscr{L}_r\} = 0.676;$$

Similarly,

$$< H, \xi > \mapsto \begin{cases} \mathscr{L}_v & = (61, 71) \\ \mathscr{L}_h & = (71, 61) \\ \mathscr{L}_r & = (74, 58) \end{cases},$$

with

$$\min\{\text{Ent}\,\mathscr{L}_v, \text{Ent}\,\mathscr{L}_h, \text{Ent}\,\mathscr{L}_r\} = 0.685;$$

and

$$< R, \xi > \mapsto \begin{cases} \mathscr{L}_v & = (41, 43) \\ \mathscr{L}_h & = (40, 44)\,, \\ \mathscr{L}_r & = (37, 47) \end{cases}$$

with

$$\min\{\text{Ent}\,\mathscr{L}_v, \text{Ent}\,\mathscr{L}_h, \text{Ent}\,\mathscr{L}_r\} = 0.680.$$

In each orbit, these are invariant summaries of components of variability, so that the interpretation is that these components do not show a substantially different variability.

5.4 The Dihedral D_3 Summaries

In this section we look at the within-orbit first-to-second preference transition counts $\mathscr{T}_\tau$, $\tau \in D_3$ described in Sect. 5.2. From Chap. 2 on page 19, the one-dimensional invariant summaries are the Fourier transforms

$$< \mathscr{T}, \xi_1 > = \sum_\tau \mathscr{T}_\tau = \begin{pmatrix} 0 & 37 & 17 & 26 \\ 34 & 0 & 52 & 23 \\ 20 & 35 & 0 & 37 \\ 34 & 15 & 24 & 0 \end{pmatrix},$$

and

$$\begin{aligned} < \mathscr{T}, \xi_\alpha > &= \mathscr{T}_1 + \mathscr{T}_r + \mathscr{T}_{r^2} - (\mathscr{T}_h + \mathscr{T}_{rh} + \mathscr{T}_{r^2h}) \\ &= \begin{pmatrix} 0 & 19 & 13 & 13 \\ 14 & 0 & 24 & 9 \\ 9 & 23 & 0 & 18 \\ 14 & 10 & 11 & 0 \end{pmatrix} - \begin{pmatrix} 0 & 18 & 4 & 13 \\ 20 & 0 & 28 & 14 \\ 11 & 12 & 0 & 19 \\ 20 & 5 & 13 & 0 \end{pmatrix}, \end{aligned}$$

where $\mathscr{T}$ is a point in the group ring $\mathscr{R}D_3$. Here, as in the previous summaries for frequency data, we evaluate the relative entropy in the rotation-reversal distributions in the corresponding matrix entries. The relative entropy is the entropy of the relative frequency distribution as a fraction of the corresponding uniform distribution. The results, summarized in (5.4), identify a potential sensitivity of (A,C) transitions to the two types of orbits.

$$\begin{pmatrix} * & 0.999473 & \boxed{0.787127} & 1. \\ 0.977418 & * & 0.995727 & 0.965636 \\ 0.992774 & 0.927527 & * & 0.999473 \\ 0.977418 & 0.918296 & 0.994985 & * \end{pmatrix}. \tag{5.4}$$

The two-dimensional invariant is the transform $< \mathscr{T}, \beta >$, for $\mathscr{T} \in \mathscr{R}D_3$, may be expressed as

$$< \mathscr{T}, \beta > = \sum \mathscr{T}_\tau \otimes \beta_\tau$$

to jointly describe the transforms evaluated at each scalar entry of $\mathscr{T}$ as points in the group algebra $\mathbb{C}D_3$ of D_3. Matrix (5.5) shows the comparison

$$\sum_{\text{rotations}} \mathscr{T}_\tau \otimes \beta_\tau - \sum_{\text{reversals}} \mathscr{T}_\tau \otimes \beta_\tau$$

between rotations and reversals. Each off-diagonal 2×2 matrix gives the above comparison for the corresponding transition frequency count. See also Problem 5.2 in this chapter.

$$\left(\begin{array}{cc|cc|cc|cc} 0 & 0 & 7.00 & 0 & 3.00 & -1.73 & 0 & 1.73 \\ 0 & 0 & 0 & -5.00 & 1.73 & 5.00 & 3.46 & -7.00 \\ \hline -3.00 & -1.73 & 0 & 0 & -4.00 & 8.66 & -8.00 & -3.46 \\ 3.46 & -2.00 & 0 & 0 & 8.66 & -2.00 & -1.73 & -1.00 \\ \hline 1.00 & 3.46 & 2.00 & -5.20 & 0 & 0 & 8.00 & -1.73 \\ 0 & -1.00 & 3.46 & -1.00 & 0 & 0 & -10.4 & 1.00 \\ \hline -1.50 & -9.53 & -5.50 & 2.60 & 1.00 & 6.93 & 0 & 0 \\ -7.79 & 8.50 & -4.33 & 1.50 & 3.46 & 3.00 & 0 & 0 \end{array}\right) \tag{5.5}$$

Problems

5.1. Show that Proposition 2.3 on page 17 holds across equivalent representations.

5.2. Verify that relative to

$$B = \begin{pmatrix} 1 & \sqrt{3} \\ 1 & -\sqrt{3} \end{pmatrix},$$

the new matrices $b_\tau = B\beta_\tau B^{-1}$, although no longer canonically unitary, are conveniently given by

$$\begin{pmatrix} 1 & 0 \\ 0 & 1 \end{pmatrix}, \begin{pmatrix} 0 & 1 \\ -1 & -1 \end{pmatrix}, \begin{pmatrix} -1 & -1 \\ 1 & 0 \end{pmatrix}, \begin{pmatrix} 0 & 1 \\ 1 & 0 \end{pmatrix}, \begin{pmatrix} 1 & 0 \\ -1 & -1 \end{pmatrix}, \begin{pmatrix} -1 & -1 \\ 0 & 1 \end{pmatrix},$$

for $\tau = 1, r, r^2, h, rh, r^2h$ respectively. Show that

$$< x, b >= \sum \tau b_\tau = \begin{pmatrix} 1 - r^2 - r^2h + rh & h + r - r^2 - r^2h \\ h - r + r^2 - rh & 1 - r + r^2h - rh \end{pmatrix},$$

or, equivalently, that

$$< x, b >= \begin{pmatrix} -\mathrm{BGR} + \mathrm{BRG} + \mathrm{GRB} - \mathrm{RGB} & -\mathrm{BGR} + \mathrm{GBR} + \mathrm{RBG} - \mathrm{RGB} \\ \mathrm{BGR} - \mathrm{BRG} + \mathrm{GBR} - \mathrm{RBG} & -\mathrm{BRG} + \mathrm{GRB} - \mathrm{RBG} + \mathrm{RGB} \end{pmatrix},$$

in terms of the D_3 orbit for the sequence BGR suggested by the construction introduced in Sect. 5.2.

5.3. Interpret, in the context of symbolic sequences, the D_3 orbit invariants obtained in Problem 5.2 above.

Chapter 6
Other Applications

6.1 Normal Modes

In this chapter we outline an application of the Fourier transform in the selection of the so-called normal modes in molecular spectroscopy, e.g., [15, p. 138], [16, p.184]. Although the Fourier transforms appear, implicitly, in [17, p.239], their usefulness in sorting out the distinct vibrational modes is not made explicit. The need for a detailed analysis of the modes comes from the fact that a typical action of a space group on the molecular framework is not transitive. Therefore, the irreducible representations appear with extra multiplicities in the factorization of the space group representation. By isolating the symmetry orbits, and thus retaining the transitivity, the separation of the modes appears with less effort. The joint vibrational scheme is then obtaining by matching the transforms according to the irreducible representations.

We will illustrate this mechanism with a simple *planar* framework, so that in each molecule we consider only the canonical (x,y) displacements. Figure 6.1 shows a five-atom framework, where atoms $1,2,3,4$, and eventually 5 as well, are interchangeable. We want to derive the normal modes effected by the action of $D_2 = \{1,h,v,o\}$ on the corresponding (x_j,y_j) displacements.

The action of D_2 on the displacements gives a representation ρ on $GL_{20}(\mathbb{R})$ that factors as

$$\rho = 6\xi^1 \oplus 5\xi^h \oplus 5\xi^v \oplus 4\xi^r,$$

where the components

	1	h	v	r
ξ^1	1	1	1	1
ξ^h	1	1	−1	−1
ξ^v	1	−1	1	−1
ξ^r	1	−1	−1	1

M.A.G. Viana and V. Lakshminarayanan, *Dihedral Fourier Analysis: Data-Analytic Aspects and Applications*, Lecture Notes in Statistics 206,
DOI 10.1007/978-1-4614-5562-2_1, © Springer Science+Business Media New York 2013

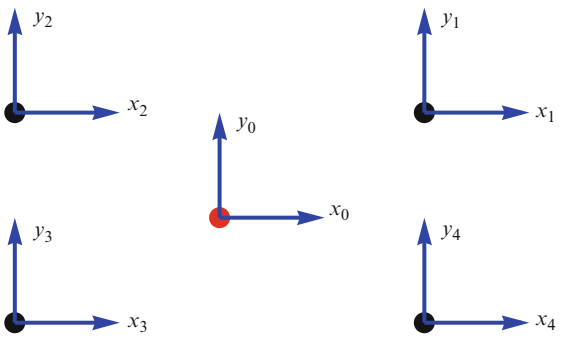

Fig. 6.1 A five-point D_2 framework

are the irreducible representations (1.9) of D_2, introduced earlier on page 5. The action of $D_2 = \{1, h, v, r\}$ gives 6 orbits, specifically:

$$\mathscr{O}_x^0 = \{x_0, x_0, -x_0, -x_0\},\ \ \mathscr{O}_x^1 = \{x_1, x_4, -x_2, -x_3\},\ \ \mathscr{O}_x^2 = \{x_2, x_3, -x_1, -x_4\},$$

$$\mathscr{O}_y^0 = \{y_0, -y_0, y_0, -y_0\},\ \ \mathscr{O}_y^1 = \{y_1, -y_4, y_2, -y_3\},\ \ \mathscr{O}_y^2 = \{y_3, -y_2, y_4, -y_1\}.$$

Next, in each orbit, we evaluate the dihedral transforms

$$\begin{aligned}
< x, \xi^1 > &= x_1 + x_h + x_v + x_r, \\
< x, \xi^h > &= x_1 + x_h - x_v - x_r, \\
< x, \xi^v > &= x_1 - x_h + x_v - x_r, \\
< x, \xi^r > &= x_1 - x_h - x_v + x_r,
\end{aligned}$$

as introduced earlier on Example 2.4 on page 19. The (component) normal modes in the x-displacement direction are obtained from the x-displacement orbits:

	$\mathscr{O}_x^0$	$\mathscr{O}_x^1$	$\mathscr{O}_x^2$
ξ^1	0	$x_1 - x_2 - x_3 + x_4$	$-x_1 + x_2 + x_3 - x_4$
ξ^h	$4x_0$	$x_1 + x_2 + x_3 + x_4$	$x_1 + x_2 + x_3 + x_4$
ξ^v	0	$x_1 - x_2 + x_3 - x_4$	$-x_1 + x_2 - x_3 + x_4$
ξ^o	0	$x_1 + x_2 - x_3 - x_4$	$x_1 + x_2 - x_3 - x_4$

,

where each component is an orbit D_2-invariant reducing as the corresponding irreducible representations ξ^1, ξ^h, ξ^v, or ξ^r. Similarly, the component normal modes in the direction of the y-displacements are

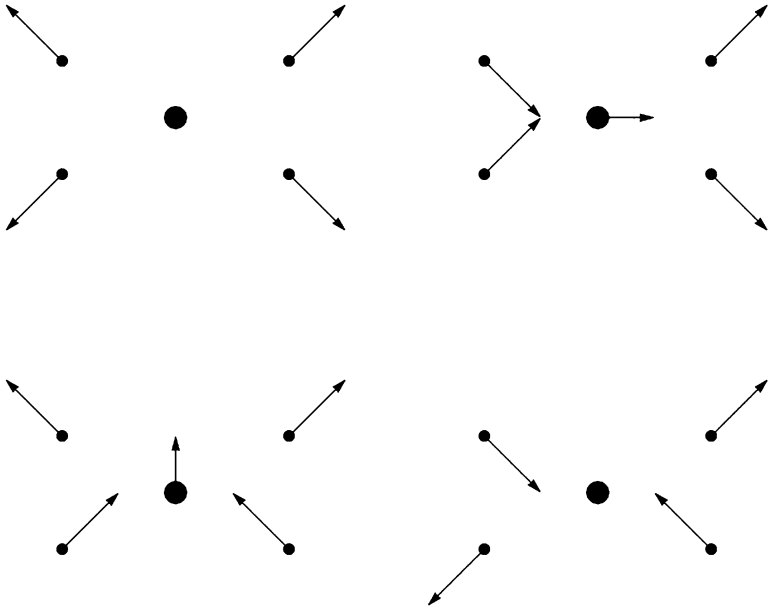

Fig. 6.2 The D_2 normal modes afforded by ξ^1 (*top left*), ξ^h (*top right*), ξ^v (*bottom left*), and ξ^r (*bottom right*)

	$\mathscr{O}_y^0$	$\mathscr{O}_y^1$	$\mathscr{O}_y^2$
ξ^1	0	$y_1+y_2-y_3-y_4$	$-y_1-y_2+y_3+y_4$
ξ^h	0	$y_1-y_2+y_3-y_4$	$y_1-y_2+y_3-y_4$
ξ^v	$4y_0$	$y_1+y_2+y_3+y_4$	$y_1+y_2+y_3+y_4$
ξ^r	0	$y_1-y_2-y_3+y_4$	$-y_1+y_2+y_3-y_4$

Figure 6.2 illustrates the superposition of the x- and y-displacements, for each irreducible representation.

It is easy to observe that in either displacements the modes induced by ξ^v and ξ^h are of the translational type (displacing the center of mass), whereas the other two are of the vibrational types.

6.2 Center of Mass Displacements

Consider effect of the D_4 field orbit

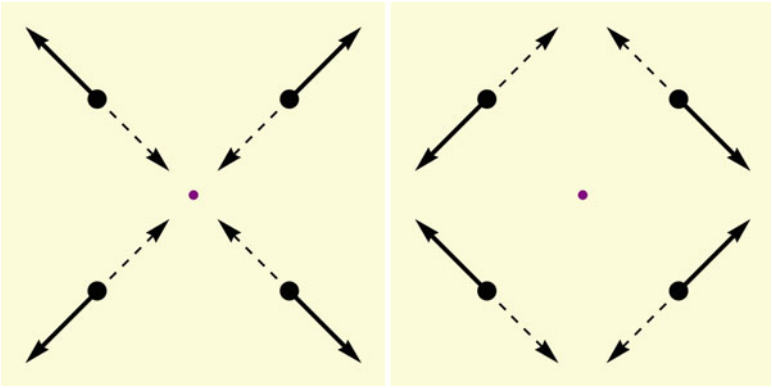

Fig. 6.3 D_4 displacements induced by the characters ξ_1 (*left*) and ξ_α (*right*). The center of mass displacement is null for homogeneous masses

$$\begin{array}{cccc} r\uparrow & \bullet_{m_1} & = & \bullet_{m_0}\rightarrow 1 \\ \| & & & \| \\ r^2 & \leftarrow\bullet_{m_2} & = & \bullet_{m_3}\downarrow r^3 \end{array} \qquad \begin{array}{cccc} r^2h\leftarrow & \bullet_{m_1} & = & \bullet_{m_0}\uparrow rh \\ \| & & & \| \\ r^3h\downarrow & \bullet_{m_2} & = & \bullet_{m_3}\rightarrow h \end{array}.$$

acting on elementary objects of mass m_0, m_1, m_2, m_3 located at the vertices

$$\{(1,1),(-1,1),(-1,-1),(1,-1)\},$$

respectively, so that the components of

$$m = (m_0, rm_1, r^2m_2, r^3m_3, rhm_0, r^2hm_1, r^3hm_2, hm_3)$$

describe the action of the position orbit on the distinct mass elements. Assuming that $m_0 + \ldots + m_3 = 1$, the (scalar components of the) Fourier transforms $< m, \xi >$ are just the center of mass for the position vectors re-oriented by the correspondent representation. Specifically, we obtain, from Example 2.6 on page 19,

$$< m, 1 >= m_0(1+rh) + m_1(r+r^2h) + m_2(r^2+r^3h) + m_3(r^3+h),$$

$$< m, \alpha >= m_0(1-rh) + m_1(r-r^2h) + m_2(r^2-r^3h) + m_3(r^3-h).$$

These are one-dimensional subspaces for the center of mass, illustrated in Fig. 6.3. Similarly,

$$< m, \gamma_+ >= m_0(1-rh) + m_1(-r+r^2h) + m_2(r^2-r^3h) + m_3(-r^3+h),$$

$$< m, \gamma_- >= m_0(1+rh) + m_1(-r-r^2h) + m_2(r^2+r^3h) + m_3(-r^3-h).$$

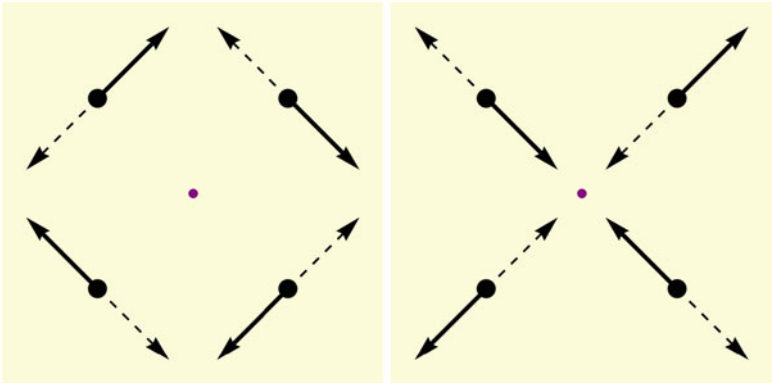

Fig. 6.4 D_4 displacements induced by the characters γ_+ (*left*) and γ_- (*right*). The center of mass displacement is null for homogeneous masses

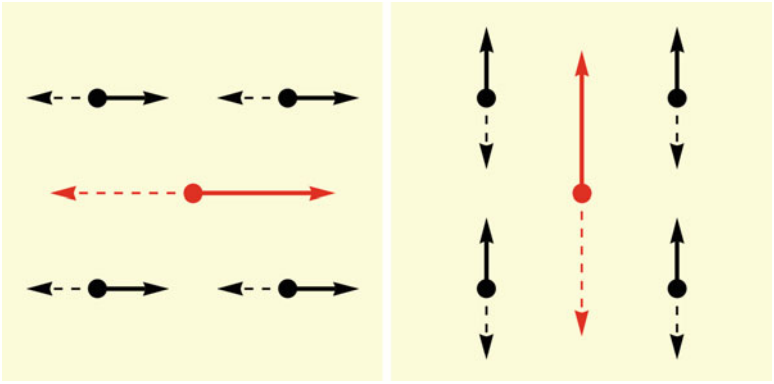

Fig. 6.5 Degenerate D_4 displacements induced by the components β_{11} (*left*) and β_{21} (*right*) of the two-dimensional character ξ_β. The center of mass is subject to a translational vibration modes

These displacements are shown in Fig. 6.4. The displacements associated with column spaces of ξ_β are given by

$$< m, \beta >_{11} = m_0 - m_1 r^2 h - m_2 r^2 + m_3 h,$$

$$< m, \beta >_{21} = m_0 r h + m_1 r - m_2 r^3 h - m_3 r^3,$$

shown in Fig. 6.5, and by

$$< m, \beta >_{12} = m_0 r h - m_1 r - m_2 r^3 h + m_3 r^3,$$

$$< m, \beta >_{22} = m_0 + m_1 r^2 h - m_2 r^2 - m_3 h,$$

shown in Fig. 6.6.

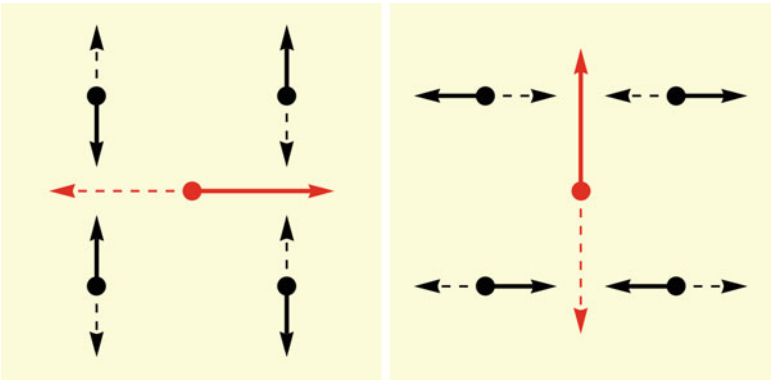

Fig. 6.6 Degenerate D_4 displacements induced by the components β_{12} and β_{22} of the two-dimensional character ξ_β. The center of mass is subject to a translational vibration modes

6.3 Polarization States

In this section we illustrate the dihedral analysis of polarimetric data from scanning laser fundus imaging, based on the method described in [18].

Imaging polarimetry gives information that is largely uncorrelated with spectral and intensity images and therefore can provide enhanced images based on mapping the state of across the field of interest. Here the polarization information is given in the form of the Stokes vector defined as a time-averaged intensity. In order to do this, the simplest way is to insert a polarization analyzer in front of the imaging optics.

A full Stokes vector is measured at every pixel in the scene. However, the Stokes vector cannot be measured directly, and several individual measurements are made and then combined to determine the Stokes vector. The most straight forward technique is the measuring of four linearly independent polarized intensities through linear and circular analyzers, as described in [18]. The elements can be then combined to recover the Stokes vector.

Indicate by $E' = (E_x, E_y)$ the complex amplitudes of the electric field, so that

$$I = |E_x|^2 + |E_y|^2,\ \ Q = |E_x|^2 - |E_y|^2,\ \ U = 2\Re(E_x\overline{E_y}),\ \ V = 2\Im(E_x\overline{E_y}),$$

are the components of the Stokes vector [19, p.256], [8, Ch.9],

$$S' = (I, Q, U, V).$$

Quantities of particular importance [20] are the degree of polarization (p) given by

$$p^2 = \frac{V^2 + Q^2 + U^2}{I^2};$$

the degree of linear polarization

$$\frac{Q^2+U^2}{I^2};$$

and the degree of circular polarization

$$\frac{V^2}{I^2}.$$

In addition, the relations

$$\tan(2\psi)=\frac{U}{Q},\quad \tan^2(2\chi)=\frac{V^2}{Q^2+U^2}$$

define the orientation (χ) of the polarization ellipse and its ellipticity (ψ). In spherical coordinates $(Ip,2\psi,2\chi)$ we have

$$Q=Ip\cos(2\psi)\cos(2\chi),\ U=Ip\sin(2\psi)\cos(2\chi),\ V=Ip\sin(2\chi),$$

so that

$$Q^2+U^2+V^2=p^2I^2,$$

with the equality $p=1$ holding for fully polarized Stokes vectors.

Dihedral Indexing

Let also, for each $\tau\in D_4$,

$$x_\tau=\frac{1}{4}E^*\beta_{\tau^{-1}}E\in\mathbb{C},$$

where β is the single irreducible representation of D_4 in dimension of 2. Direct evaluation then shows that

$$x'=\frac{1}{4}(\underbrace{I,iV,-I,-iV}_{rotations},\underbrace{Q,U,-Q,-U}_{reversals}),$$

whereas

$$<x,\beta>=\frac{1}{4}\{\,I(1-r^2)+iV(r-r^3)+Q(t-r^2h)+U(rh-r^3h)\,\},$$

or

$$< x,\beta > = \frac{1}{4}\left(I\begin{bmatrix} 1 & 0 \\ 0 & 1 \end{bmatrix} + iV\begin{bmatrix} 0 & -1 \\ 1 & 0 \end{bmatrix} + Q\begin{bmatrix} 1 & 0 \\ 0 & -1 \end{bmatrix} + U\begin{bmatrix} 0 & 1 \\ 1 & 0 \end{bmatrix}\right)$$
$$= \frac{1}{2}\begin{bmatrix} I+Q & U-iV \\ U+iV & I-Q \end{bmatrix},$$

thus recovering precisely the matrix form of the Stokes vector, in the sense of [7], and interpreted here as its scattering matrix [21]. Moreover, the dihedral (D_4) analysis retains the interpretation of the degenerate states in the standard Cartesian basis. More precisely,

- Polarization along the x,y-axes: $\pm Q \to \pm \begin{bmatrix} 1 & 0 \\ 0 & -1 \end{bmatrix}$;
- Polarization along the 45°- and 135°-lines: $\pm U \to \pm \begin{bmatrix} 0 & 1 \\ 1 & 0 \end{bmatrix}$;
- Right or left-hand circular polarization: $\pm iV \to \pm \begin{bmatrix} 0 & -1 \\ 1 & 0 \end{bmatrix}$.

We also observe that $< x,\xi >= 0$ for the remaining 4 irreducible representations of D_4 (in dimension of one) due to the definition

$$x_\tau = \frac{1}{4}E^*\beta_{\tau^{-1}}E = \frac{1}{4}\text{tr}\,[EE^*\beta_{\tau^{-1}}]$$

of x_τ and the orthogonality of the irreducible characters. As a consequence, the Parseval's equality in Corollary 2.1 on page 28 is simply

$$||x||^2 = \frac{1}{4}||\widehat{x}(\beta)||^2 = \frac{1}{2}||S||^2. \tag{6.1}$$

Jones Matrices and Dihedral Analysis

The elementary Jones matrices (J) for the distinct optical elements follow directly from the dihedral D_4 Fourier transform

$$< x,\beta >= \frac{1}{2}\begin{bmatrix} I+Q & U-iV \\ U+iV & I-Q \end{bmatrix} \equiv J(I,Q,U,V),$$

as a function of the Stokes parameters. Specifically,

$$J(1,1,0,0) = \begin{bmatrix} 1 & 0 \\ 0 & 0 \end{bmatrix},$$

for the linear polarization in the x direction;

$$J(1,-1,0,0) = \begin{bmatrix} 0 & 0 \\ 0 & 1 \end{bmatrix},$$

in the y direction;

$$J(1,0,1,0) = \frac{1}{2}\begin{bmatrix} 1 & 1 \\ 1 & 1 \end{bmatrix},$$

in the 45° direction;

$$J(1,0,-1,0) = \frac{1}{2}\begin{bmatrix} 1 & -1 \\ -1 & 1 \end{bmatrix},$$

in the 135° direction;

$$J(1,0,0,-1) = \frac{1}{2}\begin{bmatrix} 1 & i \\ -i & 1 \end{bmatrix},$$

for the left-hand circularly polarization state, and

$$J(1,0,0,1) = \frac{1}{2}\begin{bmatrix} 1 & -i \\ i & 1 \end{bmatrix},$$

for the right-hand circularly polarization state.

$$J(1,0,0,0) = \frac{1}{2}\begin{bmatrix} 1 & 0 \\ 0 & 1 \end{bmatrix},$$

gives the unpolarized state, thus proving the following result.

Proposition 6.1. *All classical Jones matrices are the dihedral Fourier transform at the irreducible representation of D_4 in dimension of 2, evaluated at distinct polarization states.*

Mueller Matrices

The defining relations for the Stokes vectors are, in matrix form,

$$S = \begin{bmatrix} 1 & 0 & 0 & 1 \\ 1 & 0 & 0 & -1 \\ 0 & 1 & 1 & 0 \\ 0 & -i & i & 0 \end{bmatrix} (E \otimes \overline{E}) \equiv T(E \otimes \overline{E}), \tag{6.2}$$

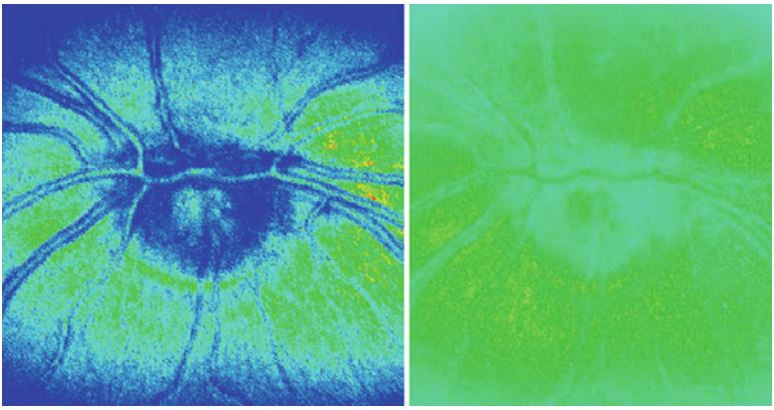

Fig. 6.7 A scanning laser fundus image, from [18], with permission and its 30° polarized rendering

so that if LE is the outgoing field leaving a linear device L then its corresponding Stokes vector is

$$T[(LE)\otimes(\overline{LE})] = T(L\otimes\overline{L})(E\otimes\overline{E}) = T(L\otimes\overline{L})T^{-1}T(E\otimes\overline{E}) = \mathscr{M}S,$$

where $\mathscr{M} = T(L\otimes\overline{L})T^{-1}$ is the Mueller matrix for the device L. We observe that $\mathscr{M}/\sqrt{2}$ is the Hermitian version of $\mathscr{M}$.

Example 6.1. If

$$P_\theta = \begin{bmatrix} \cos(\theta)^2 & \cos(\theta)\sin(\theta) \\ \cos(\theta)\sin(\theta) & \sin(\theta)^2 \end{bmatrix}$$

is the polarizer taking the projection of the electric field E in the direction making an angle θ with the x-axis, then

$$\mathscr{M}_\theta = \frac{1}{2}\begin{bmatrix} 1 & \cos(2\theta) & \sin(2\theta) & 0 \\ \cos(2\theta) & \cos(2\theta)^2 & \frac{1}{2}\sin(4\theta) & 0 \\ \sin(2\theta) & \frac{1}{2}\sin(4\theta) & \sin(2\theta)^2 & 0 \\ 0 & 0 & 0 & 0 \end{bmatrix}$$

is its Mueller matrix. From the evaluation of $\mathscr{M}_\alpha\mathscr{M}_\theta$, for example, we directly see that the analyzer's outgoing intensity I_α is related to its incoming intensity I_θ leaving the polarizer by

$$I_\alpha = \frac{1}{2}\{I\mathrm{Cos}[\alpha-\theta]^2 + Q\mathrm{Cos}[\alpha-\theta]^2\mathrm{Cos}[2\theta] + U\mathrm{Cos}[\alpha-\theta]^2\mathrm{Sin}[2\theta]\} = \mathrm{Cos}[\alpha-\theta]^2 I_\theta,$$

which is the well-known Malus' law.

Figure 6.7 shows a fundus image its polarized copy, obtained from the Mueller matrix for the polarizer with $\alpha = \pi/6$. The resulting intensity I_{pol} is obtained from

the (first entry of) the resulting Stokes vector $\mathscr{M}S$. In this case,

$$I_{pol} = \frac{1}{4}[2I + Q + \sqrt{3}U].$$

Inserting a Reflection

The $\cos^2$ law $I_\alpha = \mathrm{Cos}[\alpha - \theta]^2 I_\theta$ naturally defines an experiment in which the resulting data are then indexed by rotations, or in the finite case, by C_n. On the other hand, if $\widehat{\mathscr{M}_\theta}$ is the Mueller matrix of the polarizer preceded by a reflection, that is, the Mueller matrix of

$$P_\theta \begin{bmatrix} 1 & 0 \\ 0 & -1 \end{bmatrix},$$

then, the evaluation of $\mathscr{M}_\alpha \widehat{\mathscr{M}_\theta}$ shows that

$$I_\alpha = \frac{1}{2}\{I\mathrm{Cos}[\alpha-\theta]^2 + Q\mathrm{Cos}[\alpha-\theta]^2\mathrm{Cos}[2\theta] - U\mathrm{Cos}[\alpha-\theta]^2\mathrm{Sin}[2\theta]\} = \mathrm{Cos}[\alpha-\theta]^2 I_{-\theta}.$$

The semi-direct structure of the multiplication in D_n then leads to indexing the outgoing intensity

$$I_{\tau,\sigma} = \mathrm{Cos}[\tau - \theta]^2 I_{\delta(\sigma)\theta}, \quad (\sigma, \tau) \in D_n,$$

with the elements of D_n, where here δ is the automorphism in $C_2 \mapsto \{-1, 1\}$ that appears in the construction of the semi-direct product, in Sect. 2.2, on page 11.

Dihedral Decompositions

The dihedral decompositions of $\mathscr{M} = T(L \otimes \overline{L})T^{-1}$ can be obtained in a number of different ways. Here we will describe one approach in detail for the case in which L is an arbitrary matrix with entries $\ell_{ij} \in \mathbb{R}$. The underlying algebraic structure is the product group $D_4 \times D_4$. Similar steps would apply for the complex case and for $D_n \times D_n$.

We start with the dihedral D_4 (trace) decomposition

$$2L = (\ell_{11} + \ell_{22}) \begin{bmatrix} 1 & 0 \\ 0 & 1 \end{bmatrix} + (\ell_{21} - \ell_{12}) \begin{bmatrix} 0 & -1 \\ 1 & 0 \end{bmatrix}$$
$$+ (\ell_{11} - \ell_{22}) \begin{bmatrix} 1 & 0 \\ 0 & -1 \end{bmatrix} + (\ell_{12} + \ell_{21}) \begin{bmatrix} 0 & 1 \\ 1 & 0 \end{bmatrix}$$

of L. It then follows that $\mathscr{M}$ decomposes as a superposition of Mueller matrices of the elementary dihedral devices,

$$1 = \pm \begin{bmatrix} 1 & 0 \\ 0 & 1 \end{bmatrix}, \ \odot = \pm \begin{bmatrix} 0 & -1 \\ 1 & 0 \end{bmatrix}, \ \oplus = \pm \begin{bmatrix} 1 & 0 \\ 0 & -1 \end{bmatrix}, \ \otimes = \pm \begin{bmatrix} 0 & 1 \\ 1 & 0 \end{bmatrix}$$

corresponding to unpolarized, (L-R) circularly polarized, plane polarized along the main axes, or along the main diagonals, respectively. The additional components are generalized Mueller matrices, indicated here by $\mathbb{M}$, corresponding to the tensor products

$$L \otimes F$$

of two distinct elementary devices, interpreted as linear objects in phase-space [22–25], or the result of *entangled* outgoing fields

$$T(L \otimes \overline{F})(E \otimes \overline{E}) = T(L \otimes \overline{F})T^{-1}T(E \otimes \overline{E}) = \mathbb{M}S.$$

There are four realizable components:

$$\mathscr{M}_{11} = \begin{bmatrix} 1 & 0 & 0 & 0 \\ 0 & 1 & 0 & 0 \\ 0 & 0 & 1 & 0 \\ 0 & 0 & 0 & 1 \end{bmatrix}, \ \mathscr{M}_{\odot\odot} = \begin{bmatrix} 1 & 0 & 0 & 0 \\ 0 & -1 & 0 & 0 \\ 0 & 0 & -1 & 0 \\ 0 & 0 & 0 & 1 \end{bmatrix},$$

$$\mathscr{M}_{\oplus\oplus} = \begin{bmatrix} 1 & 0 & 0 & 0 \\ 0 & 1 & 0 & 0 \\ 0 & 0 & -1 & 0 \\ 0 & 0 & 0 & -1 \end{bmatrix}, \ \mathscr{M}_{\otimes\otimes} = \begin{bmatrix} 1 & 0 & 0 & 0 \\ 0 & -1 & 0 & 0 \\ 0 & 0 & 1 & 0 \\ 0 & 0 & 0 & -1 \end{bmatrix};$$

and six generalized components:

$$\mathscr{M}_{1\odot} + \mathscr{M}_{\odot 1} = \begin{bmatrix} 0 & 0 & 0 & -i \\ 0 & 0 & -1 & 0 \\ 0 & 1 & 0 & 0 \\ -i & 0 & 0 & 0 \end{bmatrix} + \begin{bmatrix} 0 & 0 & 0 & i \\ 0 & 0 & -1 & 0 \\ 0 & 1 & 0 & 0 \\ i & 0 & 0 & 0 \end{bmatrix} = \begin{bmatrix} 0 & 0 & 0 & 0 \\ 0 & 0 & -2 & 0 \\ 0 & 2 & 0 & 0 \\ 0 & 0 & 0 & 0 \end{bmatrix},$$

$$\mathscr{M}_{1\oplus} + \mathscr{M}_{\oplus 1} = \begin{bmatrix} 0 & 1 & 0 & 0 \\ 1 & 0 & 0 & 0 \\ 0 & 0 & 0 & -i \\ 0 & 0 & i & 0 \end{bmatrix} + \begin{bmatrix} 0 & 1 & 0 & 0 \\ 1 & 0 & 0 & 0 \\ 0 & 0 & 0 & i \\ 0 & 0 & -i & 0 \end{bmatrix} = \begin{bmatrix} 0 & 2 & 0 & 0 \\ 2 & 0 & 0 & 0 \\ 0 & 0 & 0 & 0 \\ 0 & 0 & 0 & 0 \end{bmatrix},$$

$$\mathscr{M}_{1\otimes}+\mathscr{M}_{\otimes 1}=\begin{bmatrix}0&0&1&0\\0&0&0&-i\\1&0&0&0\\0&i&0&0\end{bmatrix}+\begin{bmatrix}0&0&1&0\\0&0&0&i\\1&0&0&0\\0&-i&0&0\end{bmatrix}=\begin{bmatrix}0&0&2&0\\0&0&0&0\\2&0&0&0\\0&0&0&0\end{bmatrix},$$

$$\mathscr{M}_{\odot\oplus}+\mathscr{M}_{\oplus\odot}=\begin{bmatrix}0&0&-1&0\\0&0&0&-i\\1&0&0&0\\0&-i&0&0\end{bmatrix}+\begin{bmatrix}0&0&-1&0\\0&0&0&i\\1&0&0&0\\0&i&0&0\end{bmatrix}=\begin{bmatrix}0&0&-2&0\\0&0&0&0\\2&0&0&0\\0&0&0&0\end{bmatrix},$$

$$\mathscr{M}_{\odot\otimes}+\mathscr{M}_{\otimes\odot}=\begin{bmatrix}0&1&0&0\\-1&0&0&0\\0&0&0&-i\\0&0&-i&0\end{bmatrix}+\begin{bmatrix}0&1&0&0\\-1&0&0&0\\0&0&0&i\\0&0&i&0\end{bmatrix}=\begin{bmatrix}0&2&0&0\\-2&0&0&0\\0&0&0&0\\0&0&0&0\end{bmatrix},$$

$$\mathscr{M}_{\oplus\otimes}+\mathscr{M}_{\otimes\oplus}=\begin{bmatrix}0&0&0&-i\\0&0&1&0\\0&1&0&0\\i&0&0&0\end{bmatrix}+\begin{bmatrix}0&0&0&i\\0&0&1&0\\0&1&0&0\\-i&0&0&0\end{bmatrix}=\begin{bmatrix}0&0&0&0\\0&0&2&0\\0&2&0&0\\0&0&0&0\end{bmatrix}.$$

More specifically, given an arbitrary real matrix

$$L=\begin{bmatrix}\ell_{11}&\ell_{12}\\\ell_{21}&\ell_{22}\end{bmatrix},$$

write

$$f=\ell_{11}+\ell_{22},\ \ g=\ell_{21}-\ell_{12},\ \ h=\ell_{11}-\ell_{22},\ \ \ell=\ell_{12}+\ell_{21}.$$

Then, its Mueller matrix

$$\mathscr{M}=\frac{1}{4}\begin{bmatrix}f^2+g^2+h^2+\ell^2 & 2fh+2g\ell & -2gh+2f\ell & 0\\ 2fh-2g\ell & f^2-g^2+h^2-\ell^2 & -2fg+2h\ell & 0\\ 2gh+2f\ell & 2fg+2h\ell & f^2-g^2-h^2+\ell^2 & 0\\ 0 & 0 & 0 & f^2+g^2-h^2-\ell^2\end{bmatrix}$$

decomposes as

$$\mathscr{M}=\frac{1}{4}[f^2\mathscr{M}_{11}+g^2\mathscr{M}_{\odot\odot}+h^2\mathscr{M}_{\oplus\oplus}+\ell^2\mathscr{M}_{\otimes\otimes}]$$

$$+\frac{1}{4}\{fg[\mathscr{M}_{1\odot}+\mathscr{M}_{\odot 1}]+fh[\mathscr{M}_{1\oplus}+\mathscr{M}_{\oplus 1}]\}$$

$$+\frac{1}{4}\{f\ell[\mathscr{M}_{1\otimes}+\mathscr{M}_{\otimes 1}]+gh[\mathscr{M}_{\odot\oplus}+\mathscr{M}_{\oplus\odot}]\}$$
$$+\frac{1}{4}\{g\ell[\mathscr{M}_{\odot\otimes}+\mathscr{M}_{\otimes\odot}]+h\ell[\mathscr{M}_{\oplus\otimes}+\mathscr{M}_{\otimes\oplus}].$$

In summary, then, the Mueller matrix of an arbitrary real Jones matrix is a real-coefficient superposition of elements in a linear representation equivalent to the irreducible representation $\beta_\tau \otimes \beta_\sigma$ of $D_4 \times D_4$, where β is the irreducible representation of D_4 in dimension of two.

The dihedral analysis is then the study of the spectrum

$$\{< x, \xi >, \quad \xi \in \widehat{D_n \times D_n}\},$$

and it extends to complex Jones matrices by recalculating the Mueller matrix above. It also extends to the product $D_n \times D_{n'}$ of distinct dihedral groups.

Dihedral Actions and Orbits on the Poincare Sphere $\mathscr{S}$

Defining

$$(\tau, S) \in D_n \times \mathscr{S} \mapsto T(\beta_\tau \otimes \beta_\tau)T^*S,$$

we have $(\sigma,(\tau,S)) = (\sigma\tau,S)$ and $||(\tau,S)|| = ||s||$, due to the unitary character of β. Therefore that $(\tau,S) \in \mathscr{S}$. The resulting orbit of a point $S \in \mathscr{S}$ is given by

$$\mathscr{O}_S = \{(\tau,S),\ \tau \in D_n\}.$$

Example 6.2. A D_3 orbit in $\mathscr{S}$ has three points

$$\begin{bmatrix} I \\ Q \\ U \\ V \end{bmatrix}, \quad \begin{bmatrix} I \\ -\frac{Q}{2}+\frac{\sqrt{3}U}{2} \\ -\frac{\sqrt{3}Q}{2}-\frac{U}{2} \\ V \end{bmatrix}, \quad \begin{bmatrix} I \\ -\frac{Q}{2}-\frac{\sqrt{3}U}{2} \\ \frac{\sqrt{3}Q}{2}-\frac{U}{2} \\ V \end{bmatrix},$$

generated by the rotations and the three points

$$\begin{bmatrix} I \\ Q \\ -U \\ -V \end{bmatrix}, \quad \begin{bmatrix} I \\ -\frac{Q}{2}-\frac{\sqrt{3}U}{2} \\ -\frac{\sqrt{3}Q}{2}+\frac{U}{2} \\ -V \end{bmatrix}, \quad \begin{bmatrix} I \\ -\frac{Q}{2}+\frac{\sqrt{3}U}{2} \\ \frac{\sqrt{3}Q}{2}+\frac{U}{2} \\ -V \end{bmatrix},$$

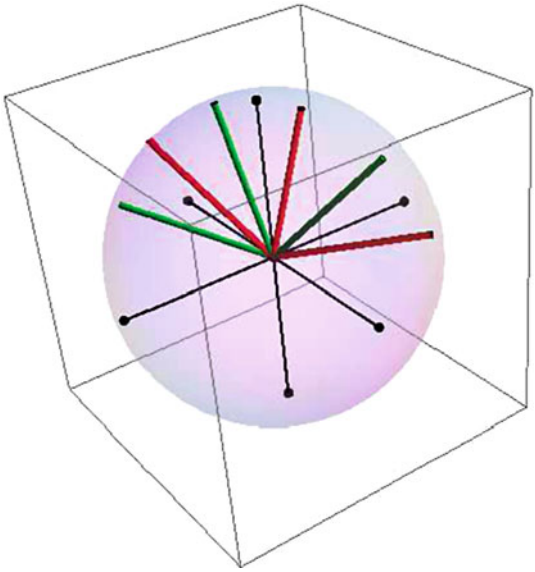

Fig. 6.8 A D_3 orbit in the Poincare sphere $\mathscr{S}$

generated by the reversals. Figure 6.8 shows the D_3 orbit generated at

$$(1, 1/\sqrt{3}, 1/\sqrt{3}, 1/\sqrt{3}) \in \mathscr{S},$$

with rotations and reversals shown with distinct colors. Note their pairwise orthogonality.

Given a dihedral orbit in $\mathscr{S}$ and the (first row m of) a Mueller matrix of an experiment, then

$$I_\tau = m \cdot (\tau, S), \quad \tau \in D_n$$

are the outgoing intensities along the dihedral orbit, amenable for the symmetry study of interest. For example, in imaging experiments in which $m = m(x, y)$ as a function of the pixel location (x, y), then

$$I_\tau(x, y) = m(x, y) \cdot (\tau, S), \quad \tau \in D_n.$$

The Intensity Indexing

The intensity indexing u_τ is defined as the intensity $|x_\tau|^2 = \overline{x_\tau} x_\tau$ of the trace indexing. More precisely,

$$u_\tau = n^2 |x_\tau|^2.$$

Therefore, in the present context $(n = 4)$, it gives

$$u' = (I^2, V^2, I^2, V^2, Q^2, U^2, Q^2, U^2).$$

The Canonical Projections for the D_4 Intensity Indexing

Evaluation of the canonical projections for the intensity data gives:

$$u' \mathscr{P}_1 u = \frac{1}{2}[I^2 + V^2 + Q^2 + U^2]^2;$$

$$u' \mathscr{P}_\alpha u = \frac{1}{2}[I^2 + V^2 - Q^2 - U^2]^2;$$

$$u' \mathscr{P}_{\gamma^+} u = \frac{1}{2}[I^2 - V^2 + Q^2 - U^2]^2;$$

$$u' \mathscr{P}_{\gamma^-} u = \frac{1}{2}[I^2 - V^2 - Q^2 + U^2]^2;$$

whereas $u' \mathscr{P}_\beta u = 0$. Evidently, then,

$$u'u = u' \mathscr{P}_1 u + u' \mathscr{P}_\alpha u + u' \mathscr{P}_{\gamma^+} u + u' \mathscr{P}_{\gamma^-} u.$$

Additional statistical tests may be obtained from combining pairs of projections into shorter canonical decompositions, such as

$$\begin{aligned} u'u &= u'(\mathscr{P}_1 + \mathscr{P}_\alpha)u + u'(\mathscr{P}_{\gamma^+} + \mathscr{P}_{\gamma^-})u \\ &= (I^2 + V^2)^2 + (Q^2 + U^2)^2 + (I^2 - V^2)^2 + (Q^2 - U^2)^2; \end{aligned}$$

$$\begin{aligned} u'u &= u(\mathscr{P}_1 + \mathscr{P}_{\gamma^+})u + u(\mathscr{P}_\alpha + \mathscr{P}_{\gamma^-})u \\ &= (I^2 + Q^2)^2 + (V^2 + U^2)^2 + (I^2 - Q^2)^2 + (V^2 - U^2)^2; \end{aligned}$$

or

$$\begin{aligned} u'u &= u'(\mathscr{P}_1 + \mathscr{P}_{\gamma^-})u + u'(\mathscr{P}_{\gamma^+} + \mathscr{P}_\alpha)u \\ &= (I^2 + U^2)^2 + (V^2 + Q^2)^2 + (I^2 - U^2)^2 + (Q^2 - V^2)^2. \end{aligned}$$

The two components in each of the shorter decompositions remain algebraic orthogonal and idempotent [2].

A Numerical Example

The estimated scattering matrix

$$\widehat{x}(\beta) = \frac{1}{2}\begin{bmatrix} I+Q & U-iV \\ U+iV & I-Q \end{bmatrix}$$

for the fundus image shown in Fig. 6.7 is

$$\frac{1}{2}\begin{bmatrix} 0.314 & 0.103-i0.097 \\ 0.103+i0.097 & 0.138 \end{bmatrix},$$

based on the estimated mean Stokes vector

$$\hat{S}' = (0.226, 0.088, 0.103, 0.097) \pm (0.122, 0.108, 0.150, 0.082).$$

The image's estimated SPAN is

$$|| < x, \beta > ||^2 = \frac{1}{2}||S||^2 = 0.03807.$$

Generalized Intensity Decomposition

The total intensity $||S||^2$ can be decomposed for arbitrary dihedral symmetries by extending the trace indexing

$$x_\tau = \frac{1}{n}E^* \beta_{\tau^{-1}} E$$

to $\tau \in D_n$. Direct evaluation shows that

$$\begin{aligned} ||x||^2 &= \frac{1}{n^2}\sum_\tau \{\underbrace{I^2\cos^2\phi_\tau + V^2\sin^2\phi_\tau}_{rotations} + \underbrace{Q^2\cos^2\phi_\tau + U^2\sin^2\phi_\tau + QU\sin(2\phi_\tau)}_{reversals}\} \\ &= \frac{1}{2n}||S||^2, \end{aligned}$$

where ϕ_τ are the dihedral angles for D_n. Consequently,

$$||S||^2 = \frac{2}{n}\sum_\tau \{I^2\cos^2\phi_\tau + V^2\sin^2\phi_\tau + Q^2\cos^2\phi_\tau + U^2\sin^2\phi_\tau + QU\sin(2\phi_\tau)\}.$$

Isotropic Vectors

The matrix

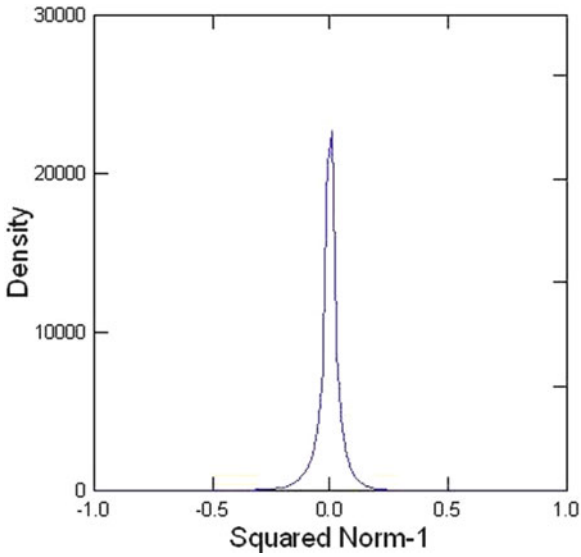

Fig. 6.9 Distribution of $||S||_1^2$ in the fundus image shown in Fig. 6.7

$$< x, \beta >= \frac{1}{2}\begin{bmatrix} I+Q & U-iV \\ U+iV & I-Q \end{bmatrix}$$

has several interesting properties, e.g. [7, Ch.3]. In particular,

$$2\det < x, \beta >= I^2 - Q^2 - U^2 - V^2 = ||S||_1,$$

so that $\det < x, \beta >= 0$ corresponds to isotropic vectors, or null vectors in the associated non-Euclidean norm $||.||_1$. Moreover,

$$||S||_1 = 2\det < x, \beta >= \begin{cases} > 0, \ S \text{ is a real space-like vector;} \\ < 0, \ S \text{ is a real time-like vector;} \\ = 1, \ S \text{ is a real unit space-like vector;} \\ = -1, \ S \text{ is a real unit time-like vector.} \end{cases}$$

Figure 6.9 shows the distribution of $||S||_1^2$ for the stokes vectors in the fundus image shown in Fig. 6.7.

6.4 Decompositions of Entropy

In this section we will apply the dihedral analysis to illustrate the interpretation of the uncertainty content in the entropy of a probability distribution indexed by a finite group. See also [26].

Example 6.3 (D_2 support). Indicate by $p = \sum_\tau p_\tau \tau$ a probability distribution indexed by D_2 and by $\ell = \sum \log p_\tau \tau$ the corresponding log probabilities.

The regular representation of K_4 gives the projections

$$\mathscr{P}_1 = 1/4 \begin{bmatrix} 1 & 1 & 1 & 1 \\ 1 & 1 & 1 & 1 \\ 1 & 1 & 1 & 1 \\ 1 & 1 & 1 & 1 \end{bmatrix}, \quad \mathscr{P}_v = 1/4 \begin{bmatrix} 1 & -1 & 1 & -1 \\ -1 & 1 & -1 & 1 \\ 1 & -1 & 1 & -1 \\ -1 & 1 & -1 & 1 \end{bmatrix},$$

$$\mathscr{P}_h = 1/4 \begin{bmatrix} 1 & 1 & -1 & -1 \\ 1 & 1 & -1 & -1 \\ -1 & -1 & 1 & 1 \\ -1 & -1 & 1 & 1 \end{bmatrix}, \quad \mathscr{P}_r = 1/4 \begin{bmatrix} 1 & -1 & -1 & 1 \\ -1 & 1 & 1 & -1 \\ -1 & 1 & 1 & -1 \\ 1 & -1 & -1 & 1 \end{bmatrix},$$

so that $I = \mathscr{P}_1 + \mathscr{P}_v + \mathscr{P}_h + \mathscr{P}_r$ is the decomposition of the corresponding identity matrix into the sum of algebraically orthogonal projections. Correspondingly, each invariant subspace is in dimension of one. The decomposition of the identity matrix carries over to

$$-H = p \cdot \ell = \sum p' \mathscr{P}_\xi \ell_p = H_1 + H_v + H_h + H_r,$$

in which:

$$H_1 = \frac{1}{4} \log(p_1 p_v p_h p_r) = \frac{1}{4} < p, \xi_1 >< \ell, \xi_1 >;$$

$$H_v = \frac{1}{4}(p_1 + p_v - p_h - p_r) \log \frac{p_1 p_v}{p_h p_r} = \frac{1}{4} < p, \xi_v >< \ell, \xi_v >;$$

$$H_h = \frac{1}{4}(p_1 + p_h - p_v - p_r) \log \frac{p_1 p_h}{p_v p_r} = \frac{1}{4} < p, \xi_h >< \ell, \xi_h >;$$

and

$$H_r = \frac{1}{4}(p_1 + p_r - p_h - p_v) \log \frac{p_1 p_r}{p_h p_v} = \frac{1}{4} < p, \xi_r >< \ell, \xi_r >,$$

where $\{\xi_1, \xi_v, \xi_h, \xi_r\}$ are the irreducible representations of D_2. Verifying Corollary 2.2 on page 29, we obtain

$$-H = p \cdot \ell = \sum_\xi \frac{1}{4} < p, \xi >< \ell, \xi > .$$

We observe that:

1. If $p_1 = p_v$ and $p_r = p_h$ then $H = -\frac{1}{2} \log(p_v p'_v) - \frac{1}{2}(p_v - p'_v) \log \frac{p_v}{p'_v}$, where $p'_v = 1 - p_v$.

2. If $p_1 = p_h$ and $p_r = p_v$ then $H = -\frac{1}{2}\log(p_h p'_h) - \frac{1}{2}(p_h - p'_h)\log\frac{p_h}{p'_h}$, where $p'_h = 1 - p_h$.
3. If $p_1 = p_r$ and $p_v = p_h$ then $H = -\frac{1}{2}\log(p_r p'_r) - \frac{1}{2}(p_r - p'_r)\log\frac{p_r}{p'_r}$, where $p'_r = 1 - p_r$.

We see that each one of these hypotheses (of pairwise, clustered distributions) leads to a decomposition of the entropy into the sum of a two-component log geometric mean and Kullback's divergence between a clustered distribution and the corresponding two-component uniform distribution.

Example 6.4 (D_3 support). To facilitate the writing, denote by

$$p' = (\underbrace{r_1, r_2, r_3}_{\text{rotations}}, \underbrace{t_1, t_2, t_3}_{\text{reversals}}),$$

a probability distribution indexed by D_3, and by

$$\ell' = (\log r_1, \log r_2, \log r_3, \log t_1, \log t_2, \log t_3)$$

the corresponding log probabilities. The dihedral action on the orbit gives three canonical projections: $\mathscr{P}_1$ is the averaging 6×6 projection $\mathscr{A}_6$ with all entries equal to $1/6$;

$$\mathscr{P}_\alpha = 1/6 \begin{bmatrix} 1 & 1 & 1 & -1 & -1 & -1 \\ 1 & 1 & 1 & -1 & -1 & -1 \\ 1 & 1 & 1 & -1 & -1 & -1 \\ -1 & -1 & -1 & 1 & 1 & 1 \\ -1 & -1 & -1 & 1 & 1 & 1 \\ -1 & -1 & -1 & 1 & 1 & 1 \end{bmatrix}; \quad \mathscr{P}_\beta = 1/3 \begin{bmatrix} 2 & -1 & -1 & 0 & 0 & 0 \\ -1 & 2 & -1 & 0 & 0 & 0 \\ -1 & -1 & 2 & 0 & 0 & 0 \\ 0 & 0 & 0 & 2 & -1 & -1 \\ 0 & 0 & 0 & -1 & 2 & -1 \\ 0 & 0 & 0 & -1 & -1 & 2 \end{bmatrix}.$$

It then follows that

$$-H = p'\ell = p'\mathscr{P}_1\ell + p'\mathscr{P}_\alpha\ell + p'\mathscr{P}_\beta\ell,$$

with the regular components of the entropy H given by

$$H_1 = p'\mathscr{P}_1\ell = \frac{1}{6}\log[r_1 r_2 r_3 t_1 t_2 t_3];$$

$$H_\alpha = p'\mathscr{P}_\alpha\ell = \frac{1}{6}\log(\frac{r_1 r_2 r_3}{t_1 t_2 t_3})^{(r_1+r_2+r_3-t_1-t_2-t_3)};$$

$$H_\beta = p'\mathscr{P}_\beta\ell = \frac{1}{3}\log[(\frac{r_1}{r_2})^{r_1-r_2}(\frac{r_1}{r_3})^{r_1-r_3}(\frac{r_2}{r_3})^{r_2-r_3}(\frac{t_1}{t_2})^{t_1-t_2}(\frac{t_1}{t_3})^{t_1-t_3}(\frac{t_2}{t_3})^{t_2-t_3}].$$

Moreover, we have, for all irreducible representations $\xi = 1, \alpha, \beta$ of D_3,

$$H_\xi = p' \mathscr{P}_\xi \ell = \frac{n_\xi}{6} < p, \xi > \cdot < \ell, \xi >,$$

so that, as stated in Parseval's equality, Corollary 2.1 on page 28,

$$-H = p \cdot \ell = \sum_\xi \frac{n_\xi}{6} < p, \xi > \cdot < \ell, \xi > .$$

We observe that

1. H_1 is the log geometric mean of the components of p.
2. H_α can be expressed as $r_\bullet D(r : u) + t_\bullet D(t : u)$, where $r_\bullet$ is the marginal probability $r_1 + r_2 + r_3$ of a rotation, $t_\bullet$ is the marginal probability $t_1 + t_2 + t_3$ of a reflection, $D(r : u)$ is Kullback's divergence between the rotation subcomposition [27, p.33]
$$r = (r_1, r_2, r_3)/(r_1 + r_2 + r_3)$$
and the uniform distribution $u = (1,1,1)/3$, and $D(t : u)$ is the divergence between the reflection subcomposition $t = (t_1, t_2, t_3)/(t_1 + t_2 + t_3)$ and the uniform distribution u.
3. H_3 can be expressed as
$$\frac{1}{3} D((r,t) : (1,1)/2) + \frac{1}{2}(r_\bullet - t_\bullet)(\bar{r} - \bar{t}),$$
where $\bar{r}$ and $\bar{t}$ indicate here the log geometric mean of r and t, respectively.

6.5 Elementary Algebraic Surfaces

Given a scalar function f defined in the plane, we are interested in describing the parametric profile

$$f_\tau = f(\beta_\tau(q + p)) - f(\beta_\tau q), \quad \tau \in D_4 \tag{6.3}$$

of the surface f obtained along the dihedral D_4 orbit $\{\beta_\tau q, \beta_\tau p\}$ generated by $q = (1,1), p = (1,0)$, as shown in Fig. 6.10. We will summarize the parametric profile of f by evaluating its D_4 spectrum

$$\{< f, 1 >, < f, \alpha >, < f, \gamma_+ >, < f, \gamma_- >, < f, \beta >\},$$

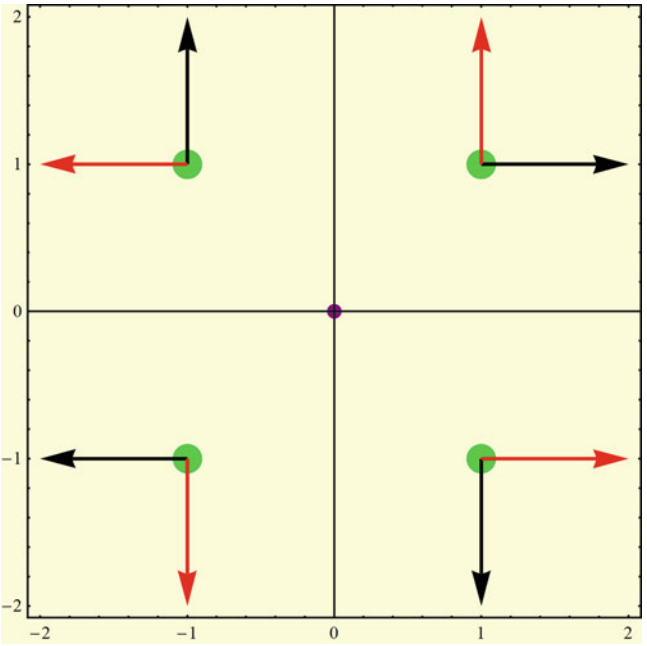

Fig. 6.10 The D_4 field orbit of $q = (1,1), p = (1,0)$

keeping in mind its relation

$$f' \mathscr{P}_\xi f = \frac{n_\xi}{8} || < f, \xi > ||^2$$

to the D_4 regular canonical projections.

Gaussian Quadratic Form

Let

$$f(x,y) = (x-\mu_x, y-\mu_y) \begin{bmatrix} {\sigma_x}^2 & \rho\, \sigma_x \sigma_y \\ \rho\, \sigma_x \sigma_y & {\sigma_y}^2 \end{bmatrix} \begin{bmatrix} x-\mu_x \\ y-\mu_y \end{bmatrix}.$$

Then, direct evaluation shows that:

$$\begin{aligned} < f, 1 > &= 12\left(\sigma_x^2 + \sigma_y^2\right), \\ < f, \alpha > &= 0, \\ < f, \gamma_+ > &= 12\left(\sigma_x^2 - \sigma_y^2\right), \end{aligned}$$

$$< f, \gamma_- > = 16\rho\sigma_x\sigma_y,$$
$$< f, \beta > = \begin{pmatrix} -8\sigma_x(\mu_x\sigma_x + \rho\mu_y\sigma_y) & 0 \\ -8\sigma_y(\rho\mu_x\sigma_x + \mu_y\sigma_y) & 0 \end{pmatrix}.$$

We observe that, sequentially, the parameters $\{\sigma_x, \sigma_y\}$ can be recovered or estimated by experimental Fourier transforms at $\{\alpha, \gamma_+\}$; ρ from an experimental transform at γ_-; and $\{\mu_x, \mu_y\}$ by the column space of the transform at β. That is, if

$$x_\tau = x_{q_\tau + p_\tau} - x_{q_\tau}, \quad \tau \in D_4$$

are experimental data observed along the orbit, then the sequential equating of

$$< x, \xi > = < f, \xi >,$$

as indicated above, will lead to solving for estimates of the corresponding parameters in the Gaussian surface.

Baker's Cornea Asphericity Model

The Baker's asphericity model [28, 29] is given by

$$f(x,y) = -2R(-a+x) + (1-Q)(-a+x)^2 + (-b+y)^2,$$

where R is a curvature parameter, Q a shape parameter, and (a,b) a centering offset. When $\mathscr{B}$ is centered at the origin, its cut along the $z = 0$ plane gives

$$y = \sqrt{x}\sqrt{2R + (-1+Q)x}$$

along which the curvature when $Q = 0$ is $-1/R$. Direct evaluation shows that:

$$< f, 1 > = -12(Q-2),$$
$$< f, \alpha > = 0,$$
$$< f, \gamma_+ > = -12Q,$$
$$< f, \gamma_- > = 0,$$
$$< f, \beta > = -8 \begin{pmatrix} a(1-Q) + R & 0 \\ b & 0 \end{pmatrix}.$$

Here we observe that all model parameters up to the x-offset can be experimentally recovered.

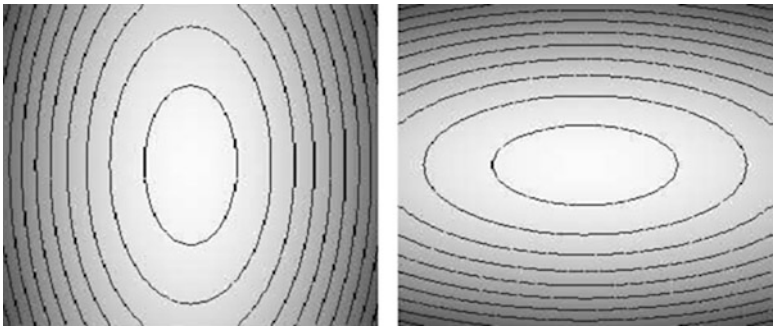

Fig. 6.11 The elliptic contours for $(c,a,b) = (1,0.5,1)$ and $(c,a,b) = (1,1,0.5)$

Ellipsoids

For the ellipsoid

$$f(x,y) = c\left(1 - \frac{x^2}{a^2} - \frac{y^2}{b^2}\right)^{1/2},$$

we have

$$< f^2, 1 > = -12c^2(\frac{1}{a^2} + \frac{1}{b^2}),\ < f^2, \alpha >= 0,$$
$$< f^2, \gamma_+ > = -12c^2(\frac{1}{a^2} - \frac{1}{b^2}),\ < f^2, \gamma_- >= 0,$$
$$< f^2, \beta > = \begin{pmatrix} 0 & 0 \\ 0 & 0 \end{pmatrix}.$$

Here we observe that $< f^2, \gamma_+ >$ can be used to assess $a = b$ (sphericity), whereas large absolute values of $< f^1, 1 >$ imply $c > a = b$ (prolate spheroid), as illustrated in Fig. 6.11.

Problems

6.1. Carry out the studies described in Problem 4.1 on page 74, using the dihedral D_3 basis introduced in Problem 5.2 on page 84, for the dihedral orbit data for the Salmonella

$\mathscr{O}$	1	2	3
AGT	385	407	318
GTA	369	351	351
TAG	176	121	36
ATG	477	559	610
TGA	581	656	754
GAT	446	547	579

,

and Tobacco

$\mathscr{O}$	1	2	3
AGT	8	19	11
GTA	13	17	18
TAG	8	11	10
ATG	22	16	14
TGA	15	27	22
GAT	26	18	13

viruses.

6.2. The following are the frequency counts for the D_3 orbit of GCT along 6 consecutive regions of the HIV1 genome. See also Sect. 4.1 on page 59.

$\mathscr{O}$	1	2	3	4	5	6
GCT	21	10	8	15	20	38
CTG	17	21	15	17	28	36
TGC	18	9	10	17	23	22
GTC	7	6	8	9	9	5
TCG	5	1	2	1	0	6
CGT	2	1	1	1	3	3

1. Show that the entropy for the estimated orbit distribution p based on the frequency counts in region 1 is Ent $p = 1.57448$.
2. With the same notation introduced in Sect. 6.4 on page 104, show that

- $< p, 1 >= 1, \quad < \ell, 1 >= -2.07906.$
- $< p, \alpha >= 0.6, \quad < \ell, \alpha >= 4.51961.$
- $< p, \beta >= \begin{pmatrix} 0.1 & 0.0494872 \\ 0.0247436 & 0. \end{pmatrix}, \quad < \ell, \beta >= \begin{pmatrix} 0.977347 & 0.843032 \\ 0.74403 & -0.611888 \end{pmatrix}.$

- Ent $p = -\sum_{\xi} n_{\xi} < p, \xi > \cdot < \ell, \xi > /6$, where the sum is over the irreducible representations $\xi = 1, \alpha, \beta$ of D_3, and n_{ξ} their corresponding dimension.

6.3. Study the D_4 parametric profile for the hyperbolic paraboloid

$$f(x,y) = c\left(\frac{x^2}{a^2} - \frac{y^2}{b^2}\right).$$

References

1. Kirillov, A.: The orbit method, I: Geometric quantization. In: Kirillov, A. (ed.) Contemporary Mathematics, vol. 145, pp. 1–32. American Mathematical Society, Providence, RI (1993)
2. Viana, M.: Symmetry studies. An introduction to the analysis of structured data in applications. Cambridge Series in Statistical and Probabilistic Mathematics. Cambridge University Press, Cambridge (2008). ISBN: 978-0-521-84103-0; 0-521-84103-8
3. Weyl, H.: The classical groups, their invariants and representations. Princeton University Press, Princeton, NJ (1953)
4. Serre, J-P.: Linear representations of finite groups. Springer, New York (1977)
5. Bishop, Y., Fienberg, S., Holland, P.: Discrete multivariate analysis: Theory and practice. MIT Press, Cambridge (1975)
6. Adkins, W., Weintraub, S.: Algebra - an approach via module theory. Springer, New York (1992)
7. Cartan, E.: The theory of spinors. MIT Press, Cambridge (1966)
8. O'Neill, E.: Introduction to statistical optics. Dover, New York (1963)
9. Viana, M.: Canonical invariants for three-candidate preference rankings. Can. Appl. Math. Q. **15**(2), 203–222 (2007)
10. Viana, M., Lakshminarayanan, V.: Data analytic aspects of chirality. Symmetry Culture Sci. 16(4), 401–421 (2005)
11. Viana, M.: Canonical decompositions and invariants for data analysis. In: Hazenwinkel, M. (ed.) Handbook of algebra, vol. 6, pp. 565–584. Elsevier/North-Holland, Amsterdam (2009)
12. Khinchin, A.: Information theory. Dover, New York (1957)
13. Kullback, S.: Information theory and statistics. Dover, New York (1968)
14. Enquist, M., Johnstone, R.: Generalization and the evolution of symmetry preferences. Proc. R. Soc. Lond. B **264**(1386), 1345–1348 (1997). http://www.jstor.org/stable/50910
15. Harris, D., Bertolucci, M.: Symmetry and spectroscopy - an introduction to vibrational and electronic spectroscopy. Oxford University Press, New York (1978)
16. Bishop, D.: Group theory and chemistry. Dover, New York (1973)
17. Heine, V.: Group theory in quantum mechanics. An introduction to its present usage. Dover, New York (1993). ISBN: 0-486-67585-8 (Reprint of the 1960 edition)
18. Bueno, J., Hunter, J., Cookson, C., Kisilak, M., Campbell, M.: Improved scanning laser fundus imaging using polarimetry. J. Opt. Soc. Am. A **24**(5), 1337–1348 (2007). http://josaa.osa.org/abstract.cfm?URI=josaa-24-5-1337
19. Doran, C., Lasenby, A.: Geometric algebra for physicists. Cambridge University Press, Cambridge (2003). ISBN: 0-521-48022-1; 978-0-521-71595-9

M.A.G. Viana and V. Lakshminarayanan, *Dihedral Fourier Analysis: Data-Analytic Aspects and Applications*, Lecture Notes in Statistics 206,
DOI 10.1007/978-1-4614-5562-2_1, © Springer Science+Business Media New York 2013

20. Kattawar, G., Adams, C.: Stokes vector calculations of the submarine light field in an atmosphere- ocean with scattering according to a Rayleigh phase matrix. Limnol. Oceanogr. **34**(8) 1453–1472 (1989). http://www.jstor.org/stable/2837031
21. Yamaguchi, Y., Moriyama, T.: Polarimetric detection of objects buried in snowpack by a synthetic aperture fm-cw radar. IEEE Trans. Geosci. Remote Sens. **34** (1996)
22. Viana, M., Lakshminarayanan, V.: Dihedral Fourier analysis in phase-space. J. Mod. Opt. **56**(21), 2318–2328 (2009)
23. Lakshminarayanan, V., Viana, M.: Dihedral representations and statistical geometric optics I: Spherocylindrical lenses. J. Opt. Soc. Am. A **22**(11), 2483–2489 (2005)
24. Viana, M., Lakshminarayanan, V.: Dihedral representations and statistical geometric optics II: Elementary instruments. J. Mod. Opt. **54**(4), 473–485 (2007)
25. Viana, M.: Invariance conditions for random curvature models. Methodol. Comput. Appl. Probab. (5), 439–453 (2003)
26. Viana, M.: Symmetry studies and decompositions of entropy. Entropy **8**(2), 88–109 (electronic) (2006)
27. Aitchison, J.: The statistical analysis of compositional data. Chapman and Hall, New York (1986)
28. Baker, T.: Ray tracing through non-spherical surfaces. Proc. Phys. Soc. **55**, 361 (1943)
29. Patel, S., Marshall, J.: Corneal asphericity and its implications for photorefractive keratectomy: a mathematical model. J. Refract. Surg. **12**(3), 347–351 (1996)

Glossary

The following is a list of selected symbols used in the text and their definitions.

- $\mathbb{C}$ and $\mathbb{R}$ the complex and real fields.
- C_n: The cyclic groups of order n.
- D_n: The dihedral groups.
- $\tau, \sigma, \ldots$: Dihedral group elements.
- $\mathbb{C}D_n$: The dihedral group algebra over the complex field.
- $x, y, \ldots$: Points in $\mathbb{C}D_n$.
- $\rho, \eta, \ldots$ dihedral homomorphisms.
- $< x, \rho >$: Dihedral linearizations $\sum_\tau x_\tau \rho_\tau$, where ρ is a dihedral homomorphism;
- ϕ: The regular module $x \mapsto \tau x$.
- $\widehat{D}_n$ (the D_n dual): The set of distinct simple submodules of CD_n, or the set of all non-equivalent irreducible representations of D_n.
- $< x, \xi >$: The dihedral Fourier transform of $x \in \mathbb{C}D_n$ evaluated at $\xi \in \widehat{D}_n$.
- $\mathscr{O}_s$: A symmetry orbit containing s.
- Diag $(a, b, \ldots)$: A diagonal matrix with diagonal entries $a, b, \ldots$.
- $GL_n(\mathbb{C})$: The general linear group of invertible $n \times n$ matrices with entries in $\mathbb{C}$.
- $A \otimes B$: The Kronecker product of matrices A and B.
- tr A: The trace of matrix A.
- $\rho \simeq m\,\beta \oplus \ldots \oplus n\,\gamma$ indicates the existence of a basis in the representation space of ρ relative to which

$$\rho_\tau = \text{Diag}\,(I_m \otimes \beta_\tau, \ldots, I_n \otimes \gamma_\tau), \quad \tau \in D_n.$$

M.A.G. Viana and V. Lakshminarayanan, *Dihedral Fourier Analysis: Data-Analytic Aspects and Applications*, Lecture Notes in Statistics 206,
DOI 10.1007/978-1-4614-5562-2_1, © Springer Science+Business Media New York 2013

Index

M.A.G. Viana and V. Lakshminarayanan, *Dihedral Fourier Analysis: Data-Analytic Aspects and Applications*, Lecture Notes in Statistics 206,
DOI 10.1007/978-1-4614-5562-2_1, © Springer Science+Business Media New York 2013